Quantification of multi-hazard risk from natural disasters

A thesis submitted in partial fulfilment of the requirements for the degree of

Doctor of Philosophy in Hazard and Disaster Management

at the

Department of Geological Sciences

University of Canterbury

by

Alexandre Dunant

University of Canterbury

2019

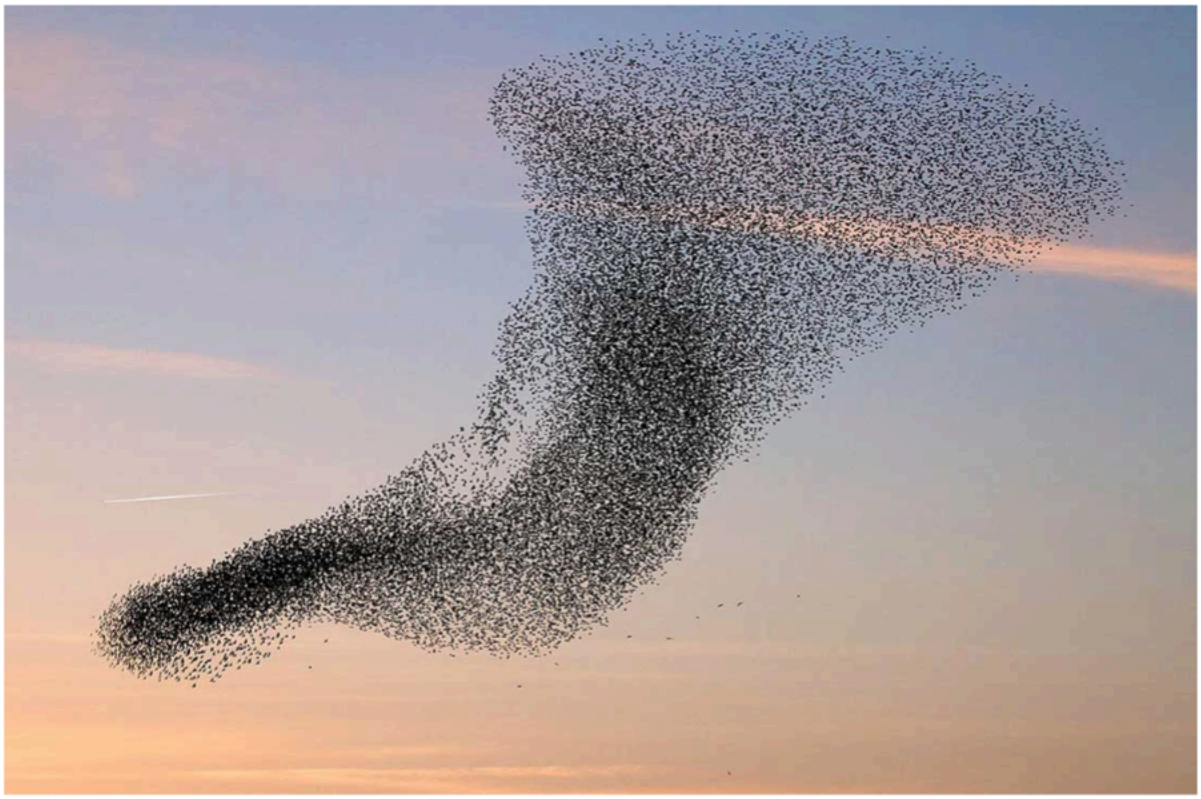

A flock of birds swarming across the sky is an example of a complex system in action

“The future ain’t what it used to be.” Yogi Berra

“Learn how to see. Realize that everything connects to everything else.” Leonardo da Vinci

“Steel isn't strong, boy, flesh is stronger! Look around you.” Thulsa Doom (Conan the barbarian)

Abstract

On a global scale, naturally-triggered disasters have killed about 60,000 people per year since 1900 and cost US$ 4,800bn of losses since 1980. Many of these catastrophes are the result of a complex combination of disastrous events. By contrast, natural disaster risk assessment is traditionally carried out on individual hazards in isolation. However, a global scientific interest has been building up over the last few years toward improving the quantification of risk by taking into account the disastrous combinations of hazards, also referred to as multi-hazard events.

This thesis develops and investigates a novel methodology to include the interacting elements of the natural disaster system in risk assessments.

A causal graphical method was found to be a promising framework for multi-hazard risk assessment. A pilot study developed and used such a framework to investigate road impacts following the Kaikōura 2016 earthquake, New Zealand, and validated further development of an iterative graphical approach by providing realistic results in line with the actual events. The potential impacts from the primary and secondary hazards were shown to be uneven for the different road segments. With the aim of leading this framework to a probabilistic risk assessment, the Franz Josef area was selected early on as an interesting case study. Franz Josef township, New Zealand, is located downstream of steep valleys of the Southern Alps and experiences considerable annual precipitation. We identified that the risk from landslide dam blockage and outburst flood could have a strong influence on the multi-hazard risk to the township.

Because of the complexity of the task, pre-emptive quantifiable output associated with landslide dams is often a missing link in the cascading chain of events from an earthquake. An automated tool was developed to forecast potential outburst floods from landslide dam blockages at a regional scale, which could be used for risk reduction and resource allocation. A test study of the Callery river on the West Coast of the South Island showed a strongly positively skewed

distribution of the outburst discharges that could be attributed to the known fractal dimensions of mountainous landscapes and river networks. The results point to the need for a comprehensive review of the stopbank inventory in New Zealand.

This tool formed part of the work undertaken to further develop a fully probabilistic risk assessment for the Franz Josef area using a causal graphical framework. The resulting methodology is the ultimate outcome of this thesis: it allows quantification of multi-hazard impacts on a range of vulnerable assets while providing an extensive discrete data output.

This methodology provides several advantages:

i) the unifying aspect of the framework proposed, which allows flexibility to encapsulate multiple elements into the risk "spectrum" (hazard, exposure and vulnerability) with very little friction.

ii) the forward nature of the assessment, which is predictive (use of threshold values and empirical relationships) rather than explanatory (inverse model fitting data).

The application of the framework to Franz Josef township, New Zealand, demonstrates the benefits of multi-hazard assessment. It has shown that differences between single and multi-hazard approaches increase in the low-frequency/high-magnitude tail of the loss distributions where impact aggravation occurs. Because disaster mitigation decisions are often made on higher-frequency (e.g. 100-year), or quantile (e.g. 99^{th} percentile) events, standard risk assessments would miss or, in the best case, underestimate the risk and lead to misplaced mitigation measures.

Deputy Vice-Chancellor's Office
Postgraduate Research Office

UNIVERSITY OF CANTERBURY
Te Whare Wānanga o Waitaha
CHRISTCHURCH NEW ZEALAND

Co-Authorship Form

This form is to accompany the submission of any thesis that contains research reported in co-authored work that has been published, accepted for publication, or submitted for publication. A copy of this form should be included for each co-authored work that is included in the thesis. Completed forms should be included at the front (after the thesis abstract) of each copy of the thesis submitted for examination and library deposit.

Please indicate the chapter/section/pages of this thesis that are extracted from co-authored work and provide details of the publication or submission from the extract comes:

Chapter 2

The submission was done on the 6th February 2019 to the Risk Analysis journal. A reply was given by the journal on the 6th August 2019 calling for revisions. The version presented here is the revision number 1 which is going to be sent to the journal in the near future.

Please detail the nature and extent (%) of contribution by the candidate:

The concept of the manuscript was developed through discussions between Alexandre Dunant, Tim Davies and Mark Bebbington. Alexandre Dunant, Tim Davies, Mark Bebbington designed the research objectives. The flood modeling was provided by Matthew Gardner. The PSHA source model was provided by Quakecore (University of Canterbury) and run by Alexandre Dunant. The Landslide modelling was done using the Flow-R model provided by Pascal Horton (University of Bern) and run by Alexandre Dunant. Alexandre Dunant created the graphical multi-hazard methodology, modeling and wrote the manuscript. All co-authors carried out in-depth reviews of the manuscript and offered much useful discussion of results and interpretations.

Alexandre Dunant account for 60% of the work , Tim Davies 20%, Mark Bebbington 20%

Certification by Co-authors:

If there is more than one co-author then a single co-author can sign on behalf of all

The undersigned certifies that:

The above statement correctly reflects the nature and extent of the Doctoral candidate's contribution to this co-authored work

In cases where the candidate was the lead author of the co-authored work he or she wrote the text

Name: Tim Davies Signature: Date:18 Dec 2019

Deputy Vice-Chancellor's Office
Postgraduate Research Office

UNIVERSITY OF CANTERBURY
Te Whare Wānanga o Waitaha
CHRISTCHURCH NEW ZEALAND

Co-Authorship Form

This form is to accompany the submission of any thesis that contains research reported in co-authored work that has been published, accepted for publication, or submitted for publication. A copy of this form should be included for each co-authored work that is included in the thesis. Completed forms should be included at the front (after the thesis abstract) of each copy of the thesis submitted for examination and library deposit.

Please indicate the chapter/section/pages of this thesis that are extracted from co-authored work and provide details of the publication or submission from the extract comes:
Chapter 3
The paper is still to be submitted to a journal for publication.

Please detail the nature and extent (%) of contribution by the candidate:
The concept of the manuscript was developed through discussions between Alexandre Dunant and Tim Davies. Alexandre Dunant and Tim Davies designed the research objectives. The flood modeling was provided by Matthew Gardner. Alexandre Dunant created the landslide dam outburst flood methodology, modeling and wrote the manuscript. Tim Davies carried out in-depth reviews of the manuscript and offered much useful discussion of results and interpretations.
Alexandre Dunant account for 80% of the work , Tim Davies 20%

Certification by Co-authors:

If there is more than one co-author then a single co-author can sign on behalf of all

The undersigned certifies that:

The above statement correctly reflects the nature and extent of the Doctoral candidate's contribution to this co-authored work

In cases where the candidate was the lead author of the co-authored work he or she wrote the text

Name: Tim Davies Signature: Date:18 Dec 2019

Deputy Vice-Chancellor's Office
Postgraduate Research Office

UNIVERSITY OF CANTERBURY
Te Whare Wānanga o Waitaha
CHRISTCHURCH NEW ZEALAND

Co-Authorship Form

This form is to accompany the submission of any thesis that contains research reported in co-authored work that has been published, accepted for publication, or submitted for publication. A copy of this form should be included for each co-authored work that is included in the thesis. Completed forms should be included at the front (after the thesis abstract) of each copy of the thesis submitted for examination and library deposit.

Please indicate the chapter/section/pages of this thesis that are extracted from co-authored work and provide details of the publication or submission from the extract comes:

Chapter 4

The manuscript was submitted on the 17th December 2019 to the International Journal of Disaster Risk Reduction.

Please detail the nature and extent (%) of contribution by the candidate:

The concept of the manuscript was developed through discussions between Alexandre Dunant, Tim Davies and Mark Bebbington. Alexandre Dunant, Tim Davies, Mark Bebbington designed the research objectives. The flood modeling was provided by Matthew Gardner. The PSHA source model was provided by Quakecore (University of Canterbury) and run by Alexandre Dunant. The Landslide modelling was done using the Flow-R model provided by Pascal Horton (University of Bern) and run by Alexandre Dunant. Alexandre Dunant created the graphical multi-hazard methodology, modeling and wrote the manuscript. All co-authors carried out in-depth reviews of the manuscript and offered much useful discussion of results and interpretations.

Alexandre Dunant account for 60% of the work , Tim Davies 20%, Mark Bebbington 20%

Certification by Co-authors:

If there is more than one co-author then a single co-author can sign on behalf of all

The undersigned certifies that:

The above statement correctly reflects the nature and extent of the Doctoral candidate's contribution to this co-authored work

In cases where the candidate was the lead author of the co-authored work he or she wrote the text

Name: Tim Davies Signature: Date:18 Dec 2019

Acknowledgements

I would like to express my deepest appreciation to my supervisors, Professor Tim Davies and Professor Mark Bebbington, for offering this opportunity and for their constant support, rigour, insight, guidance and willingness to entertain wild ideas. I would also like to thank Associate Professor Tom Wilson, for his shrewdness and useful remarks as an unofficial mentor. You have all been instrumental in changing my professional outlook for the better and helped to “bring a fish to water”.

I would like to thank my fellow PhD students for the fun in a place far away from home.

Thank you to all the people that provided technical assistance with the modeling and professional support - this thesis would not have been possible without you; Pascal Horton, Chris Massey, Graeme Smart and the NIWA crew, Matthew Gardner, Brendon Bradley, Sung Bae and Quakecore.

Thanks to Xavier Bellagamba for helping out a beginner with the dark art of programming.

Thank you to the administrative and technical staff at the University of Canterbury. John Southward, I will now stop bothering you I promise.

I want to extend my acknowledgments to the people that were kind enough to host me during my visit in Europe; thank you again for the interesting discussions: Professor Warner Marzocchi, Professor Bruce Malamud, Professor Michel Jaboyedoff, Dr Tom Robinson, Dr Arnaud Mignan.

Financial support from the Resilience to Nature’s Challenges and the Mason Trust is gratefully acknowledged.

Thank you to my family to understand that, sometimes, you have to answer the call to adventure.

To Marie, obviously. 3 babies in 3 years and I only delivered this one! Thank you for your endless support and energy.

To Suzie and Léon for making me a man fulfilled … and tired.

Table of Contents

List of Figures

List of Tables

Terminology

The study of natural hazards and disaster risk involves specific terminologies. The following definitions will help clarify the terms used and facilitate the understanding of the thesis.

Assets (elements at risk): Humanly/socially valued entities threatened by a hazard. (Schmidt et al., 2011)

Exposure: People, property, systems, or other elements present in hazard zones that are thereby subject to potential losses (UNISDR, 2009).

Hazard: A dangerous phenomenon, substance, human activity or condition that may cause loss of life, injury or other health impacts, property damage, loss of livelihoods and services, social and economic disruption, or environmental damage (UNISDR, 2009).

Hazard assessment: The process of identifying the nature, location, probability and magnitude of a potentially damaging event.

Impact: is the total effect, including negative effects (e.g., economic losses) and positive effects (e.g., economic gains), of a hazardous event or a disaster (UNISDR, 2009).

Multi-Hazard assessment: The implementation of methodologies and approaches aimed at evaluating all identified individual hazards relevant to a defined spatial area and characterize all possible interactions between these identified hazards (Gill & Malamud, 2016).

Natural hazard: Natural process or phenomenon that may cause loss of life, injury or other health impacts, property damage, loss of livelihoods and services, social and economic disruption, or environmental damage (UNISDR, 2009).

Risk: The combination (i.e. product) of the probability of an event and its negative consequences (UNISDR, 2009).

Risk assessment: A methodology to determine the nature and extent of risk by analyzing potential hazards and evaluating existing conditions of vulnerability that together could potentially harm exposed people, property, services, livelihoods and the environment on which they depend (UNISDR, 2009).

Vulnerability: The characteristics and circumstances of a community, system or asset that make it susceptible to the damaging effects of a hazard (UNISDR, 2009)

Chapter 1
Introduction

On a global scale, natural disasters have killed about 60,000 people per year since 1900 and cost US$ 4,800bn in losses since 1980. Many of these catastrophes are the result of a complex combination of disastrous events. By contrast, natural hazard risk assessment is traditionally carried out on individual hazards in isolation. This type of approach can be referred to as “single hazard”, or “multilayer single hazard” when several hazard layers overlap spatially (Gill & Malamud, 2014), as opposed to a more holistic “multi-hazard” approach where the interactions between hazards are considered (Figure 1.1). Global scientific interest has been building over the last few years toward improving the quantification of risk by taking into account impacts from a combination of hazards, also referred as “multi-hazard”.

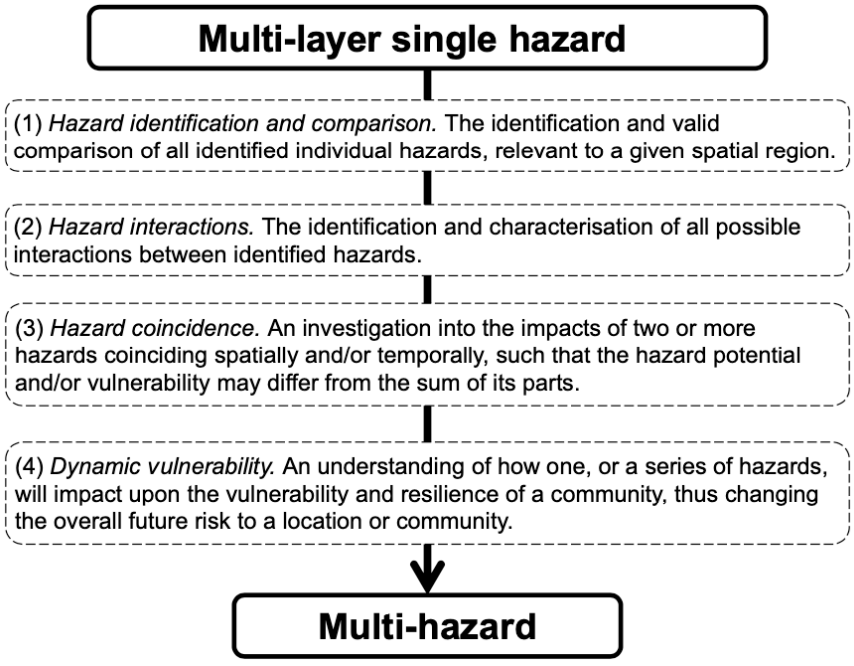

Figure 1.1 Progression from a Multi-layer single hazard to a Multi-hazard assessment (Gill et al., 2014, 2016)

Indeed, natural hazard experts recognize the disastrous effects of multi- and cascading hazards and many papers emphasize the complex aspect of disasters (Kumasaki et al. , 2016) (see Figure 1.2) As part of the Hyogo Framework for Action the necessity for a ‘‘holistic and multi-hazard approach to disaster risk management” (UNISDR, 2005) is mentioned.

The 2011 Tohoku earthquake which precipitated the 2011 Fukushima nuclear disaster (Pescaroli & Alexander, 2015), and the 2008 Wenchuan earthquake with seven episodes of extraordinary hazards impacting the Beichuan area (earthquake, multiple large landslides, dam-breaching floods, large-scale debris flows, severe sedimentation, change of river course, and flooding/scouring; Zhang et al.,2014), are two examples highlighting the amplifying effect of cascading and multi-source hazard systems. New Zealand recently experienced the disruptive effect of multiple hazards and cascading effects through the 2010 – 2012 Canterbury earthquake sequence and the 2016 Kaikōura earthquake (earthquake, landslides, landslide dams and floodplain subsidence; Hughes et al., 2015; Robinson & Rosser, 2017).

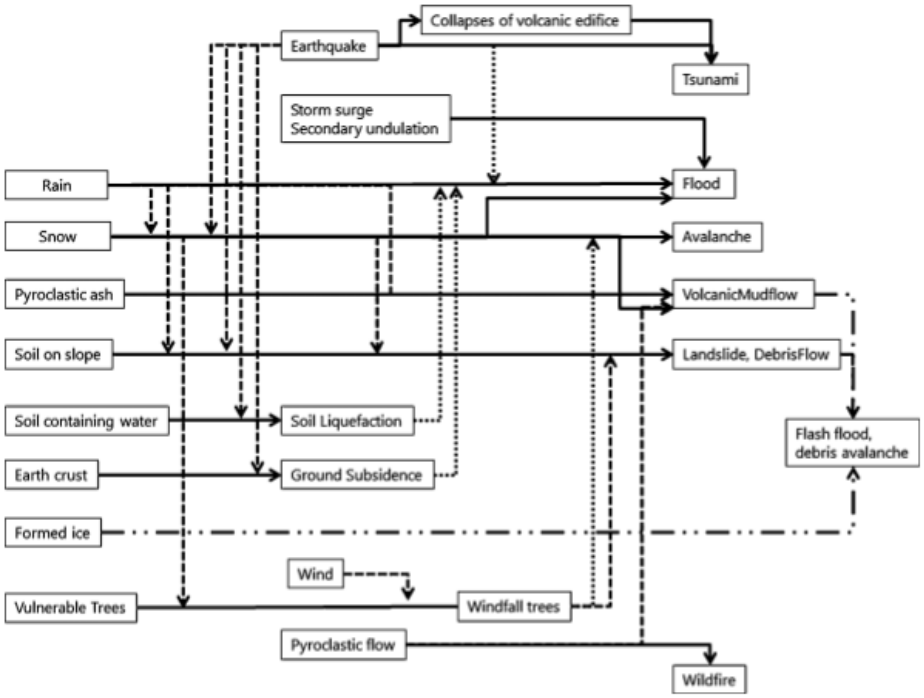

Figure 1.2 Relationships of cascading natural hazards in Japan by Kumasaki et al., (2016)

It is important to note that several terms exist to explain the different interactions between hazards; a list of terminology from publications is presented in Table 1.1 (from Kappes et al., 2012).

Table 1.1 List of terminology in use to described relations between hazard types, compiled by Kappes et al., (2012)

Cascades, cascading effects, cascading failures, or cascade events	Delmonaco et al. (2006b), Carpignano et al. (2009), Zuccaro and Leone (2011), European Commission (2011)
Chains	Shi (2002), Erlingsson (2005)
Coincidence of hazards in space and time	Tarvainen et al. (2006)
Coinciding hazards	European Commission (2011)
Compound hazards	Hewitt and Burton (1971), Alexander (2001)
Coupled events	Marzocchi et al. (2009)
Cross-hazards effects	Greiving (2006)
Domino effects	Luino (2005), Delmonaco et al. (2006b), Perles Roselló and Cantarero Prados (2010), European Commission (2011)
Follow-on events	European Commission (2011)
Interactions	Tarvainen et al. (2006), dePippo et al. (2008), Marzocchi et al. (2009), Zuccaro and Leone (2011)
Interconnections	Perles Roselló and Cantarero Prados (2010)
Interrelations	Delmonaco et al. (2006b), Greiving (2006)
Knock-on effects	European Commission (2011)
Multiple hazard	Hewitt and Burton (1971)
Synergic effects	Tarvainen et al. (2006)
Triggering effects	Marzocchi et al. (2009)

In contrast to single hazards, the relationships and interactions between multiple hazards create an additional layer of complexity (Kappes et al., 2012). For example, assessing the cascading effect of various hazards on a common vulnerable asset means quantifying processes with different units and measures (e.g. earthquake, landslide, flood etc.). In addition to estimating the characteristics of the individual hazardous events, a complete hazard assessment would need to assess “their mutual interactions and interrelations (e.g., landslide induced earthquake, floods and landslides triggered by extreme rainfall, natural disasters as secondary effect from main

disaster types)" (Delmonaco et al., 2007). From a response perspective, the complexity of multi-hazard occurrences extends to their impacts and their management.

1.1 Current methods of multi-hazard assessment

1.1.1 Terminology

Multi-hazard definitions have proliferated over recent years (Tilloy et al., 2019). This section will review some of the existing terms and clarify the meaning of the "multi-hazard" definition used in this paper to avoid confusion.

Terms like "cascade", "chains", "coincidence", "compound", "coupled", "domino effects", "triggering" have been widely used to describe the interaction between hazards (Kappes et al., 2012). Tilloy et al., (2019) reviewed the interrelationships between hazards and summarized them in the following set of concepts:

i. Independence, where the impact can be sustained from independent hazards;
ii. Triggering or Cascading, where a primary hazard triggers a secondary hazard;
iii. Change condition, where a primary hazard alter the probability of a secondary hazard;
iv. Compound hazard, where large scale processes influence the occurrence of simultaneous hazards;
v. Mutual exclusion, where a primary hazard excludes a secondary hazard.

The purpose of the method developed herein is to create a unifying quantitative framework under which these concepts can be applied. To do so, the following quote has been used to define a "multi-hazard framework"; the implementation of a framework "aimed at evaluating all identified

individual hazards relevant to a defined spatial area and characterize all possible interactions between these identified hazards" (Gill & Malamud, 2016).

1.1.2 Qualitative and semi-quantitative multi-hazard assessments

Paradoxically, given the need for complex risk assessment, relatively few research papers exist quantifying systemic risks of hazards (Kappes et al., 2012). Several qualitative methods have been published but few quantitative methods are available.

Existing methods have been classified in qualitative, semi-quantitative and quantitative terms. Nevertheless, two methods are mainly used to by-pass the difficulty of combining hazards of different types: (1) the categorization of hazards (qualitative) and (2) the use of indices (semi-quantitative approach; Kappes et al., 2012).

In order to categorize hazards, intensity and recurrence intervals limits are predefined to assign each of the hazards into several classes. The boundaries are specifically determined by the location, or the objectives of the assessment. This allows for the comparison between threats, for example, "high earthquake and high flood hazard" (Delmonaco et al., 2007). Table 1.2 illustrates this point.

Table 1.2 Classes of hazards from the Armonia project (Applied Multi Risk Mapping of Natural Hazards for Impact Assessment) (Delmonaco et al., 2007). The purpose of the Armonia project was to define a methodology to harmonise risk maps aimed at spatial planning in Europe.

Natural Hazard	Intensity Scales			
	Low	Medium	High	Parameters
Flood	<0.25	0.2–1.25	>1.25	Flood depth (m)
Forest Fire	<350	350–1,750	>1,750–3,500	Predicted fire line intensity (*)(kW/m)
Forest Fire	<1.2	1.2–2.5	>2.5–3.5	Approximate flame length (m)
Volcanoes	<5	5–10	>10	Intensity = volcanic explosive index $\log_{10}$(mass eruption rate, kg/s) + 3
Landslide (fast and slow movements)	<5	5–15	>15	Percentage of landslide surface (m^2, km^2, …) vs. stable surface (%)
Seismic	<10	10–30	>30	Peak Ground Horizontal Acceleration (%g)

Differing from the classification approaches, indices offer a way to standardize and, hence, compare parameters (see Table 1.3). Also, they permit the quantification of coupled hazard threats not provided by qualitative indices. The values in Table 1.3 are the results of the weighted sum of the different hazards from a study in the Eastern Mediterranean region by El Morjani et al. (2007).

Table 1.3 Indices used by El Morjani et al. (2007)

Hazard	Normalized weight
Seismic	0.41
Flood	0.36
Wind speed	0.09
Heat	0.08
Landslide	0.06
Sum	1

A popular tool for standardization of multi-hazard occurrence is the use of matrices. Matrices are grids that represent the occurrence probabilities and intensities of contiguous hazards. These often result in qualitative delineation such as “low”, “medium” or “high” represented by a color code (Fleming et al., 2014). The same principle has been applied to represent spatial overlap of disaster risk using GIS tools (e.g. multi-hazard map of China, Figure 1.3). This makes it possible to geographically assess the combined risk of hazards or the relative preponderance of one hazard over others (Liu et al., 2019; Pourghasemi et al., 2019). In innovative work, Pourghasemi et al. (2020) used machine learning to map the relative susceptibility of flood, forest fire and landslide in the Fars province, Shiraz City, Iran.

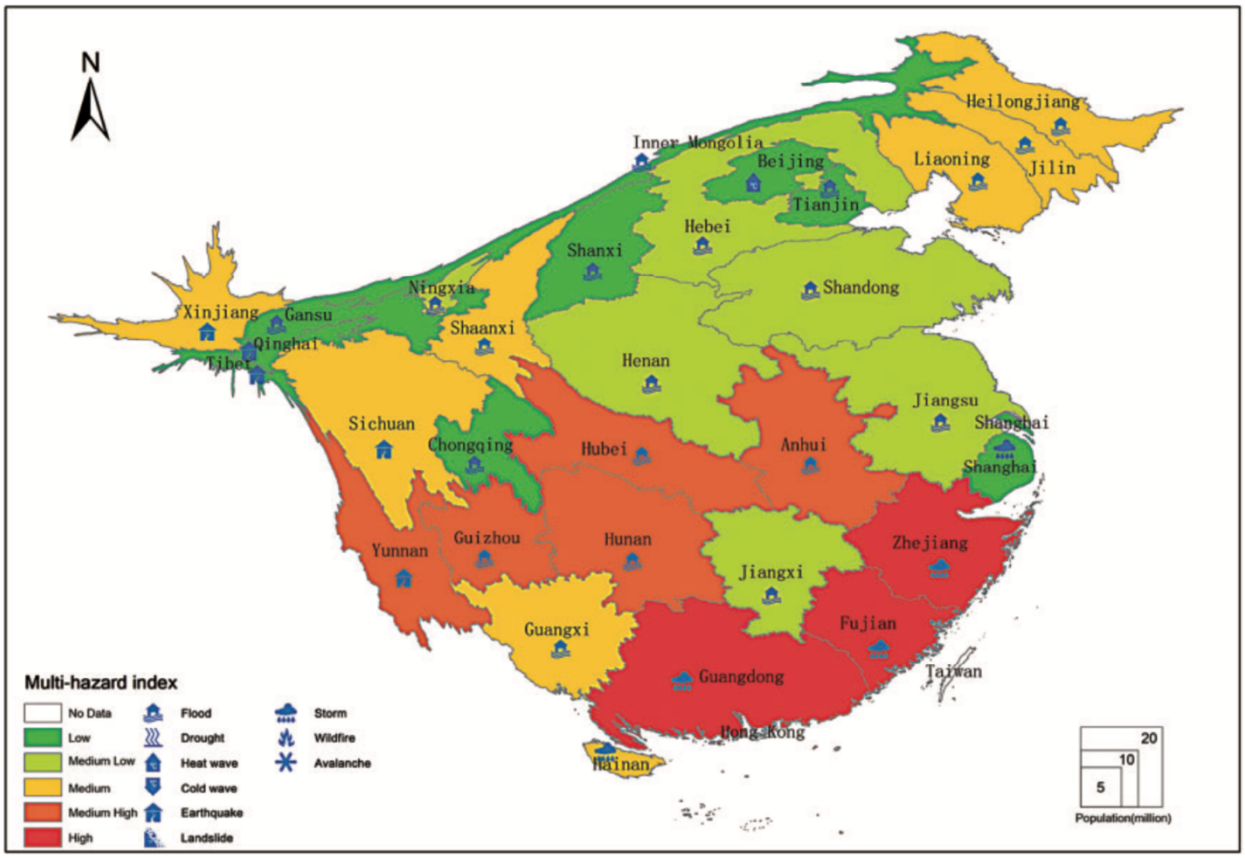

Figure 1.3 Multi-hazard map of China (Liu et al., 2019)

1.1.3 Quantitative multi-hazard assessments

The need for quantification relates to the necessity for decision support systems to quantify risk and hence help in reducing it to an optimum or acceptable level. Indeed, most regions and organizations preparing for disasters need to evaluate (often costly) risk reduction measures. The specific need to put these risk reduction initiatives in the broader multi-hazard scope is pointed out by McGee et al. (2015), stating that it is important for "… developed models to represent causal relationships triggering cascading disaster spreading, allowing to compare the effectiveness of…response strategies". Recently Tilloy et al., (2019) conducted an extensive review of the quantification methods dealing with interconnected hazards (Figure 1.4). This

literature review led to the classification of the quantification methods into three techniques; stochastic, empirical and mechanistic. Tilloy et al., (2019) defined the techniques as follows:

- Stochastic: “models based on samples of different variables with random behavior”
- Empirical: “models are based on measurements and are observation oriented. In empirical models, empirical distributions are fitted directly to the observed data.”
- Mechanistic: “Mechanistic models are mathematically idealized representations of real phenomena. They are based upon physical processes and mechanisms that rule the considered system operations.”

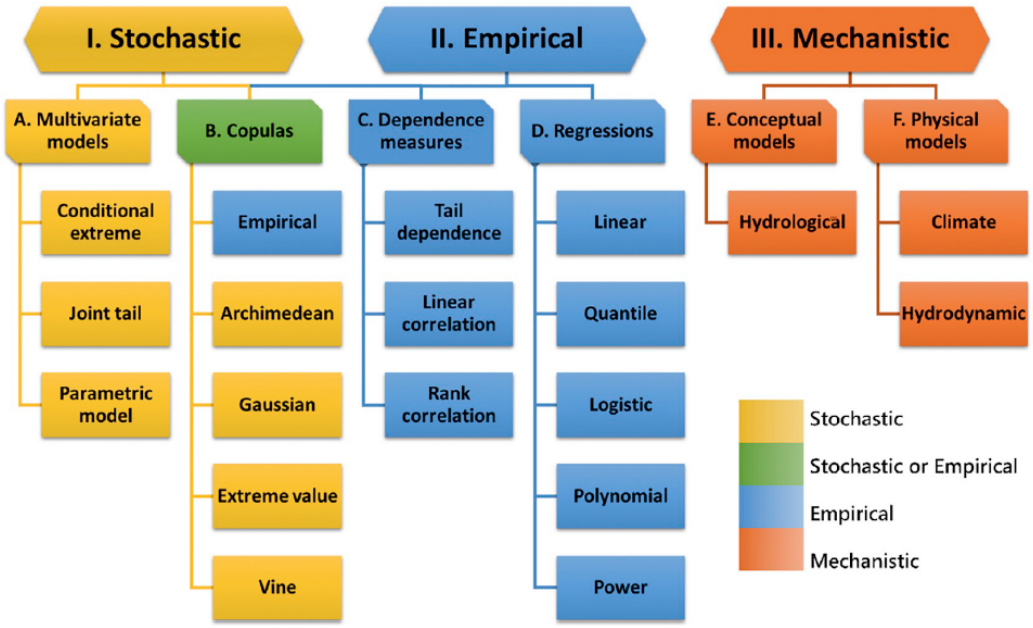

Figure 1.4 Different types of multi-hazard quantification and modeling techniques from Tilloy et al., (2019)

The aims and limitations are specific to each of the quantification classes.

The stochastic methods take into account the statistical relationships between the occurrence and intensity of hazards. For stochastic methods, the purpose is either to model the distribution of each individual hazard (Hao & Singh, 2016; Liu et al., 2018), or to model the joint probability

between hazards (Sadegh et al., 2018). The results from this type of modelling are extremely dependent on the statistical distribution used, which, in itself, can be difficult to assess with scarce or low-quality datasets. Also, the spatial representation of stochastic models might be challenging, which could impair risk communication to practitioners.

The empirical method is based on fitting existing datasets to probability distributions. The accuracy of the fit can be quantified by the use of dependence measures such as Pearson or Spearman, or regressions (Petroliagkis et al., 2016). The limitation of empirical methods is their dependency on data. Damaging natural hazards are rare and with limited records, hence limiting the use of empirical methods. Fitting correlations may be more challenging as models evolve to consider multiple hazard combinations.

Mechanistic methods have been widely used by risk scientists for computing the potential impact of natural hazards. But the intensive nature of the computation makes them difficult to use for probabilistic risk assessment and hence they are biased toward a particular set of outcomes (Geist et al., 2009).

To summarize, quantification techniques have been attempted, but limitations remain including:

- Restrictions on the number of hazards interacting
- Difficulties in providing spatial outputs
- The amount of data required to set a joint probability distribution and the intrinsic constraints of the risk analysis within the data boundaries
- The computing resources necessary for a combined physical model, which limits the flexibility of such a model to expand to additional hazards or to provide a probabilistic assessment.

It is quite clear that “the assessment of the impact of different catastrophic events in a given area requires innovative approaches that allow risks comparison and that account for all the possible risk interactions” (Marzocchi et al., 2012). Hence, to address existing limitations, a unifying multi-hazard framework should be pursued. In the following Graph Theory is investigated in this context.

1.2 Graph theory

Risk scientists are required to deal with complex and highly interconnected hazard systems. Phillips et al. (2015) mentioned that many disciplines of Earth Science could benefit from a network approach: “ ‘Graph theory’ or ‘network theory’ has been used to analyze and quantify complex systems in geography, ecology and atmospheric sciences for several decades” (Phillips et al., 2015). However, it hardly features in the discipline of natural hazard related risk assessment.

Networks refer to objects composed of multiple components and their interactions. The main purpose of graph or network theory is to “represent, measure and model the relational structure of networks” (Barabasi, 2009; Butts, 2009; Newman, 2018; Phillips, 2012). The model of networks is the graph, and the study of these graphs is termed graph theory. Graph theory allows one to deal with several issues of complex systems, i.e. “describing and assessing network structure, understanding exchange of matter, energy and information in networks, modelling propagation of system changes through networks, modelling the effects of changes in network structure and finding universality in network topology” (Phillips et al., 2015). Networks seems ubiquitous as their frameworks can be applied to a variety of systems as illustrated Figure 1.5.

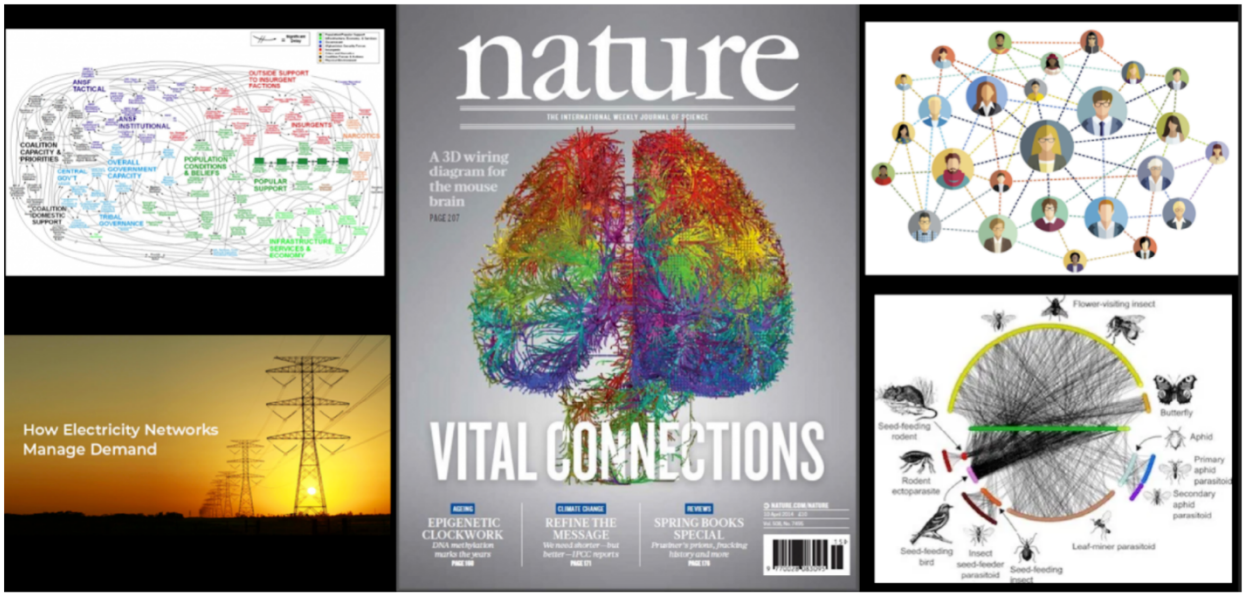

Figure 1.5 Illustration of the breadth of disciplines leveraging networks as a frame of study (from political systems – top left – to social networks and ecosystem – right-hand side.

Networks use nodes and edges to represent matter, energy or information. Hence, the absence of standard units or specific measurements allows different networks to be connected across disciplines (e.g. geological hazards and power grid). Using networks gives several notable advantages. Indeed, the connectivity among hazards, and the connectivity between hazards and elements at risk, allow for the understanding of direct as well as indirect risk (i.e. risk resulting from cascading hazards). By filtering the system to consider only the important point in space, complex spatial attributes can be converted into implicit representations. From a hardware point of view, compared to standard physical hazard models, the limited use of complex terrain data in the use of graphs limits the requirement for computer-intensive calculations. This permits the creation of numerous scenarios, giving a more complete knowledge of the spectrum of hazards present.

In addition to hazard assessment, exposure assessment can benefit from this approach. Many exposed elements that are poorly represented in traditional risk assessments are naturally

modelled as networks e.g. social networks, lifeline networks, communication networks, business and commercial networks etc. Cascading multi-hazards can propagate through an exposed societal network with disastrous consequences (Buldyrev et al., 2010; Buzna et al., 2006; Pescaroli & Alexander, 2016). Many publications already leverage graphical frameworks for risk study in various disciplines: supply chains analysis (Faisal et al., 2007), economic markets (Huang et al., 2013; Lautier & Raynaud, 2013) and infrastructure systems (Chang & Wu, 2011; Hines et al., 2013; Zhu et al., 2014; Zorn et al., 2020) are a few examples. The application of graph theory for infrastructure systems is framed with the connectivity between components represented by nodes and edges. The graph is then used to test the risk of cascading failures based on the components' dependencies. To simplify, the network method can be divided into two approaches: i) topology-based and ii) flow-based (Ouyang, 2014). The topology-based approach examines failures at the node or link level, by considering their vulnerabilities, and then examines cascading failures to other nodes or links (Dunn & Wilkinson, 2013). Flow-based methods are established by supplying the topological structure with flow-dynamic models that communicate information between nodes (Duenas-Osorio & Hernandez-Fajardo, 2008).

An interesting feature of the network approach is that hazard and exposure networks can be connected without the difficulties or limitations intrinsic in "standard" approaches. As explained earlier, networks deal with nodes and edges, but not with actual units or measures, which allows for a streamlining of the workflow. The use of networks potentially enables linking of the entirety of the hazard-exposure system, giving a complete overview of the spreading effect of initial hazards in a systems approach.

1.3 Thesis goal and objectives

The purpose of the present work is to create a novel framework for quantitative multi-hazard risk assessment. This framework was created and developed following the objective of developing a fully probabilistic multi-hazard assessment that could be leveraged to improve risk reduction and preparedness for New Zealand.

1.4 Thesis structure

The thesis is a chronological report, from Chapter 2 to Chapter 4, of the development and improvement of the framework to quantify multi-hazard risk. These chapters comprise scientific manuscripts submitted to international peer-reviewed journals. Aside from formatting to provide a consistent flow for the thesis, the content of each chapter and appendix is identical to that of the manuscript version submitted to the journals.

The multi-hazard framework is first explored by creating and testing the graphical methodology in a pilot study investigating impacts from the 2016 Kaikōura earthquake (Chapter 2). Subsequently, it focuses on landslide dam outburst flood, which is regarded as a potential threat for communities living downstream of mountain ranges. Unfortunately, no forward model exists to predict the potential for landslide dam break at a regional scale in New Zealand. A multi-hazard framework presented itself as an interesting opportunity to add this geomorphological process to the multi-hazard capability. To address this, Chapter 3 quantifies the risk from landslide dams as part of the multi-hazard cascade. To do this, an automated tool was developed to assess the peak outburst flood discharge from landslide dam scenarios in the Callery river on the west coast of South Island, New Zealand (Chapter 3). In Chapter 4, the overarching objective of this thesis is answered by applying a fully probabilistic multi-hazard assessment to Franz Josef township,

providing a “real-life” application of the methodology, demonstrating its relevance and providing new insights into the natural hazard risk to the township.

The methodologies, applications and results described in the chapters are direct outcomes of my own research with the invaluable contribution from co-authors.

1.5 References

Barabasi, A.-L. (2009). Scale-Free Networks: A Decade and Beyond. *Science*, *325*(5939), 412–413. https://doi.org/10.1126/science.1173299

Buldyrev, S. V., Parshani, R., Paul, G., Stanley, H. E., & Havlin, S. (2010). Catastrophic cascade of failures in interdependent networks. *Nature*, *464*(7291), 1025–1028. https://doi.org/10.1038/nature08932

Butts, C. T. (2009). Revisiting the foundations of network analysis. *Science (New York, N.Y.)*, *325*(5939), 414–416. https://doi.org/10.1126/science.1171022

Buzna, L., Peters, K., & Helbing, D. (2006). Modelling the dynamics of disaster spreading in networks. *Physica A: Statistical Mechanics and Its Applications*, *363*(1), 132–140. https://doi.org/10.1016/j.physa.2006.01.059

Chang, L., & Wu, Z. (2011). Performance and reliability of electrical power grids under cascading failures. *International Journal of Electrical Power & Energy Systems*, *33*(8), 1410–1419.

Delmonaco, G., Margottini, C., & Spizzichino, D. (2007). *ARMONIA methodology for multi-risk assessment and the harmonisation of different*. (January).

Duenas-Osorio, L., & Hernandez-Fajardo, I. (2008). Flow-based reliability assessment of infrastructure systems (Vol. 31, pp. 157–167). Presented at the 14th World Conference on Earthquake Engineering (14WCEE).

Dunn, S., & Wilkinson, S. M. (2013). Identifying critical components in infrastructure networks using network topology. *Journal of Infrastructure Systems*, *19*(2), 157–165.

El Morjani, Z. E. A., Ebener, S., Boos, J., Abdel Ghaffar, E., & Musani, A. (2007). Modelling the spatial distribution of five natural hazards in the context of the WHO/EMRO Atlas of Disaster Risk as a step towards the reduction of the health impact related to disasters. *International Journal of Health Geographics*, *6*, 8. https://doi.org/10.1186/1476-072X-6-8

Faisal, M. N., Banwet, D. K., & Shankar, R. (2007). Quantification of risk mitigation environment of supply chains using graph theory and matrix methods. *European Journal of Industrial Engineering*. Retrieved from https://www.inderscienceonline.com/doi/abs/10.1504/EJIE.2007.012652

Fleming, K., Zschau, J., & Gasparini, P. (2014). The New Multi-HAzard and MulTi-RIsK Assessment MethodS for Europe (MATRIX) Project-An overview of its major findings (Vol. 16). Presented at the EGU General Assembly Conference Abstracts.

Geist, E. L., Lynett, P. J., & Chaytor, J. D. (2009). Hydrodynamic modeling of tsunamis from the Currituck landslide. *Marine Geology*, *264*(1–2), 41–52. https://doi.org/10.1016/j.margeo.2008.09.005

Gill, J. C., & Malamud, B. D. (2014). Reviewing and visualizing the interactions of natural hazards: Interactions of Natural Hazards. *Reviews of Geophysics*, *52*(4), 680–722. https://doi.org/10.1002/2013RG000445

Hao, Z., & Singh, V. P. (2016). Review of dependence modeling in hydrology and water resources. *Progress in Physical Geography*, *40*(4), 549–578.

Hines, P. D., Dobson, I., Cotilla-Sanchez, E., & Eppstein, M. (2013). " Dual Graph" and" Random Chemistry" Methods for Cascading Failure Analysis (pp. 2141–2150). Presented at the 2013 46th Hawaii International Conference on System Sciences, IEEE.

Huang, X., Vodenska, I., Havlin, S., & Stanley, H. E. (2013). Cascading Failures in Bi-partite Graphs: Model for Systemic Risk Propagation. *Scientific Reports*, *3*(1), 1219.

https://doi.org/10.1038/srep01219

Hughes, M. W., Quigley, M. C., Van Ballegooy, S., Deam, B. L., Bradley, B. A., Hart, D. E., & Measures, R. (2015). The sinking city: Earthquakes increase flood hazard in Christchurch, New Zealand. *GSA Today*, *25*(3–4), 4–10. https://doi.org/10.1130/GSATG221A.1

Kappes, M. S., Keiler, M., von Elverfeldt, K., & Glade, T. (2012). Challenges of analyzing multi-hazard risk: A review. *Natural Hazards*, *64*(2), 1925–1958. https://doi.org/10.1007/s11069-012-0294-2

Kumasaki, M., King, M., Arai, M., & Yang, L. (2016). Anatomy of cascading natural disasters in Japan: Main modes and linkages. *Natural Hazards*, *80*(3), 1425–1441. https://doi.org/10.1007/s11069-015-2028-8

Liu, Z., Cheng, L., Hao, Z., Li, J., Thorstensen, A., & Gao, H. (2018). A Framework for Exploring Joint Effects of Conditional Factors on Compound Floods. *Water Resources Research*, *54*(4), 2681–2696. https://doi.org/10.1002/2017WR021662

Liu, B., Fan, J., Siu, Y. L., & Mitchell, G. (2019). A multi-hazard map of China. *Environment and Planning A: Economy and Space*, *51*(1), 8–10. https://doi.org/10.1177/0308518X18791171

Marzocchi, W., Garcia-Aristizabal, A., Gasparini, P., Mastellone, M. L., & Ruocco, A. D. (2012). Basic principles of multi-risk assessment: A case study in Italy. *Natural Hazards*, *62*(2), 551–573. https://doi.org/10.1007/s11069-012-0092-x

McGee, S., Frittman, J., Ahn, S. 'James', & Murray, S. (2015). Risk relationships and cascading effects in critical infrastructures: Implications for the Hyogo framework. *International Journal of Disaster Resilience in the Built Environment, 7(2), 144-157.*, *7*(2), 144–157.

Newman, M. (2018). Networks. Oxford university press.

Ouyang, M. (2014). Review on modeling and simulation of interdependent critical infrastructure systems. *Reliability Engineering and System Safety*, *121*, 43–60. https://doi.org/10.1016/j.ress.2013.06.040

Pescaroli, G., & Alexander, D. (2015). A definition of cascading disasters and cascading effects: Going beyond the 'toppling dominos' metaphor. *GRF Davos Planet@Risk*, *Volume 3*.

Pescaroli, G., & Alexander, D. (2016). Critical infrastructure, panarchies and the vulnerability paths of cascading disasters. *Natural Hazards*, *82*(1), 175–192. https://doi.org/10.1007/s11069-016-2186-3

Petroliagkis, T. I., Voukouvalas, E., Disperati, J., & Bidlot, J. (2016). Joint probabilities of storm surge, significant wave height and river discharge components of coastal flooding events. *European Commission-JRC Technical Reports, Italia Http://Bookshop. Europa. Eu/En/Joint-Probabilities-of-Storm-Surge-Significant-Wave-Height-and-River-Discharge-Components-of-Coastal-Flooding-EventspbLBNA27824*, 0KABstXJMAAAEjt5AY4e5L.

Phillips, J. D. (2012). Synchronization and scale in geomorphic systems. *Geomorphology*, *137*(1), 150–158. https://doi.org/10.1016/j.geomorph.2010.09.028

Phillips, J. D., Schwanghart, W., & Heckmann, T. (2015). Graph theory in the geosciences. *Earth-Science Reviews*, *143*, 147–160. https://doi.org/10.1016/j.earscirev.2015.02.002

Pourghasemi, H. R., Gayen, A., Panahi, M., Rezaie, F., & Blaschke, T. (2019). Multi-hazard probability assessment and mapping in Iran. *Science of The Total Environment*, *692*, 556–571. https://doi.org/10.1016/j.scitotenv.2019.07.203

Pourghasemi, H. R., Kariminejad, N., Amiri, M., Edalat, M., Zarafshar, M., Blaschke, T., & Cerda, A. (2020). Assessing and mapping multi-hazard risk susceptibility using a machine learning technique. *Scientific Reports*, *10*(1), 3203. https://doi.org/10.1038/s41598-020-60191-3

Robinson, T., & Rosser, N. (2017). Rapid landslide risk assessment of transport infrastructure following the 13 November 2016 Kaikōura, New Zealand, earthquake. *Geophysical Research Abstracts EGU General Assembly*, *19*, 2017–5180.

Sadegh, M., Moftakhari, H., Gupta, H. V., Ragno, E., Mazdiyasni, O., Sanders, B., … AghaKouchak, A. (2018). Multihazard Scenarios for Analysis of Compound Extreme

Events. *Geophysical Research Letters*, *45*, 5470–5480. https://doi.org/10.1029/2018gl077317

Tilloy, A., Malamud, B. D., Winter, H., & Joly-Laugel, A. (2019). A review of quantification methodologies for multi-hazard interrelationships. *Earth-Science Reviews*, *196*, 102881. https://doi.org/10.1016/j.earscirev.2019.102881

UNISDR. (2005). *Hyogo framework for action 2005-2015: Building the resilience of nations and communities to disasters.* In Extract from the final report of the World Conference on Disaster Reduction (A/CONF. 206/6) (Vol. 380). Geneva: The United Nations International Strategy for Disaster Reduction.

Zhang, L. M., Zhang, S., & Huang, R. Q. (2014). Multi-hazard scenarios and consequences in Beichuan, China: The first five years after the 2008 Wenchuan earthquake. *Engineering Geology*, *180*, 4–20. https://doi.org/10.1016/j.enggeo.2014.03.020

Zhu, Y., Yan, J., Sun, Y., & He, H. (2014). Revealing cascading failure vulnerability in power grids using risk-graph. *IEEE Transactions on Parallel and Distributed Systems*, *25*(12), 3274–3284.

Zorn, C., Pant, R., Thacker, S., & Shamseldin, A. Y. (2020). Evaluating the magnitude and spatial extent of disruptions across interdependent national infrastructure networks. *ASCE-ASME J Risk and Uncert in Engrg Sys Part B Mech Engrg*, *6*(2).

Chapter 2
Multi-hazards scenario generator: A network-based simulation of natural disasters

---

Alexandre Dunant[1], Mark Bebbington[2], Tim Davies[1]

[1] Department of Geological Sciences, University of Canterbury, Christchurch

[2] Institute of Fundamental Sciences, Massey University, Palmerston North

Overview

A pilot study of a novel causal graphical multi-hazard assessment is described in this Chapter as a way to present the method applicability and its potential for the future. The method relevance is tested using the Kaikōura 2016 earthquake and the comparison with the actual cascading impacts of earthquake, rainfall & landslides.

Contributions

The concept of the manuscript was developed through discussions between Alexandre Dunant, Tim Davies and Mark Bebbington. Alexandre Dunant, Tim Davies and Mark Bebbington designed the research objectives. The flood modeling was provided by Matthew Gardner. The PSHA source model was provided by QuakeCoRE (University of Canterbury) and run by Alexandre Dunant. The Landslide modelling used the Flow-R model provided by Pascal Horton (University of Bern) and was run by Alexandre Dunant. Alexandre Dunant created the graphical multi-hazard methodology, undertook the modeling and wrote the manuscript. All co-authors carried out in-depth reviews of the manuscript and offered much useful discussion of results and interpretations.

ABSTRACT

The impact of natural disasters has been increasing in recent years. Despite the developing international interest in multi-hazard events, few studies quantify the dynamic interactions that characterize these phenomena. It is argued that without considering the dynamic complexity of natural catastrophes, impact assessments will underestimate risk and misinform emergency management priorities. The ability to generate multi-hazard scenarios with impacts at a desired resolution is important for emergency planning and resilience assessment. This paper demonstrates a framework for using graph theory and networks to generate and model the complex impacts of multi-hazard scenarios. First, the combination of maximal hazard footprints and exposed nodes (e.g. infrastructure) is used to create the risk network. Iterative simulations of the network, defined by actual hazard magnitudes, are then used to estimate the overall compounded impact from a sequence of hazards. Outputs of the modelling are used to study distributional ranges of multi-hazard impact.

The 2016 Kaikōura earthquake is used as a calibrating event to demonstrate that the method can reproduce the same scale of impacts as a real event. The cascading hazards included numerous landslides, allowing us to show that the scenario set generated includes the actual impacts that occurred during the 2016 events.

2.1 Introduction

2.1.1 Context & background

Many areas of the world are prone to complex and interconnected natural hazards. In recent years, several disasters have shown the importance of the complex nature of contributing hazards; disasters can be triggered by a single event that cascades into multiple hazards, widely

distributed in both space and time. The 2016 Kumamoto strike-slip earthquake, with several deaths attributed to landsliding (Goda et al., 2016), and the 2008 Wenchuan earthquake, with seven consequential episodes of extraordinary hazards (which “included [. . .]multiple large landslides, dam-breaching floods, large-scale debris flows, severe sedimentation, change of river course, and flooding/scouring”) impacting the Beichuan area (Zhang et al., 2014), are examples highlighting the amplifying effect of cascading and multisource hazard systems.

The Sendai Framework for Disaster Risk Reduction highlights the need for a focus on multi-hazards with an emphasis on solution-driven methods to assess risks from “all hazards” (UNISDR, 2015). In this context, the Sendai Framework echoes the Hyogo Framework for Action (ISDR, 2005) as well as pronouncements by The European Geosciences Union (Gill & Malamud, 2014), all of which clearly demonstrate the international challenges of, and interest in, multi-hazard impacts.

New Zealand recently experienced the disruptive effect of multi-hazards and cascading impacts as part of the Canterbury earthquake sequence (Cubrinovski et al., 2012; Stahl et al., 2014; Bannister & Gledhill, 2012; Cox et al., 2012), particularly through liquefaction and rockfall; and associated with the 2016 Kaikōura earthquake (Robinson & Rosser, 2017; Stahl et al., 2014), through slope-failure hazards triggered by the original shaking and subsequent rainfall. The New Zealand Civil Defence and Emergency Management (CDEM) Act 2002 recognizes the need to study hazards for the good of New Zealand communities by “identifying, assessing, and managing risks”.

2.1.2 Definitions and hazard interactions

Despite the fact that natural hazard experts recognize the disastrous effects of multi- and cascading hazards, and many papers emphasise the complex aspects of disasters (e.g. Kumasaki et al., 2016; Pescaroli & Alexander, 2016; Pescaroli & Alexander, 2018), no consensus

on exact definition(s) exists, even though the notion is used extensively by practitioners (Marzocchi et al., 2012; Pescaroli & Alexander, 2015). While the point of the present work is not the semantics of multi-hazard assessment, it is recognised that a common understanding, between the reader and the authors, on the purpose of the methodology presented herein, is needed to avoid confusion. It is quite clear, from the references above, that multi-hazard assessment methodologies must tackle the issue of complexity by addressing the multi-dimensionality of the disaster system they are assessing. This requires that the methods must be flexible enough to allow a systemic assessment incorporating the internal and external linkages existing across domains (i.e. physical, social, economic) and dimensions (time and space). This aim is followed throughout the methodology presented herein.

It is also important to emphasise that the present methodology is essentially a test of a framework; the underlying question is, “does graph theory provide a robust basis for developing multi-hazard impact scenarios?” The paper demonstrates that it does.

2.1.3 Gaps in current methods and research opportunities

Paradoxically, given the urgent need for complex risk assessment, a relatively limited number of research papers quantify the systemic risk assessment of multiple hazards (Kappes et al., 2012). As pointed out by Hergarten (2004), hazard magnitude and impact (or damage) might not follow a straightforward relationship because of the complex nature of natural hazards and exposure to them. In fact, the impact of a hazard is a function of magnitude of the event within a specific area and time interval, and the consequent damage sustained by the exposed elements. Indeed, Arosio et al., (2018a) indicate that the approach to natural hazard risk assessment needs to be holistic as “the whole is more than the sum of its parts”. Also, in another recent article, AghaKouchak et al., (2018) remind scientists that research gaps on multi-hazards remain to be filled. This calls for an expansion of the current quantitative risk assessment paradigm, and for

measures to frame the study of interlinked disasters. Gill and Malamud (2016) point out that hazard and risk assessments often take “multi-layer single-hazard approaches”, in which the hazard potential or risk from one particular physical phenomenon is considered in isolation. Indeed, several of those approaches combine distinct cloistered hazards through “standardisation schemes” (Kappes et al., 2012) leading to the use of indices and semi-quantitative approaches to address the issue of working with different reference units. Another approach is to combine the hazards (with exposure and vulnerability) at the risk level using common metrics such as monetary loss or probabilities. These approaches implicitly assume that hazards are always independent occurrences; whereas, in reality, natural hazards interact and thus may amplify their potential impacts (Mignan et al., 2014). Hence, the use of the “multi-layer single hazard approach” is liable to underestimate risk and limit risk reduction and preparedness (Gill and Malamud, 2014). The problem we face is that the dynamic complexity of multi-hazard assessment can be daunting (Liu et al., 2015), which may explain the current lack of methods for quantitative multi-hazard assessment (Mignan et al., 2014).

In a rare attempt to go beyond the “multiple single hazards” quantitative assessment, Mignan et al., (2014) used a Monte-Carlo simulation of dynamic exposure and vulnerability to represent the dynamic evolution of risk and hence introduce the potential for extreme loss events. Mignan et al., (2014) showed that taking the interaction between several hazards into account leads to the emergence of extremes through clustering of losses (risk migration) and loss amplification at higher values (risk amplification). Those observations follow the work on extreme events categorized as “perfect storms” or “black swans” or “dragon kings” (Sornette, 2009; Paté-Cornell, 2012; Sachs et al., 2012; Helbing, 2013; Taleb & Blyth, 2011).

In the work of Mignan et al., (2014), the artificial nature of the exercise and the lack of geographical reference combined with the complexity inherent in multi-risk assessment made it difficult to communicate the outcomes to non-specialists (i.e. emergency services, communities). Indeed, it has been acknowledged that such a complex model is difficult for a non-specialist to comprehend

(Komendantova et al., 2014). In general, the understanding of the end-user(s) (i.e. authorities, community, business owners, emergency services etc.) is critical to the usability of the method. This may be achieved by shaping the output toward simplification and visually "appealing" methods to convey multi-hazard complexity.

To summarise, analysis of multi-hazards is a complex problem with a variety of challenges (as mentioned in Chapter 1). In principle, the complexity of the natural system needs to be tackled by implementing a method that considers the dynamic nature of hazards and their potential overlaps in time and space; but the difficulty of this endeavor leads also to a major problem of communication. Indeed, as the methods grow more complex, the visualization and transfer of information to external parties becomes more laborious. However, over-simplification of the hazard assessment potentially means that some of the risks are not realistically articulated.

2.1.4 Filling in the gaps through complexity

2.1.4.1 Reductionism

In the attempt to make sense and respond to the constraints of the natural world, natural disaster risk assessment methods (like in many other disciplines) employ reductionism (Fang, 2011). In the context of earth sciences, this is represented by the division of the risk "system" into organizational subsystems and technical specialties (e.g. seismologist, geomorphologist, hydrologist etc.). The behavior of these individual systems is easier to analyze, leading to successful mitigation of natural disasters through engineering, policy and planning. On the other hand, the study of isolated components leads to methodological limitations that can explain the gaps identified in paragraph 1.1 of this paper.

As mentioned earlier, current multi-hazard assessment treats the natural phenomena (hazards) mostly in isolation. This isolation of phenomena leads to the omission of relational behaviors,

causal processes, and their resulting emergent properties (e.g. risk amplification; Mignan et al., 2014). To address these gaps and map out the potential behavior of correlated phenomena, many disciplines are moving toward complex system approaches.

2.1.4.2 Complex systems

Many sciences and disciplines can be described as complex systems, for example, social systems, infrastructure (e.g. power grid and transport), medicine, literature, economic markets and ecosystems. Natural phenomena in the earth sciences, including natural disasters, can also be described as complex systems (Bak & Paczuksi, 1993; Pescaroli & Alexander, 2018). Systems that are "complex" have distinctive characteristics that emerge from the collective behavior of the system, such as nonlinearity, emergence and feedback loops, among others (Ladyman et al., 2012). Modeling such systems is challenging due to the, sometimes complicated, dependencies between their parts.

One solution is to represent such a system as a network where nodes represent the components and the links their interactions; such networks are described by Graph theory.

2.1.4.3 Graphs

A network is often mathematically called a graph (Bondy & Murty, 1976). As explain by (Boccara., 2010), “A graph G is an ordered pair of disjoint sets (V, E), where V is a set of elements called vertices, nodes, or points, and a subset E of ordered pairs of distinct elements of V, called directed edges, arcs, or links”. Thus, networks or graphs are objects composed of multiple components (nodes) and their interactions via links or ties (also known as edges) (Figure 2.1). A network with directional edges is often called a “directed graph” or “digraph”.

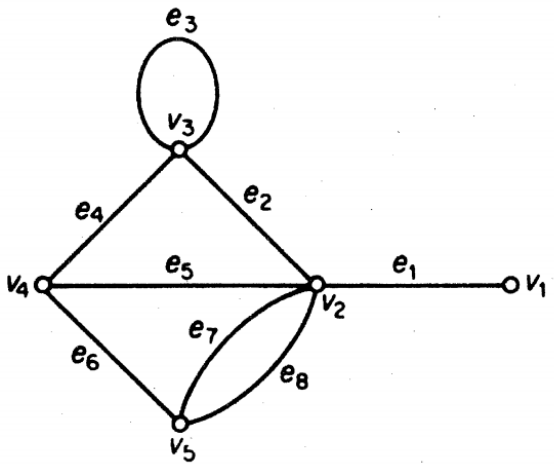

Figure 2.1 Network made of vertices (v) and edges (e) and their different configurations (Bondy et al., 1976)

The use of graphs allows one to deal with several issues of complex systems by understanding the causality between the network components (Butts, 2009; Phillips et al., 2015). Graphs have been used to study complex system such as food webs, genome and protein networks, Internet web pages, and human languages (Dorogovtsev & Mendes, 2003).

This paper advocates that a graphical approach can also be taken to assess complex systems of multi-hazard risk and provides a novel holistic framework going beyond the restricted “multi-layer single hazard approach”.

2.2 Methodology

One means of planning for preparedness for multi-hazard disasters is by using scenarios that can test capabilities to mitigate or become resilient to disasters. The standard approach in this space is to use empirical models to inform deterministic disaster scenarios. Even though such scenarios are often practical and useful, ‘the devil is often in the detail’, in particular when it comes to impacts. Thus, one or a few scenarios cannot test the full spectrum of capabilities at an appropriate impact level. For risk scientists to answer the question “what is going to happen?” can

be a daunting assignment indeed.

In this section we will outline a novel methodology that fills some of the identified gaps by the use of graphs and a complex system approach to model a distribution of multi-hazard impacts. First, we describe how a network of interconnected hazards has been constructed. Then, the multi-hazard risk framework is used to generate a multitude of disaster scenarios by cascading from node to node, flowing along the network edges according to a set of rules and conditions. The discrete events from the initial node to the most distal end point(s) of the network represent a single disaster scenario. Using an iterative process, thousands of varied scenarios are created. From these numerous iterative scenarios, a large database of possible impacts is produced and can be analysed.

The basis of the method is that through conceptualising the different elements of the risk system, and their empirical expression, it is possible to draw a stochastic network of the interconnections and the causal relationships between those elements. Based on this network, stimuli (initial activations) can be propagated along the network branches according to pre-determined sets of conditions. Repeated simulations (via Monte Carlo sampling) can test the various “branches” of the network to cover a broad spectrum of potential disaster scenarios, from mild to catastrophic. This kind of simulation of multi-hazard cascade is similar to previous work on virus spreading simulations or cascading power outages (Dezso & Barabási, 2002; Buzna et al., 2006; Perez & Dragicevic, 2009; Papic et al., 2011). A general overview of the methodology is given Figure 2.2:

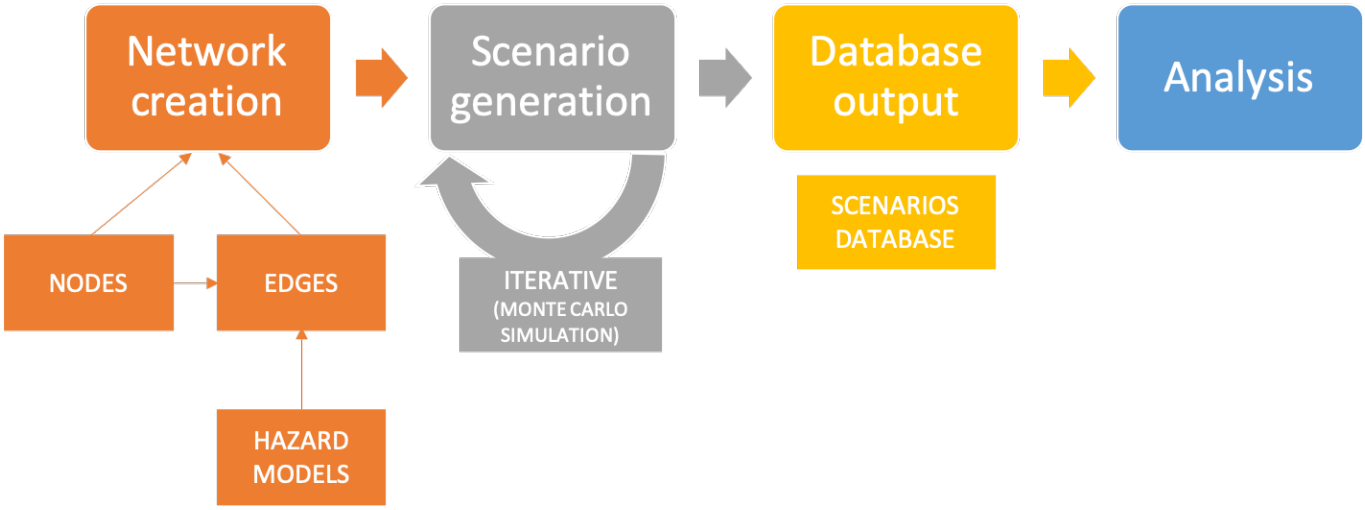

Figure 2.2 Overview of the framework. The Analysis box would comprised stochastic post-processing efforts such as risk analysis and/or impact analysis.

The present work investigates the possibility that, using a graph framework, multi-hazard assessments can be improved by simulating the full range of possible multi-hazard scenarios. The following sections will discuss how the general idea of using graph theory can be applied for scenario generation. The detailed setup of the network through the selection of nodes and edges is explained in the subsequent sections.

2.2.1 Construction of the network

The elements comprising the system must be established with the objective of the exercise firmly in mind. The model needs to reflect the known behavior of the system (Grimm et al., 2005) as well as end-user aspiration(s). The elements of a system interact in a hierarchical scale of complexity (an analogy in biology would be atoms, cells, organisms, ecosystems etc.) and finding the right level of analysis is essential. The Medawar Zone describes the “sweet” spot for incorporating complexity, between an over-simplistic response to a given problem and an over-complicated data overload (Grimm et al., 2005). The model must be guided by thoroughly

quantified output, computing limitations and a comprehensible way to convey the results.

Hence, some underlying processes will not be explicitly included in the model as they would add too much complexity (e.g. internal processes of gravity mass movement or fault network structure underlying earthquake behavior (Abe & Suzuki, 2006; Pastén et al., 2017)), and would not be useful for the final purpose of the method, which is to quantify the risk from multi-hazards in a way that remains comprehensible for the end-user (in this specific case, communities and emergency managers). Our chosen approach to determining the hierarchical scale of the analysis is to consider only the physical effects or measures that are “observed or felt” (e.g. shaking, gravity mass movement, water depth).

This method assumes that an area of interest (AOI) can be considered as a disaster macro-system composed of hazard nodes (or sources, e.g. earthquake, river) and exposed nodes (e.g. houses, roads). It is stressed that a “conceptualisation” is needed whereby the objects of the system are drawn as points (nodes) (e.g. Figure 2.3). Hence a node could represent a fault segment, a contributing source area of landslides, a storm, a river, a road segment, a house or any other “entity” depending on the specific purpose of the exercise and the hazard characteristic of the AOI.

The various nodes are considered as separate entities with their own spatial patterns and behaviors. They relate to each other by specific sets of rules based on empirical data, mathematical models and expert opinion.

Figure 2.3 Worldwide airport network 2013 (Xiaoqian et al., 2017). The nodes represent airport locations and their sizes, i.e. the number of connections they process. The edge lines represent flight connections.

In this paper, the nodes are considered "connected" if the geographical effect of one node overlaps that of another node. For example, if an earthquake "effect" (i.e. shaking) can possibly impact a house, the earthquake node and the house node are considered connected, hence an edge exists between the two. The effect must be considered relevant based on existing empirical relation or expert judgment. For example, the rainfall footprint might overlap road nodes (conceptualizing rain falling on the road) but the direct impact of rainfall on the road is considered negligible, so rain and road are not deemed to be directly connected, hence no edge exists. Taking this example further, if a flood / river node existed, a connection could be made between the rainfall node and the flood node and then from the flood node to the road node(s), conceptualizing that a rainfall can cause a flood that could then impact the road. Further, the connections are based on the "worst" or largest possible effect, so the risk network is maximally connected. Indeed, if no edges exist between the nodes, it means that no significant relationship can exist between the nodes. Figure 2.4 introduces the basic idea of how to build the network.

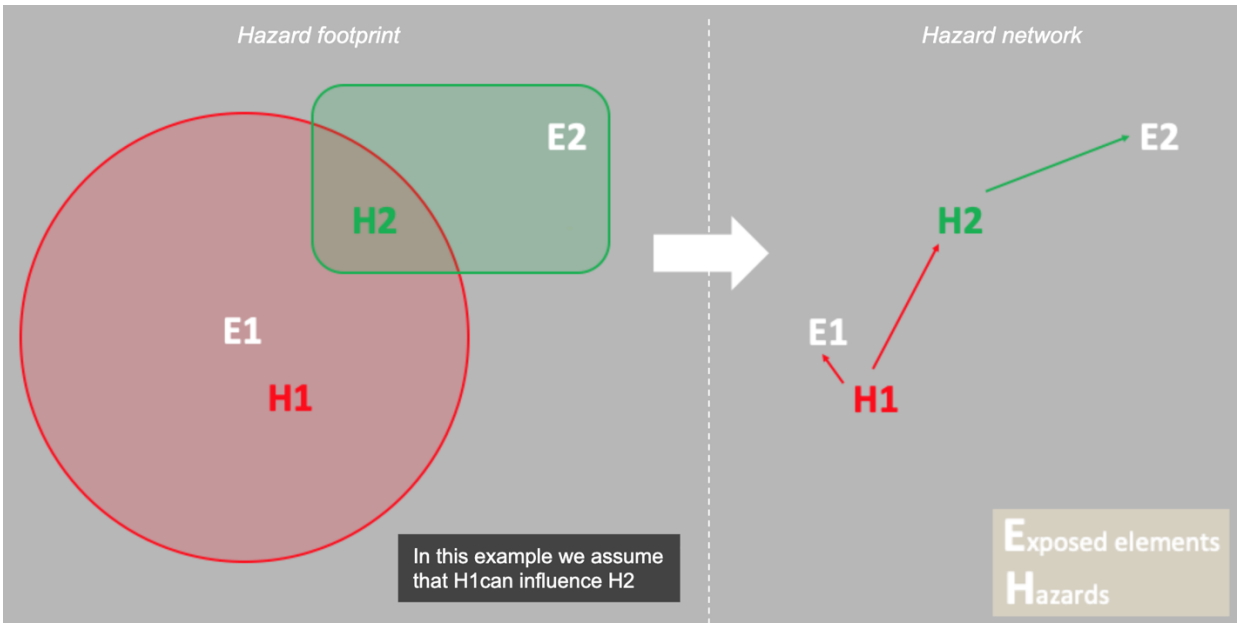

Figure 2.4 High level overview of the network creation process and how the standard approach, using footprints, can be translated into a network based approach.

As illustrated in Figure 2.4, a hazard has a specific effect which can be displayed as a geographical footprint (e.g. shake map). That footprint might overlap with other elements relevant to the disaster system (e.g. another hazard, houses etc.). Based on the nature of the hazard and the overlapped elements, a connection can be drawn, thus, creating a network incorporating hazard footprints. In Figure 2.4, Hazard H_1 can have an impact on Hazard H_2 and the exposed element E_1. Hence a connection (H_1, H_2) and (H_1, E_1) is made. In the same way, H_2 can be connected to E_2.

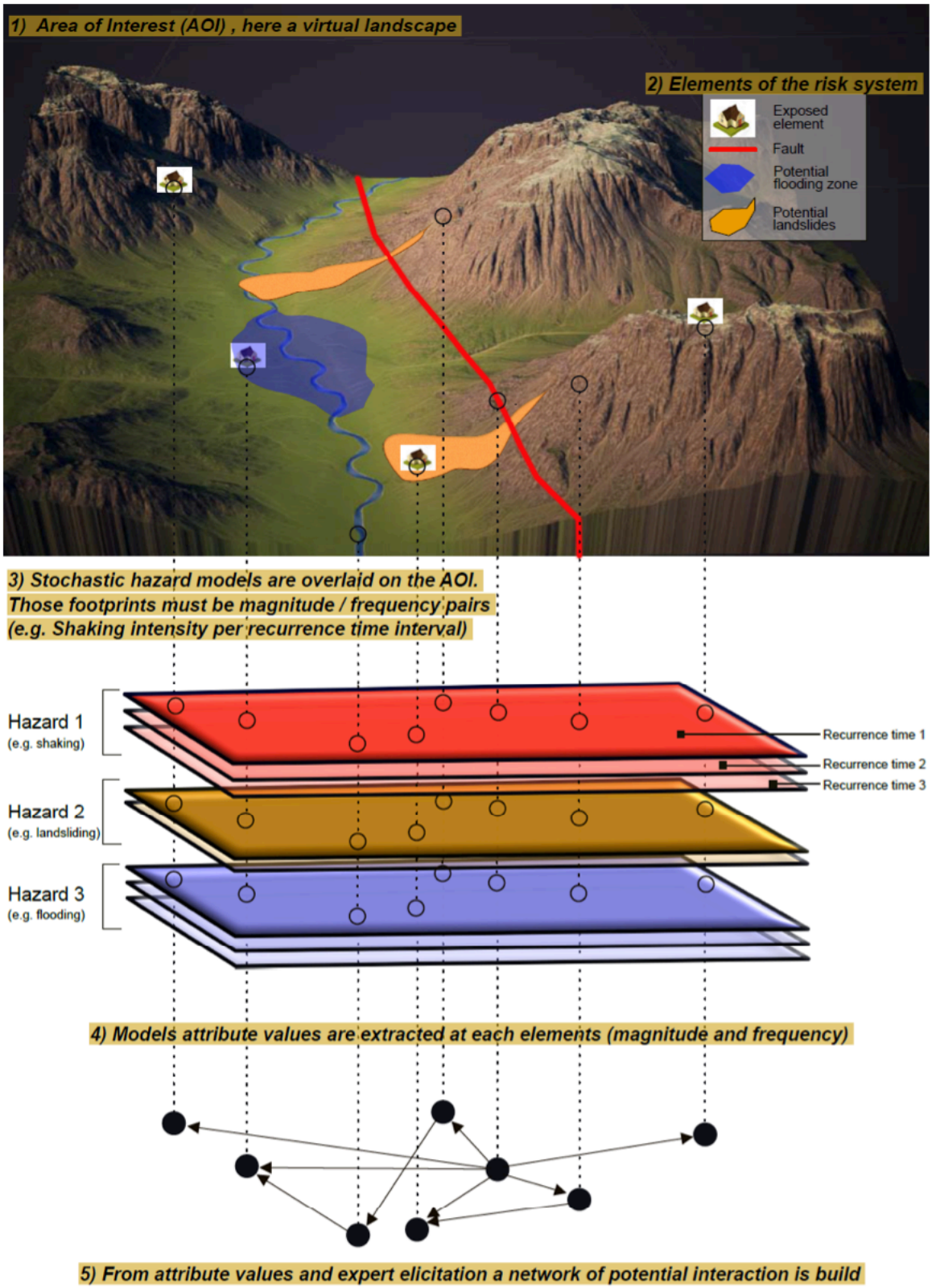

Figure 2.5 Diagram of the network creation process, explained from 1) to 5). The point locations on the landscape are for explanation only and different locations can be used depending on the question to be answered.

Figure 2.5 shows in more detail the process of network creation. The top picture shows a landscape with elements of the disaster system (in this case: fault line, river, landslide source areas, and houses). These elements are then conceptualised as points on a map with XY coordinates. For each hazard type, a set of magnitude intensity / frequency pairs is represented as GIS layers (Figure 2.5). Attributes are extracted at each point location (further explanation of the point location is given in paragraph 2.3.1). From the magnitude / frequency information, expert opinions and known empirical relationships (e.g. can an earthquake affect a building? can a flood influence an earthquake?), connections (edges) can then be established or dismissed between the points. This way, a network of potential interactions can be displayed as an edge list (i, j) where a source node (i) is associated with a target node (j). In this paper, the network is a directed graph as the edges have a specific direction where:

$$(i, j) \neq (j, i) \quad (1)$$

Because of the large number of potential interconnections, the creation or dismissal of an edge is automated based on a routine algorithm (written in the coding language Python). Many parameters can be used to discriminate what is considered a valid connection (e.g. types of nodes, presence of magnitude values above zero, maximum distance etc.). The process can be applied to any hazard or exposure settings.

2.2.2 Multiple multi-hazards disaster scenarios

Graph theory studies generally regard the network architecture to be the final aim (Keeling & Eames., 2005). Similar to epidemiological studies that concentrate on virus transmission through a social network, this paper argues that a “multi-hazard” network can be used to investigate cascading hazard propagation and, hence, assess risk.

The simulation, representing the cascading impact of initial events or stimuli, uses the model’s information contained on the network edges (from the network building exercise, Figure 2.5) to

select the pathway to the next node.

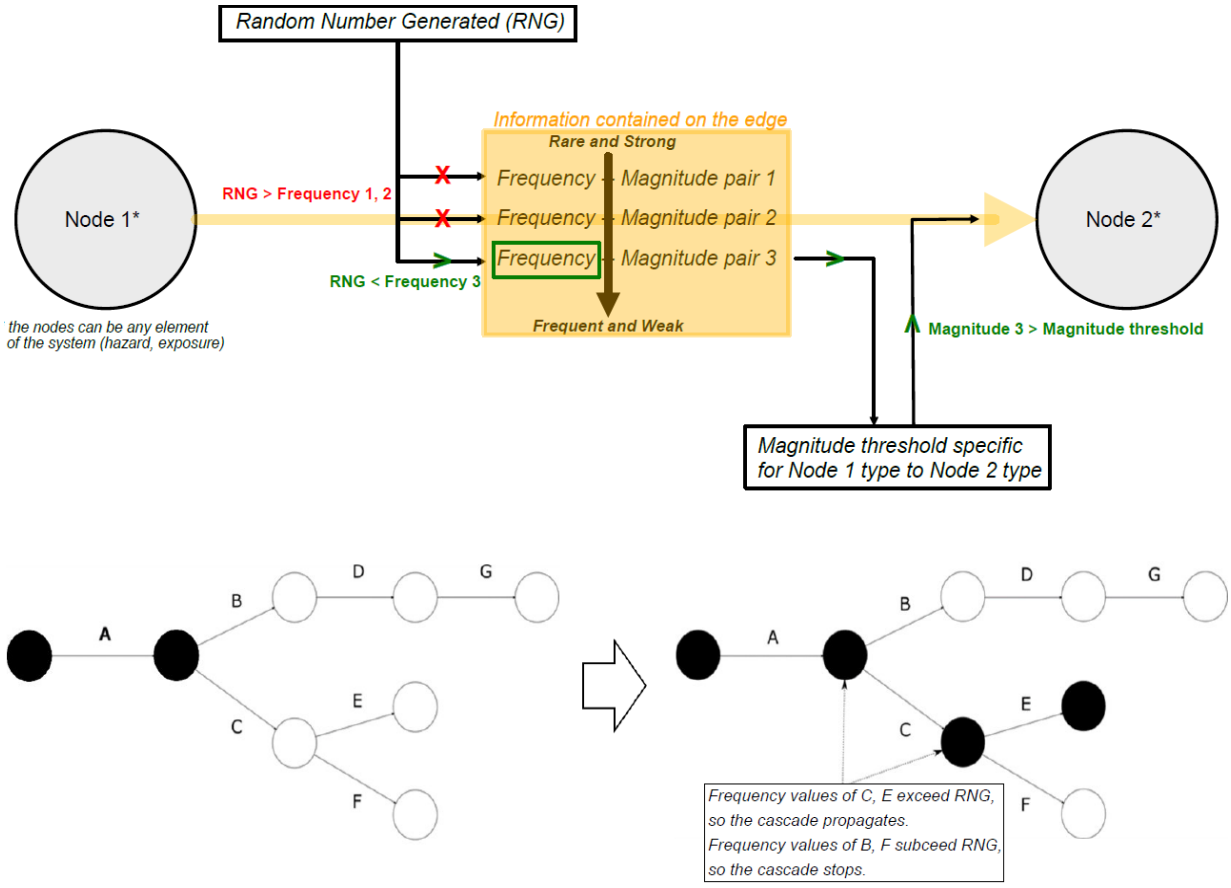

Figure 2.6 Schematic of the network propagation protocol. Upper: zoom-in on the node to node process. Lower: a zoomed-out version of the propagation protocol. The letters are used to illustrate the cascading effect.

The cascading effect from one node to another is based on frequency and magnitude thresholds. Figure 2.6 shows the process of node activation and cascade propagation. In the first step, a random number is generated and compared, one by one, with frequency values which are ordered from the smallest (rarest) to the highest (most frequent). When the frequency value exceeds the random number generated (RNG), the second phase begins. In the second phase, the magnitude value corresponding to the frequency exceeded is compared with a magnitude threshold specific for the node types (e.g. the minimum shaking value to trigger a landslide). If this magnitude value is also exceeded, then node 2 (Figure 2.6) is reached and the propagation continues. The condition for the magnitude threshold can be set based on the nature of the source node, the

nature of the target node, and empirical relationships or expert knowledge of the behavior between the node types.

The simulation of discrete cascades from an initial triggered node to the network end points would represent only one scenario. As many different scenarios can happen within the multi-hazard network structure, an iterative process is required to test a variety of scenarios. Using a Monte Carlo method, multiple trials can simulate a range of cascading scenarios. During Monte Carlo simulation, random numbers controlling the propagation along edges need to be generated in such a way that the widest possible scale of scenario impacts are achieved. As propagation along edges is conditionally independent given upstream nodes and occurs with probabilities less than or equal to one, if we select random numbers from a uniform distribution, almost all cascade chains will be short, hence the resulting scenario will not be 'disastrous'. Instead, we transform the uniform random variate U by raising it to the power α:

$$RNG = U^{\alpha} \tag{2}$$

Where $0 < \alpha < \infty$. The resulting RNG is still between 0 and 1 but is now biased towards 0 if $\alpha > 1$, towards 1 if $\alpha < 1$. Here we will use $\alpha > 1$ to 'encourage' longer cascades and hence make disastrous scenarios less infrequent (larger values of α biasing the RNG to smaller values). Multiple values of α can be attributed at different levels of the network to vary the severity thresholds and bring heterogeneity to the modelling. For instance, the level of landsliding associated with a given level of ground shaking can be varied.

When the distribution of impacted nodes reaches a steady state (achieves convergence), the number of simulations is deemed to have encompassed the range of potential scenarios and the simulation is ended. The final model output is a list of all the scenarios created. This list contains the nodes activated, edge pathway taken as well as the magnitude and frequency of each discrete event. These data can be analyzed further depending on the initial purpose of the modelling. It is

important to specify that the simulation outputs would then need to be weighted to correct for the use of a biased distribution (α). In the current state, the process cannot be used for probabilistic analysis.

2.3 2016 Kaikōura earthquake case study

In 2016, a Mw 7.8 earthquake occurred in the Canterbury region, in the north east of the South Island of New Zealand. The complex fault rupture (Cesca et al., 2017) and its effects severely impacted the South Island transportation network and isolated Kaikōura Township (Davies et al., 2017). The Kaikōura region was affected by fault rupture, periods of intense rainfall and landsliding, thus is considered a multi-hazard event.

As a tentative first step to apply graph theory to simulate multi-hazard disaster scenarios, we set out to assess the achievability and reliability of the methodology outlined above against the Kaikōura event. Stochastic model validation is challenging, especially in the multi-hazard context (Sperotto et al., 2017). We have only one datum (Kaikōura 2016 event) but a range of impacts were observed at various locations (especially on the roads). Hence a statistical test is possible whereby the actual multivariate impacts (road impacts) can be used as the test statistics against the empirical distribution derived from the model simulations.

A specific goal was to produce a large array of disaster scenarios and compare the modelled impact on the road network against the actual impact recorded. As the method should be applicable in other settings, no post-event modelling was used as it would bias the results toward the Kaikōura outcome (e.g. no shake map from the actual event was used). Therefore, the outcome would help understand the relevance and limitations of the methodology and indicate if further development is justified.

The area south west of Kaikōura (Figure 2.8) was been selected as a pilot study, to build the network model and test the method proposed herein. For an initial evaluation of the method, a

simple cascade scheme representing the Kaikōura cascading event was used (Figure 2.7).

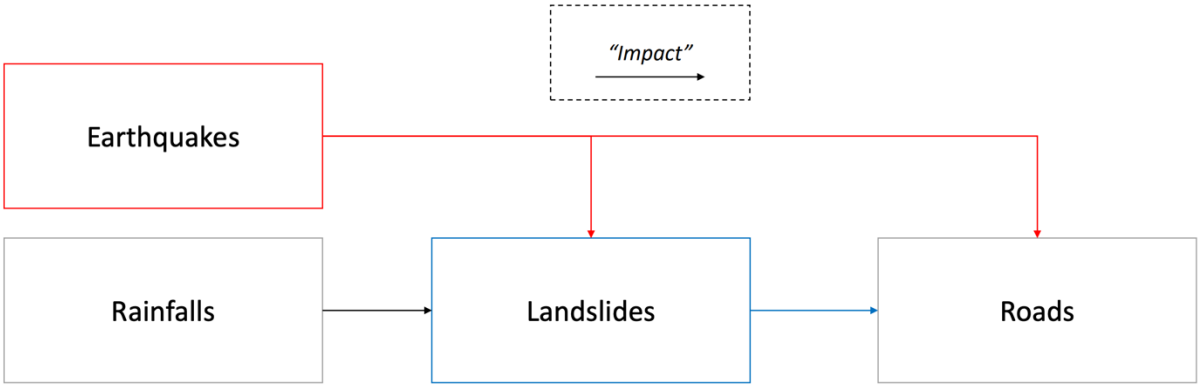

Figure 2.7 Diagram of interactions during the Kaikōura events and used in the modelling. The Kaikōura "sequence" saw a combined effect of earthquake, rainfall and the consequent landslides (debris avalanche and rock slides (Dellow et al., 2017). The arrows indicate the impact from one element to the next element of the system.

Figure 2.8 Location of the case study area in the South Island of New Zealand. The AOI is focused on the area south-west of Kaikōura Township. Modified from Davies et al. (2017).

2.3.1 Nodes or components of the system

Based on the Kaikōura events, the nodes used in the system represent the earthquake source, rainfall source, landslide sources and road segments. It should be remarked that the nodes can be displayed either with a relevant geographic location (in this case, landslide nodes are the centroid points of order 1 catchments (Strahler, 1957) and the road nodes are points on the road system separated by 500m), or conceptually represented at a random geographical location (earthquake and rainfall nodes are regional nodes, hence do not have a precise location). For convenience, they are nominally positioned at a random location in Figure 2.9.

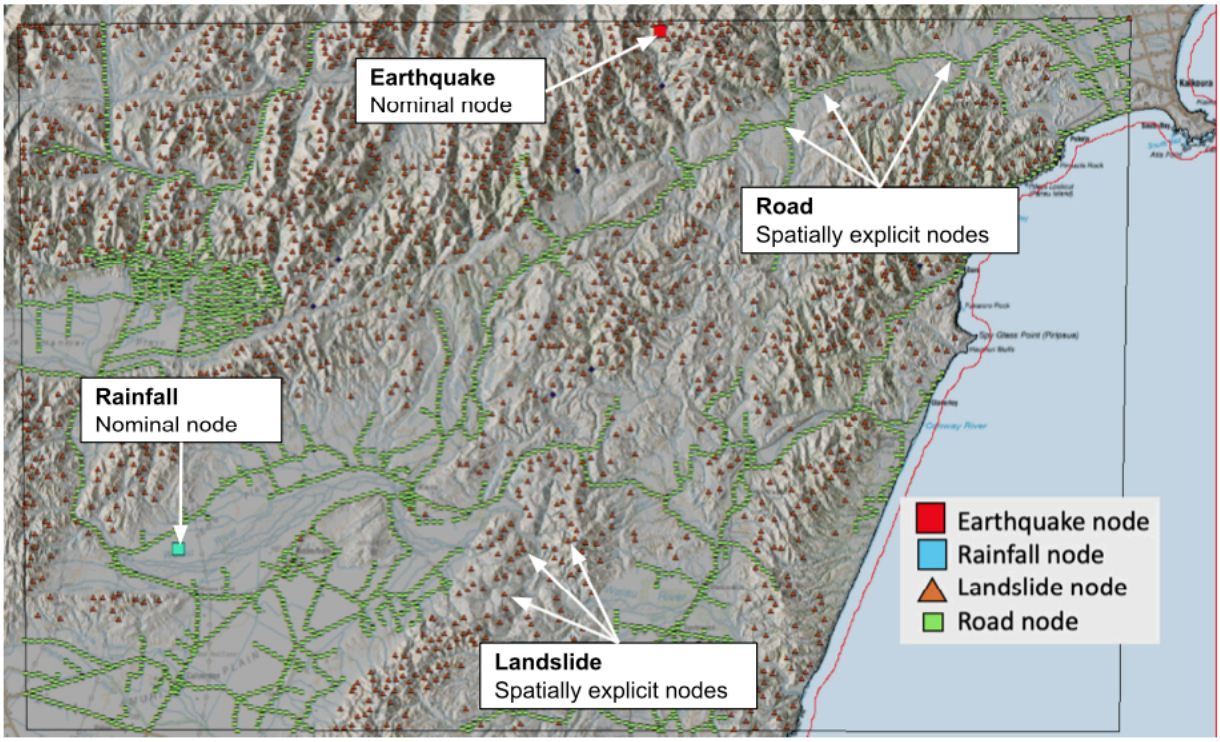

Figure 2.9 Examples of the nodes used for the method in the Kaikōura case study

(Earthquake)The red square node represents the nominal (random) "earthquake source". The location of the node is not depicting a specific epicentre and is used to conceptualize the regional effect of "earthquakes".

(Landslide)The red triangular nodes represent the potential "landslides". The location of the nodes represents the centroid points of order 1 catchments in the study area. In this case, and contrary to the earthquake node, the aim of the landslide node locations is to delineate a coherent geographical area to be affected by either earthquake (co-seismic) landslides or rainfall (rainfall-induced) landslides. Using a random "conceptual" location (as for the earthquake node) would cause an erroneous triggering effect as the landslide nodes are linked to the earthquake and rainfall effects by the local PGV and the rainfall intensity values respectively.

(Rainfall)The blue square node represents the "rainfall" source. As for the earthquake node, the rainfall node is set as a concept for "rainfall" at a random location (the current location is actually in the vicinity of the station from where the probability has been calculated – but didn't have to be for the purpose of the exercise).

(Road)The green squares represent the roads. The road node locations are set by creating a node every 500m along the road line.

2.3.2 Edges (links) between the nodes, based on hazard footprints

Earthquake - As different earthquake intensities create potentially different cascading effects, four different PSHA (Probabilistic Seismic Hazard Analysis) maps have been used with recurrence times of respectively 1 year, 10 years, 100 years and 1000 years. The footprints were built using the National QuakeCoRE model (Tarbali & Bradley, 2014). National-scale PSHA models have been built based on the ground motion prediction equation (GMPE) developed by Bradley (2013). In this case the median percentile of the GMPE model was used to predict the peak ground velocity associated with each recurrence interval. Note that the model has not been revised since the occurrence of the Kaikōura event and is, therefore, unbiased by that occurrence.

The use of PSHA maps for simulating scenarios carries limitations. The limitations of using PSHA are related to the size of the studied area, the tectonic setting and the number of faults contributing to the model. In the case of the area studied herein, the seismic activity above the 5-year recurrence interval is dominated by the Hope fault. Hence, the results remain correct for the damaging scenarios presented herein. In the future, the study of larger areas would be problematic as contribution from multiple faults would cause an overestimation of the shaking intensities. The option to use OpenQuake (Pagani et al., 2014) is already being implemented in recent projects to generate stochastic earthquake event simulations.

In addition to shaking intensity, another potential impact of earthquakes is surface rupture. It is difficult to predict fault rupture from ground motion as there are several local parameters that might influence the displacement. Fault ruptures damaged roads during the Kaikōura 2016 event

(Benson et al., 2016). Hence, in an attempt to represent the surface rupture events in the modeling based on the sole availability of PGV maps, we used information from the Darfield 2010 earthquake, New Zealand, as an analogue. The surface ruptures observed during the 2010 Darfield earthquake exhibited a minimum threshold PGV value close to 40 cm/s (Cubrinovski et al., 2010; Nicol et al., 2010; Van Dissen et al., 2011; Buxton et al., 2014). Based on 2010 Darfield experience, the value of 40 cm/s was used to assess the direct impact of the earthquake on road segments.

Landslides - Landslides are often described as a cascading effect from an initial tremor (coseismic) and/or intense rainfall, as this was certainly the case during the Kaikōura sequence (Davies et al., 2017). It is to be noted that for the methodology developed in this paper, a stochastic model of landsliding had to be created. A physical model of landslides corresponding to a particular shaking intensity would not contain the frequency content required. Indeed, a specific shaking intensity from an earthquake could cascade into a range of potential landsliding scenarios (from no landslides to extreme landslide counts and volumes). For the model developed herein, a map representing the "stacked" susceptibility of landslide deposits from every potential landslide source area was required (cumulative runout susceptibility, Figure 2.9). Few software codes have this capability at a regional scale. The Flow-R software (Horton et al., 2013) was used to provide landslide runout susceptibility maps for the two potential triggers (earthquake and rainfall). The inputs for the Flow-R model are a DEM and a source area in a binary format (a pixel value of "0" is not triggered, a value of "1" is triggered). To test the methodology and capture the worst-case scenarios, a simple approach was taken, assuming that every slope above 10° could potentially be triggered (so given a value of 1), and that a minimum PGV value of 0.7 cm/s would trigger a coseismic landslide (Tanyas et al., 2017). The parameters needed to model the runout in Flow-R are the scar depth of the landslide source area and the angle of reach (among other options). A distinction is made between earthquake-triggered landslides and rainfall-triggered landslides. In reality, the trigger event affects the volume of material collapsing in part because of

the varying depth of failure (scar depth; Larsen et al., 2010). Based on the inventory collected by Larsen et al., (2010), and the potential for a worst-case scenario, the scar depth values related to rainfall and earthquake were selected using the 50^{th} percentile scar depth value for, respectively, 10^4 m^2 soil landslide area and 10^5 m^2 bedrock landslide area. Thus, the scar depths assumed for rainfall and earthquake triggers were 2 m and 50 m respectively. Consequently, two distinct runout models were created. Following Legros (2002), the maximum angle of reach used was 10° with the aim of accounting for extreme runout events. It is to be noted that angle of reach is strictly independent of the gradient of the source and that the values used for the angle of reach and slope gradient are conservative. The end product of the modelling is a distribution of the cumulative susceptibility of run-out values based on the number of times a pixel has been "covered" by a modelled landslide runout. As expected, the modelled susceptibility values decrease further away from the source area. The threshold value to sustain an impact is given by the specific susceptibility value at the node location (road node in this case). Hence, impact from low susceptibility / long runout landslides would be rare and from high susceptibility / short runout landslide frequent.

Rainfall was also considered as a potential trigger for landslides. Intense rainfall has often been recorded as a primary mechanism for generating landslides (Keefer et al., 1987; Benn, 2005; Kritikos, 2013). For the purpose of the method discussed herein, a simplified approach to rainfall-induced landslide assessment was taken. The intrinsic variable considered for rainfall-induced landslides is the slope gradient only (as explained in the previous section) and the extrinsic variable considered is the rainfall intensity over a 24h period (Dahal et al., 2008). From previous New Zealand case studies (e.g. Glade, 1998), the threshold rainfall intensity for triggering landslides seems to be 20 mm/24 h. For our area of interest, rainfall stations are used to assess the distribution of rainfall intensity (NIWA CliFlo database). Based on the station database, rainfall of intensity 20 mm/24 h occurred on an average of 2% of the days per year over the last 20 years in the AOI (Thompson, 2002). Hence, a spatially uniform footprint of value 2% was used as a

rainfall intensity threshold for potential landslide triggering.

A matrix of interdependencies between the various hazards is summarized in Figure 2.10.

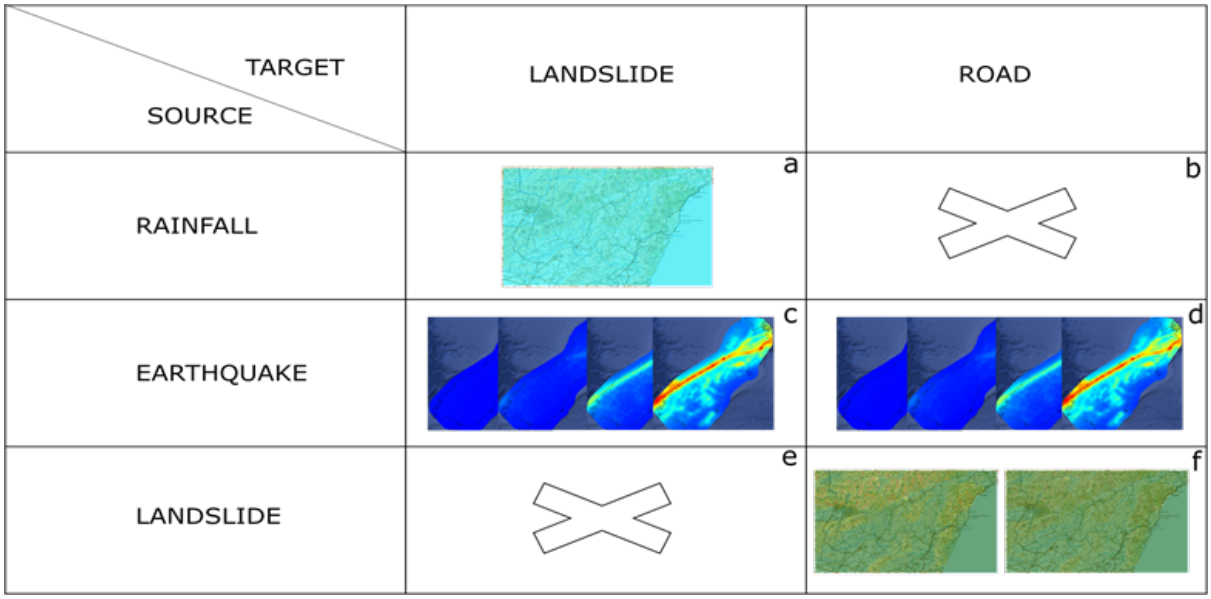

Figure 2.10 The correlation matrix illustrates the assumed connectivity between the various elements of the disaster system in the Kaikōura example.

(a) Rainfall and landslide are connected by the probability of a threshold intensity of 20 mm/24 h.

(b)(e) The cross represents non-connectivity. In particular, landslides are not considered to trigger other landslides and rainfalls are not considered to have a direct impact on the road.

(c)(d) Earthquakes are considered to trigger a landslide node if the PGV threshold value is reached. In the same way, earthquakes can impact the road if a different threshold value of PGV is reached.

(f) Landslide and road nodes are connected by the two runout susceptibility models. The runout models selected depend on the initial triggering event (earthquake or rainfall in this case).

It is recognised that many more hazard types might be relevant for the area. The purpose of the exercise is to develop and test the methodology, in which context, constraining the model to a relatively simple approach was considered the best way forward. More work is currently ongoing in this space with added complexity.

2.3.3 Network building & scenarios generation

The previous sections have identified the key parameters to build the network through the creation of nodes and edges. The methodology presented in paragraph 2.2 is applied to the AOI. The hazard footprints are used to connect the nodes and create edges as per Figure 2.5, and based on the conditions summarized Figure 2.10. An algorithm (scripted in Python) is used to go from a node list (points on the maps with hazard attributes) to an edge list with source node, target node, source coordinates, target coordinates, and numerous frequency and magnitude pairs (e.g. annual recurrence time and related PGV value at the target node). The script uses node types and conditional statements to establish which connections are legitimate or not. GIS software is used to display the connections by providing an edge list with the source node and target node IDs and coordinates. As the number of nodes and edges can impair the geographical display, network software (Gephi in this case) can be used to display the network based on non-spatial parameters (Figure 2.11).

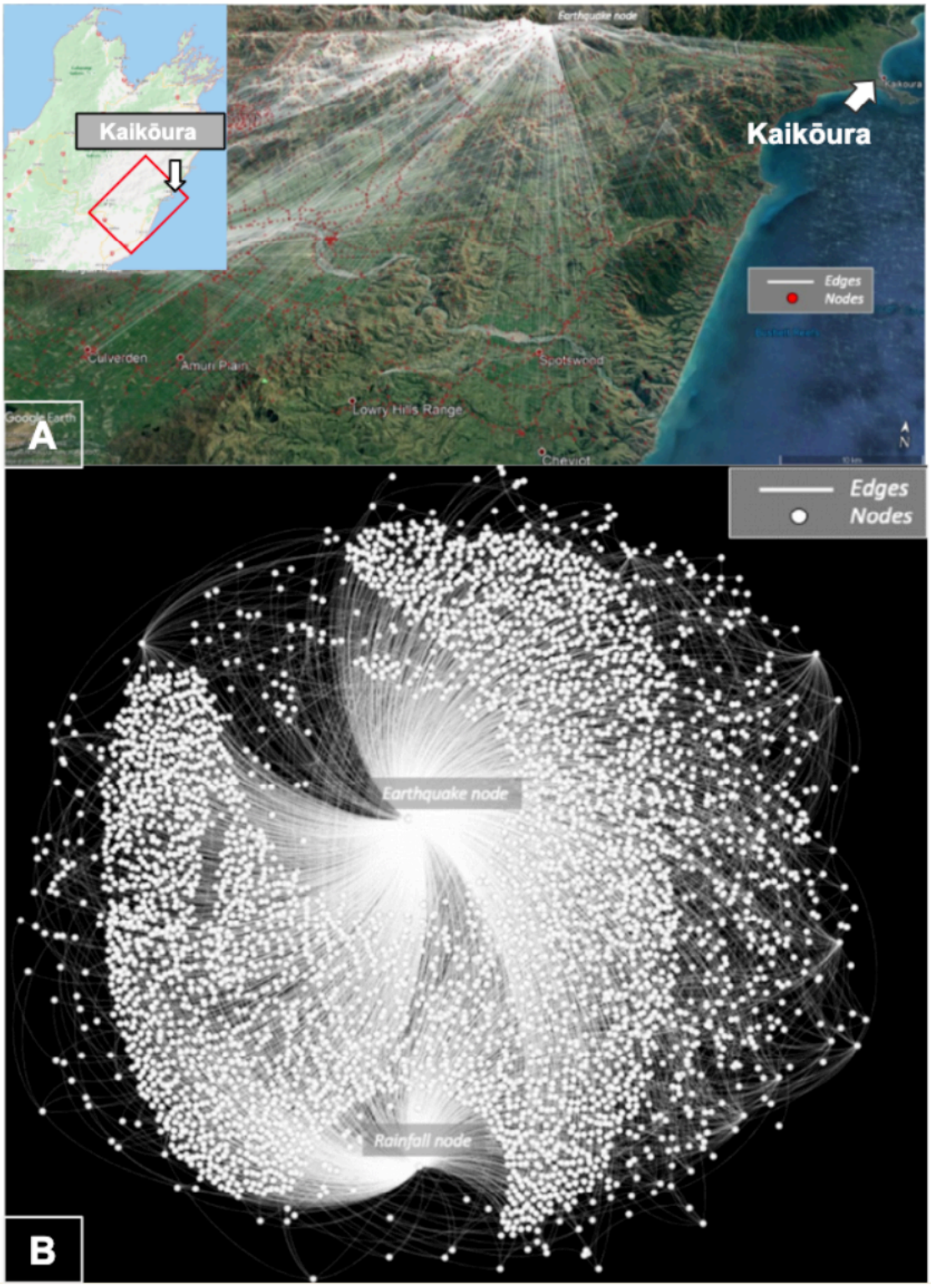

Figure 2.11 Representation of the network in ArcGIS (A), and by the degree of centrality (number of links incident upon a node) to sort the various nodes (B) (using Gephi).

2.3.4 Multi-hazard scenario creation

As discussed in the methodology section, whether cascades happen or not is based on a randomisation exercise whereby the “likeliness” of an edge is compared with a random number generated (RNG) (1).

In the algorithm presented herein, two tuning parameters are used, $\alpha 1$ and $\alpha 2$. The first, $\alpha 1$, tunes the severity of the top-level stimuli events (earthquake and rainfall), while $\alpha 2$ tunes the secondary cascading effects (landslides). Using two tuning parameters permits a more heterogenous set of severities to be investigated. The secondary tuning parameter $\alpha 2$ is varied from 1 (mild) to 20 (severe) for each specific value of the top-level tuning parameter $\alpha 1$ (e.g. for $\alpha 1 = 1$, $\alpha 2$ varies from 1 to 20, then for $\alpha 1 = 2$, $\alpha 2$ varies from 1 to 20 and so on). The value range of α is based on the lower annual probability of occurrence on the edge list. Indeed, the scenario simulations must be able to trigger even the most unlikely events (i.e. increasing α progressively triggering lower-probability events). The parameter U is randomised in the interval [0,1] for each α pair and for each hazard node. In the model presented herein, each α pair is iterated over 150 times (Figure 2.12, in the following section, gives more information on the selection of the value 150). The 150 iterations permit variation of the scenarios within a severity bracket (i.e. $\alpha 1$ and $\alpha 2$ set). It is emphasised that a new RNG is created for each activated node and every single neighboring edge, so several thousand distinct scenarios can be created (e.g. one scenario could cause strong shaking on a rainy day with some landslide sources providing a few landslides with long-runout, and other landslide sources generating numerous landslides but limited runout). The detailed workflow is shown Figure 2.12.

A dual activation of a landslide node by both rainfall and earthquake can happen. In this case, as earthquake triggered landslides have greater expected volume and runout, only the earthquake triggering is considered. Compounding triggers are not considered in this paper but are mentioned as an area of development in the Discussion section.

To summarise, initial hazard events (earthquake and/or rainfall) are randomly triggered based on frequencies. These initial events might trigger landslide nodes. Every “activated” landslide node undergoes, independently, a randomisation process whereby, as landslides don’t have a frequency component *per se*, a random number is compared with the susceptibility of runout to a target node (as already explained, susceptibility values used are specific to the nature of the trigger events: earthquake or rainfall). Thus, long runout - high volume landslides will occur more rarely than short runout - low volume landslides. The impact of landslides on exposed elements (road segments) is then recorded. When this is done, the scenario is concluded, as the roads are terminal nodes in the network. A new scenario can then start.

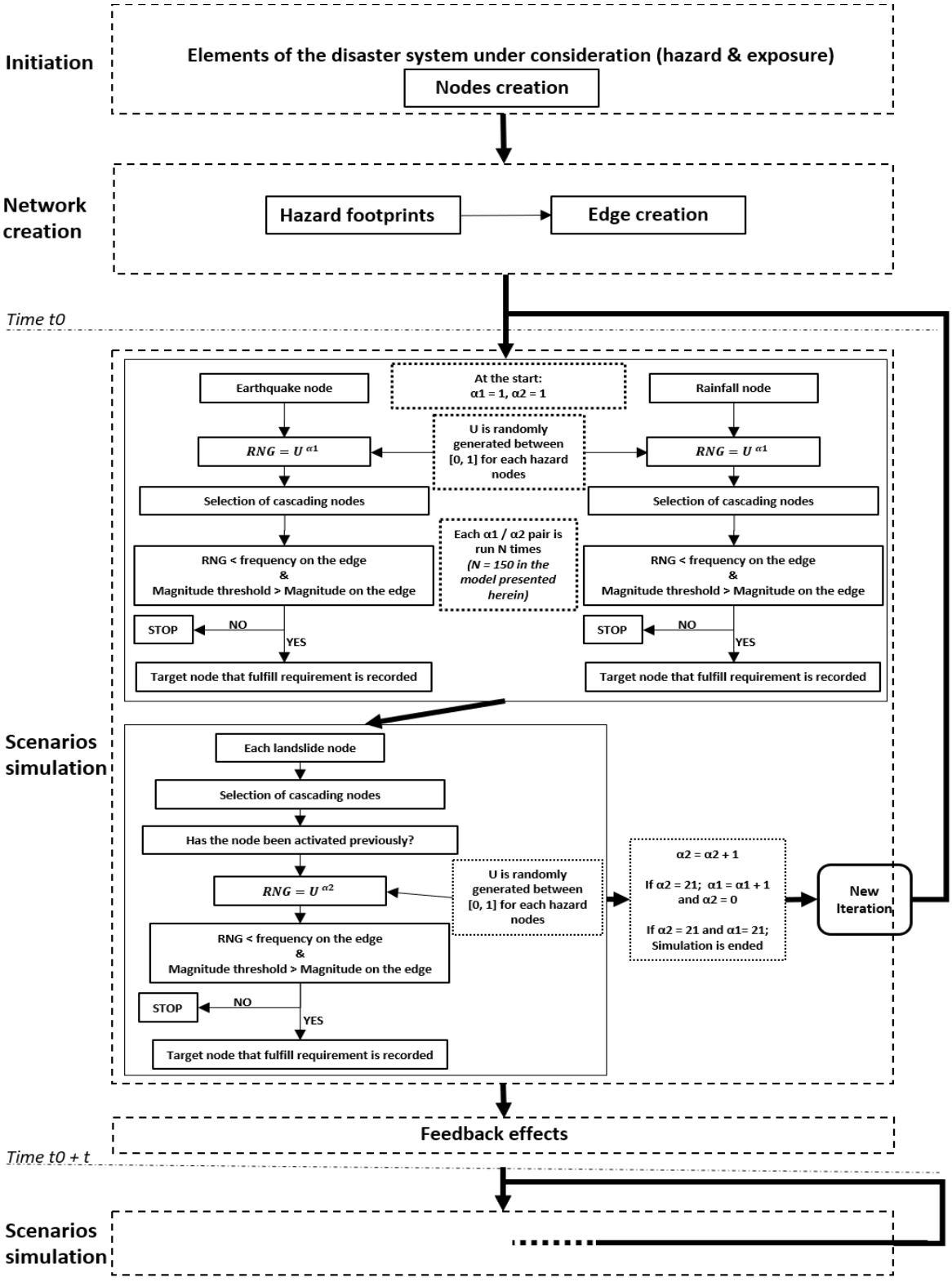

Figure 2.12 Flow chart of the main processes of the multi-hazard graphical quantitative assessment. RNG stands for "Random Number Generated" and is calculated as per the equation (1). α1 and α2 are used at different stages of the algorithm as tuning parameters for RNG. Results of frequency and magnitude are logged after each scenario simulation.

2.4 Results from the Kaikōura 2016 test case study

A recurring problem with predictive models, particularly simulation models, is the necessity to validate the predictions of the model (Beck et al., 1997). Even though this paper is trying to test the methodology proposed against an actual event (2016 Kaikōura earthquake consequences), it should be further emphasised that the workflow generates a wide range of scenarios, while the actual events comprise one possible realisation among a vast range of potential scenarios that could have happened.

The methodology described above has been applied to our area of interest (AOI). The roads have been divided into segments to constrain the impact analyses to a more local scale instead of using the full length of the road. The road segments are separated by the town locations (white circles, Figure 2.13). The heat map (blue to red color band, Figure 2.13) represents the number of times a road node has been impacted after simulating a total of sixty thousand scenarios. The heat map was generated by gridding the impact count on the road nodes.

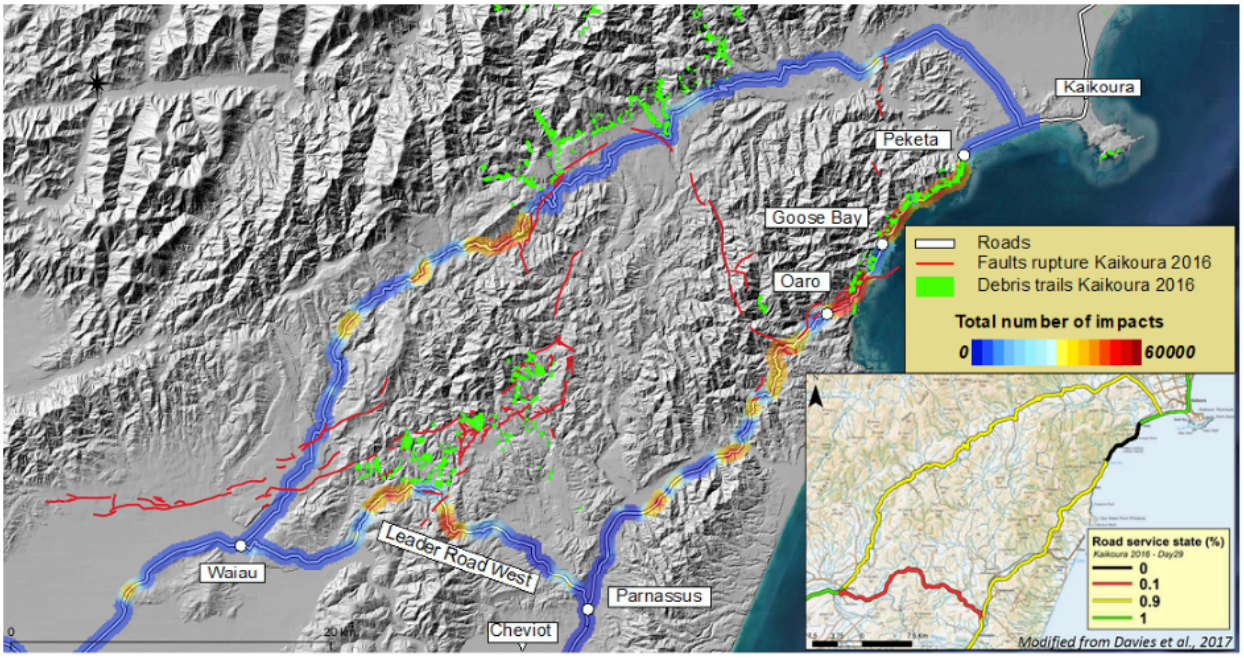

Figure 2.13 Output impact count map on the road nodes over the actual damaged area of the AOI. The road service values refer to the state of service; 0 means that the main road is closed, 0.1 means that local roads are closed, 0.9 means controlled access of highway, 1 means open.

Hence, it is possible to discriminate which areas are prone to being affected by a disaster scenario considering the complex interactions between the hazards.

The plot presented in Figure 2.14 shows the evolution of the average number of nodes impacted for each of 200 scenarios where U is a random variable, and α1 and α2 both equal 20. In the network presented in Figure 2.1, the attainable part of the network is the entirety of the network as it represents the more "severe" scenarios possible (when both *α1* and *α2* equal 20). Figure 2.14 illustrates the stabilisation of the number of nodes impacted after 130 iterations for the maximum values of *α1 and α2*, and suggests that the simulation has reached a stable level. Hence, the value used of 150 randomisations seems adequate to cover the range of frequencies contained in the network.

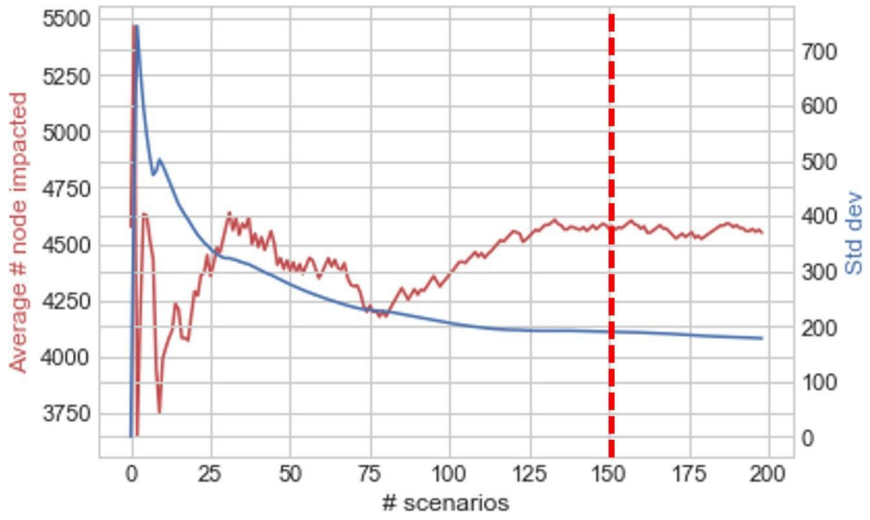

Figure 2.14 Plot showing the evolution of the average number of impacted nodes during the scenario simulations and the associated standard deviation. The "cut-off" of 150 randomisations is highlighted by the red dotted line.

The distribution of impacts per road segment compared with the actual impact on the road resulting from the Kaikōura earthquake is presented in Figure 2.15. To clarify, the results are based on the entire seismic hazard (all PSHA maps) and rainfall, both simulated with gradual sampling (increasing *α1* and *α2*). The distribution represents the spectrum/range of impacts on

each road segment from the severity “escalation” modeling. The actual number of impacts on the roads is calculated by assessing the number of hazards (surface rupture and/or landslide run out) that occurred within 250 m of a road node. The results from Figure 2.15 show that, for most of the road segments, the impact sustained by the road system after the 2016 Kaikōura earthquake and the associated landsliding, fall within the range modelled by the complex multi-hazard model. Hence it gives confidence that, despite the simplistic approach taken, the method is providing realistic results and justifies further development.

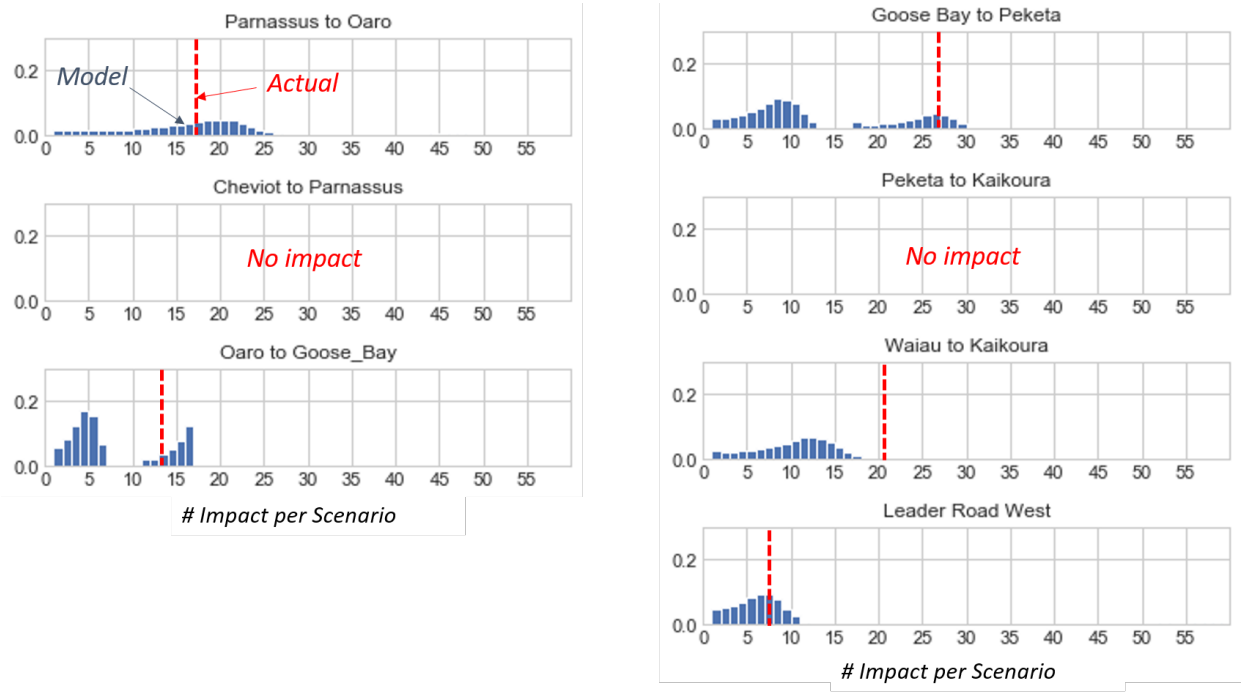

Figure 2.15 The predicted distribution of the numbers of impacts for different road segments in the AOI (blue histogram). Dashed red vertical line indicates the actual number of impacts on the road segment during the Kaikōura 2016 earthquake.

Another significant finding is the volatile nature of potential impacts, highlighted by the variability from one road segment to another. The volatility is attributed to the particular geomorphology of the areas. Depending on the road proximity to hazard sources (steep slopes and active faults), the impacts can be constrained or highly dependent on fine level details within the model. These correspond to equally fine level (unknown) variability within the physical system. Some impact

profiles highlight different populations of impacts likely based on the effect of secondary hazards (e.g. Oaro to Goose Bay, Goose Bay to Peketa). In other areas, where the geomorphological features (sources of hazards) are localised, the range of scenario outcomes is limited to a spatially constrained hotspot. Hence, those road segments are sheltered from compounding scenarios and extreme impact events (e.g. localized topographic highs on the Waiau to Kaikōura road segment). Most of the actual impact on the Waiau to Kaikōura segment came from surface rupture from the earthquake, hence the mismatch observed with the model could be attributed to the low resolution of the earthquake model used initially (national scale model, not event specific) and the assumptions on the fault rupture parameters. Hence, it points to the (known) fact that shaking intensity and surface rupture hardly correlate and that alternative options should be found to integrate the risk of surface rupture to the model.

The variation in tuning parameters α1 and *α2* is further studied in Figure 2.16 by plotting the tuning parameters against the error in impact prediction. The impact prediction is calculated as the average number of nodes impacted per α pair minus the actual number of impacts sustained after the Kaikōura events in 2016, for a total of 400 points (combination of 20 α1 values and 20 *α*2 values).

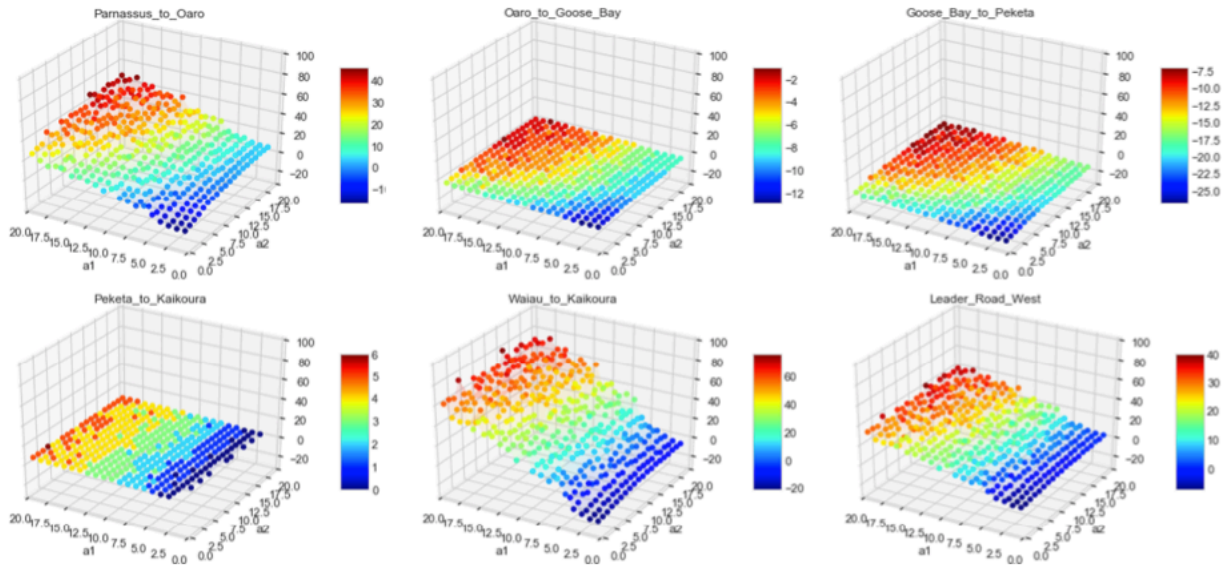

Figure 2.16 Impact of tuning parameters on the prediction of impact per road segment. The different axes of the 3D plot represent tuning parameters α1, α2 and the difference between the number of actual impacts & modelled impacts (from small/negative differences in blue – less or equal modelled impact than actual impact - to high differences in red – more modelled impact than actual impact).

Figure 2.16 illustrates that, for certain road segments, the 2016 Kaikōura events were close to the worst-case scenario modelled herein (e.g. Oaro to Goose Bay, Goose Bay to Peketa), while other road segments seemed to sustain relatively mild impacts among the potential outcomes modelled herein (e.g. Waiau to Kaikōura, Parnassus to Oaro, Leader Road West). Figure 2.16 exemplifies that the variation of potential impacts across the various scenarios can be either small (Peketa to Kaikōura) or large (Waiau to Kaikōura), represented, respectively, by a flat surface or a steep surface. Also, the distribution of impacts highlights the strong contribution of the "$\alpha 2$" cascading events (landsliding) for some road segments (e.g. Oaro to Goose Bay, Goose Bay to Peketa), while other road segments (e.g. Peketa to Kaikōura) are mainly impacted by the initial stimuli (impact from earthquakes in this case) with less contribution from the cascading events.

2.5 Discussion

The methodology is currently at an early stage of development and some key points are discussed below.

2.5.1 Added value of a complex and graphical framework

This methodology is potentially answering several of the gaps highlighted in Chapter 1 of this thesis. Contrary to the siloed approach of the *multi-layer single hazard* (Gill & Malamud, 2016), the dynamic nature of hazards and their consequences can be captured by a graphical approach in a genuine *multi-hazard* approach. The iterative graphical simulation leads to a bottom-up assessment where the interconnectivity between hazards is the basis for the risk assessment. The theoretical work of Mignan et al., (2014) highlighted that taking into account the interdependency between hazards will alter the result of a loss assessment. Unlike multi-layer single hazard methods, it is expected that the approach presented in this paper would capture those behaviors while being applicable for “real-world” studies. Also, compared to standard methods, the network approach can be used to input more complex behavior such as conditional changes, compounding effects, and exclusion (further discussion on this point is found in the next section), which is difficult to achieve with more rigid models. The use of graphs for risk quantification is a radical change from the standard risk assessment framework. It widens the possibilities for innovative approaches by, for example, tapping into potential development in other disciplines (e.g. dynamic network in epidemiology; Enright & Kao, 2018). In addition, this framework permits remarkable reduction in computation time compared to entangled physical multi-hazard models. A hidden “by-product” of the method is to drive the user to deeply consider “what-if” possibilities beyond the standard risk assessment practice. It also lends itself to a multi-disciplinary approach to risk assessment as expert opinion is crucial to constrain the behavior of

each element in a system approach. The spatial properties of the graph (by contrast to non-spatial e.g. distribution plot) enhances the results comprehensibility and clarifies to non-scientists by allowing spatial display in GIS software. Analogies with other types of networks (e.g. social networks) can also help to convey the interdependency aspect of the method to the end user for better comprehension.

2.5.2 Time and feedbacks

The method presented here only considers the immediate aftermath of the hazard effects. It is clear that the time dimension is a key component of a disaster (Marzocchi et al., 2012) and is an ongoing limitation in natural disaster assessment tools (Zerger & Smith, 2003; Gallina et al., 2016). For example, what is the effect of a delay in landslide triggering after an initial earthquake? What about the time delay for a landslide dam to overtop and fail? And how do their impacts propagate in the mid- to long term?

This raises two issues related to time-dependent effects; first, it is understood that the temporal aspect of disaster scenarios has increasing relevance if the damaged state of the exposed elements is susceptible to delayed effects of hazards (e.g. compounded impact, repair time extended). By integrating sampling of fragility functions following scenarios, it would become possible to take into account parameters such as time to repair damaged assets or cumulative damage due to successive impacts. Second, continuous feedback effects will have either amplification or reduction effects on the impact over time (e.g. earthquakes cause landslides, which can result in aggradation of the riverbed and increase the risk of flooding). These two points can be addressed by using the framework presented herein to move from static simulation to discrete event simulation, in which the “memory” of the model can be used to amplify or diminish the values of frequency and magnitude on the connections. This highlights one of the main benefits of translating the elements of a disaster system to a network of connections: the flexibility

of the framework to respond to the dynamic aspect of natural disasters.

2.5.3 Uncertainties and limitations

The methodology is aimed at properly representing the large aleatoric uncertainty and improving the epistemic uncertainty, compared to a multi-layer single hazard approach (Gill & Malamud, 2016), by producing numerous scenarios via Monte Carlo simulations. The current model follows a consistent set of rules with relatively limited complexity but, also, a lack of flexibility (e.g. no variance on threshold values, binary approach to vulnerability). Options to improve the framework toward further enhancing the epistemic error representation could arise at a later stage, even at the cost of tending toward more complex models (e.g. bias-variance trade-off; Fortmann-Roe, 2012). Secondly, hazard footprints consider the potential case for each specific occurrence, so the network is maximally connected. Incorporating a wider range of intensity-dependent hazard footprints in the workflow could be an efficient way to improve the numerical properties of the procedure. Overall, a slightly “fuzzier” approach could reduce the overall epistemic error, better quantify the aleatoric uncertainty, and thus improve quantification of the potential risk.

At present, the network is set up based on expert opinion, observation and existing databases. Therefore, it is inherently expected that “unknown unknowns” (Logan, 2009) will be left out of the model despite the willingness to test the “real world” to the best of one’s capability and knowledge. Nevertheless, as human knowledge of the behavior of the natural world develops, these improvements can be incorporated into the model framework.

2.5.4 Extension to connected impacts

Like natural systems, most man-made systems can be summarised as networks (i.e. infrastructure, societal, commercial etc.). Networks use nodes and edges instead of matter,

energy or information. The work done by Arosio et al. (2018b) on Mexico City demonstrates how infrastructure can be put into a graphical framework to assess the risk by studying the topology of the network. Hence, an interesting potential development of the network approach is that hazard and exposure networks can be merged together without the difficulties or limitations intrinsic in non-graphical approaches (i.e. methods that do not use “graphs” or networks). As highlighted in previous publications (Buzna et al., 2006; Buldyrev et al., 2010; Pescaroli & Alexander, 2016), a cascading multi-hazard event can impact and propagate through infrastructure and societal networks with disastrous consequences. The method presented herein would allow an understanding of the spreading of impacts through connected and merged networks, and permit deeper insights into potential adverse consequences.

To summarise, the use of networks potentially allows linkage of the entirety of the hazard-exposure system (e.g. hazards, social, economic etc.), giving a complete overview of the spreading effect of initial hazards and their propagation through a system-of-systems framework (Ackoff, 1971; Jackson & Keys, 1984; Cavallo & Ireland, 2014; Pant et al., 2017).

2.5.5 Forecasting capabilities

Finally, the method should naturally evolve towards simulation-type forecasting. To do so, the RNG simulation would need to be redesigned to reduce the control of the current method (by using combination of two α values) as it currently impairs the capacity to produce probabilistic results. The computationally efficient approach of transforming the random variable would now only be feasible at the top level of the hierarchy (importance sampling), as the likelihood needs to be corrected for, and this cannot be done at the lower levels because of the complex interactions. More use will need to be made of precalculated impacts from each node, and thresholds established based on the individual node below. Rainfall would need to be made more variable, but highly spatially correlated.

2.6 Conclusion

The method presented here develops an innovative workflow for the study of multi-hazard and complex cascading effects in the realm of natural disasters by providing a framework for associating empirical models in a network and simulating disaster scenarios. It answers many limitations of the current “multi-layer single hazard” approach to risk assessment by integrating hazard interconnectivity at its core. Despite the simple approach taken, the Kaikōura test case demonstrates that the method is able to generate realistic results. Furthermore, several useful outputs can be derived from the method and can lead to specific actions to reduce potential impact over studied areas (e.g. resource allocation for preparedness). Several aspects of the method can be developed further, depending on the purpose of the exercise. Numerous avenues are available (and currently in progress), through the addition of natural hazards (e.g. flooding, landslide dam events), sophistication of the hazard models and vulnerability components (e.g. use of fragility functions for the road network), and the study of “deeper” and dynamic impacts (e.g. impacts on tourism, supply chains, social networks). This framework has the potential to inspire the emergence of novel ideas for complex impact assessment and to evolve toward probabilistic risk assessment.

2.7 Acknowledgements

The authors would like to thank Resilience to Nature’s Challenges (RNC) for funding this research. We would like to thank the many contributors that provided models and information without whom this work would not have been possible. Thanks also for the discussion, comments and interest from Graeme Smart, Pascal Horton, Arnaud Mignan, Bruce Malamud and Warner Marzocchi

2.8 References

Abe, S. and Suzuki, N. (2006). Complex-network description of seismicity. Nonlinear Processes in Geophysics, 13, 145–150.

Ackoff, R. L. (1971). Towards a System of Systems Concepts. Management science, 17(11), 661-671.

AghaKouchak, A., Huning, L. S., Chiang, F., Sadegh, M., Vahedifard, F., Mazdiyasni, O., Moftakhari, H., and Mallakpour, I. (2018). How do natural hazards cascade to cause disasters? Nature, 561, 458-460.

Arosio, M., Martina, M. L., and Figueiredo, R. (2018a). Natural hazard risk of complex systems-the whole is more than the sum of its parts: I. A holistic modelling approach based on Graph Theory. Natural Hazards Earth System Science Discussion. In review.

Arosio, M., Martina, M. L. V., and Figueiredo, R. (2018b). Natural hazard risk of complex systems - the whole is more than the sum of its parts: II. A pilot study in Mexico City. Natural Hazards Earth System Science Discussion. In review.

Bannister, S. and Gledhill, K. (2012). Evolution of the 2010–2012 Canterbury earthquake sequence. New Zealand Journal of Geology and Geophysics, 55, 295–304.

Beck, M. B., Ravetz, J. R., Mulkey, L. A., and Barnwell, T. O. (1997). On the problem of model validation for predictive exposure assessments. Stochastic Hydrology and Hydraulics, 11, 229–254.

Benn, J. L. (2005). Landslide events on the West Coast, South Island, 1867-2002. New Zealand Geographer, 61(1), 3–13.

Bradley BA. (2013). A New Zealand-Specific Pseudospectral Acceleration Ground-Motion Prediction Equation for Active Shallow Crustal Earthquakes Based on Foreign Models. Bulletin of the Seismological Society of America, 103(3):1801–1822.

Buldyrev, S. V., Parshani, R., Paul, G., Stanley, H. E., and Havlin, S. (2010). Catastrophic cascade of failures in interdependent networks. Nature, 464, 1025.

Butts, C. T. (2009). Revisiting the foundations of network analysis. science, 325, 414–416.

Buxton, R., Mcverry, G., and Goded, T. (2014). Ground motion maps based on recorded motions for the earthquakes in the canterbury earthquake sequence. In Proc. of the Australasian Structural Engineering Conference (ASEC).

Buzna, L., Peters, K., and Helbing, D. (2006). Modelling the dynamics of disaster spreading in networks. Physica A: Statistical Mechanics and its Applications, 363, 132–140.

Cavallo, A. and Ireland, V. (2014). Preparing for complex interdependent risks: a system of systems approach to building disaster resilience. International journal of disaster risk reduction, 9, 181–193.

Clark-Ginsberg, A., Abolhassani, L., and Rahmati, E. A. (2018). Comparing networked and linear risk assessments: From theory to evidence. International Journal of Disaster Risk Reduction.

Cox, S. C., Rutter, H. K., Sims, A., Manga, M., Weir, J. J., Ezzy, T., White, P. A., Horton, T. W., and Scott, D. (2012). Hydrological effects of the MW 7.1 Darfield (Canterbury) earthquake, 4 September 2010, New Zealand. New Zealand Journal of Geology and Geophysics, 55, 231–247.

Cubrinovski, M., Green, R., Allen, J., Ashford, S., Bowman, E., Bradley, B. A., Cox, B., Hutchinson, T., Kavazanjian, E., and Orense, R. (2010). Geotechnical reconnaissance of the 2010 Darfield (New Zealand) earthquake. Bulletin of the New Zealand Society for Earthquake Engineering, 43, 243–320.

Cubrinovski, M., Robinson, K., Taylor, M., Hughes, M., and Orense, R. (2012). Lateral spreading and its impacts in urban areas in the 2010–2011 Christchurch earthquakes. New Zealand Journal of Geology and Geophysics, 55, 255–269.

Dahal, R. K., Hasegawa, S., Nonomura, A., Yamanaka, M., Masuda, T., and Nishino, K. (2008). GIS-based weights-of- evidence modelling of rainfall-induced landslides in small catchments for landslide susceptibility mapping. Environmental Geology, 54(2), 311–324.

Davies, A. J., Sadashiva, V., Aghababaei, M., Barnhill, D., Costello, S. B., Fanslow, B., Headifen, D., Hughes, M., Kotze, R., and Mackie, J. (2017). Transport infrastructure performance and management in the South Island of New Zealand, during the first 100 days following the 2016 Mw 7.8 "Kaiko¯ura" earthquake. Bulletin of the New Zealand Society for Earthquake Engineering, 50, 2.

Dellow S, Massey CI, Cox SC. (2017). Response and initial risk management of landslide dams caused by the 14 November 2016 Kaikōura earthquake, South Island, New Zealand. New Zealand, 2017:8.

Dezso˝, Z. and Barabási, A.-L. (2002). Halting viruses in scale-free networks. Physical Review E, 65(5), 055103.

Enright J, Kao RR. (2018). Epidemics on dynamic networks. Epidemics, 24:88–97.

Fang FC, Casadevall A. (2011). Reductionistic and Holistic Science. Infection and Immunity, 79(4):1401–1404.

Fortmann-Roe, S. (2012). Understanding the bias-variance tradeoff. http://scott.fortmannroe.com/docs/BiasVariance.html.

Gallina, V., Torresan, S., Critto, A., Sperotto, A., Glade, T., and Marcomini, A. (2016). A review of multi-risk methodologies for natural hazards: Consequences and challenges for a climate change impact assessment. J Environ Manage, 168, 123–32.

Gill, J. C. and Malamud, B. D. (2014). Reviewing and visualizing the interactions of natural hazards. Reviews of Geophysics, 52, 680–722.

Gill, J. C. and Malamud, B. D. (2016). Hazard interactions and interaction networks (cascades) within multi-hazard methodologies. Earth System Dynamics, 7, 659–679.

Glade, T. (1998). Establishing the frequency and magnitude of landslide-triggering rainstorm events in New Zealand. Environmental Geology, 35(2-3), 160–174.

Goda, K., Campbell, G., Hulme, L., Ismael, B., Ke, L., Marsh, R., Sammonds, P., So, E., Okumura, Y., and Kishi, N. (2016). The 2016 Kumamoto earthquakes: cascading geological hazards and compounding risks. Frontiers in built environment, 2, 19.

Grimm, V., Revilla, E., Berger, U., Jeltsch, F., Mooij, W. M., Railsback, S. F., Thulke, H.-H., Weiner, J., Wiegand, T., and DeAngelis, D. L. (2005). Pattern-oriented modeling of agent-based complex systems: lessons from ecology. science, 310, 987–991.

Heckmann, T. and Schwanghart, W. (2013). Geomorphic coupling and sediment connectivity in an alpine catchment—Exploring sediment cascades using graph theory. Geomorphology, 182, 89–103.

Heckmann, T., Schwanghart, W., and Phillips, J. D. (2015). Graph theory—Recent developments of its application in geo- morphology. Geomorphology, 243, 130–146.

Helbing, D. (2013). Globally networked risks and how to respond. Nature, 497, 51.

Hergarten, S. (2004). Aspects of risk assessment in power-law distributed natural hazards. Natural Hazards and Earth System Science, 4, 309–313.

Horton, P., Jaboyedoff, M., B et, a. R., and Zimmermann, M. (2013). Flow-R, a model for susceptibility mapping of debris flows and other gravitational hazards at a regional scale. Natural Hazards and Earth System Sciences, 13, 869–885.

ISDR, U. N. (2005). Hyogo framework for action 2005-2015: building the resilience of nations and communities to disasters.

Jackson, M. C. and Keys, P. (1984). Towards a system of systems methodologies. Journal of the operational research society, 35, 473–486.

Kappes, M. S., Keiler, M., von Elverfeldt, K., and Glade, T. (2012). Challenges of analyzing multi-hazard risk: a review. Natural hazards, 64, 1925–1958.

Keefer, D. K., Wilson, R. C., Mark, R. K., Brabb, E. E., Brown, W. M., Ellen, S. D., Harp, E. L., Wieczorek, G. F., Alger, C. S., and Zatkin, R. S. (1987). Real-time landslide warning during heavy rainfall. Science, 238, 921–925.

Keeling MJ, Eames KTD. (2005). Networks and epidemic models. Journal of The Royal Society Interface, 2(4):295–307.

Komendantova, N., Mrzyglocki, R., Mignan, A., Khazai, B., Wenzel, F., Patt, A., and Fleming, K. (2014). Multi-hazard and multi-risk decision-support tools as a part of participatory risk governance: Feedback from civil protection stakeholders. International Journal of disaster risk reduction, 8, 50–67.

Kritikos, T. (2013). Geomorphic hazard analyses in tectonically-active mountains: application to the Western Southern Alps, New Zealand. University of Canterbury.

Kumasaki, M., King, M., Arai, M., and Yang, L. (2016). Anatomy of cascading natural disasters in Japan: Main modes and linkages. Natural Hazards, 80, 1425–1441.

Larsen, I. J., Montgomery, D. R., and Korup, O. (2010). Landslide erosion controlled by hillslope material. Nature Geoscience, 3, 247.

Legros, F. (2002). The mobility of long-runout landslides. Engineering Geology, 63:301–331.

Liu, Z., Nadim, F., Garcia-Aristizabal, A., Mignan, A., Fleming, K., and Luna, B. Q. (2015). A three-level framework for multi-risk assessment. Georisk: Assessment and Management of Risk for Engineered Systems and Geohazards, 9, 59–74.

Logan, D. C. (2009). Known knowns, known unknowns, unknown unknowns and the propagation of scientific enquiry. Journal of experimental botany, 60, 712–714.

Marzocchi, W., Garcia-Aristizabal, A., Gasparini, P., Mastellone, M. L., and Ruocco, A. D. (2012). Basic principles of multi-risk assessment: a case study in Italy. Natural hazards, 62, 551–573.

Mignan, A., Wiemer, S., and Giardini, D. (2014). The quantification of low-probability–high-consequences events: part I. A generic multi-risk approach. Natural Hazards, 73, 1999–2022.

Nicol, R., Cox, S., Langridge, R., and Pedley, K. (2010). Surface rupture of the Greendale fault during the Mw 7.1 Darfield (Canterbury) earthquake, New Zealand: Initial findings. Bulletin of the New Zealand Society for Earthquake Engineering, 43.

Pagani, M., Monelli, D., Weatherill, G., Danciu, L., Crowley, H., Silva, V., ... & Simionato, M. (2014). OpenQuake engine: An open hazard (and risk) software for the global earthquake model. *Seismological Research Letters*, *85*(3), 692-702.

Pant, R., Thacker, S., and Hall, J. W. (2017). System-of-systems framework for global infrastructure vulnerability assessments. In Paper for GGKP Annual Conference, WorldBank, Washington, DC, November. http://www.greengrowthknowledge.org/resource/system-systems-framework-global-infrastructure-vulnerability-assessments.

Papic, M., Bell, K., Chen, Y., Dobson, I., Fonte, L., Haq, E., Hines, P., Kirschen, D., Luo, X., and Miller, S. S. (2011). Survey of tools for risk assessment of cascading outages. In Power and Energy Society General Meeting, IEEE, 1-9.

Pastén, D., Torres, F., Toledo, B., Muñoz, V., Rogan, J., and Valdivia, J. A. (2017). Time-Based Network Analysis Before and After the M w 8.3 Illapel Earthquake 2015 Chile. Pure and Applied Geophysics, 173, 2267-2275

Paté-Cornell, E. (2012). On “Black Swans” and “Perfect Storms”: risk analysis and management when statistics are not enough. Risk Analysis: An International Journal, 32, 1823–1833.

Perez, L. and Dragicevic, S. (2009). An agent-based approach for modeling dynamics of contagious disease spread. International journal of health geographics, 8, 50.

Pescaroli, G. and Alexander, D. (2015). A definition of cascading disasters and cascading effects: Going beyond the “toppling dominos“metaphor. Planet@ Risk, 3.

Pescaroli, G. and Alexander, D. (2016). Critical infrastructure, panarchies and the vulnerability paths of cascading disasters. Natural Hazards, 82, 175–192.

Pescaroli, G. and Alexander, D. (2018). Understanding Compound, Interconnected, Interacting, and Cascading Risks: A Holistic Framework. Risk Analysis.

Phillips, J. D., Schwanghart, W., and Heckmann, T. (2015). Graph theory in the geosciences. Earth-Science Reviews, 143, 147– 160.

Robinson, T. and Rosser, N. (2017). Rapid landslide risk assessment of transport infrastructure following the 13 November 2016 Kaikōura, New Zealand, earthquake. In EGU General Assembly Conference Abstracts, Vol. 19, p. 5180.

Sachs, M. K., Yoder, M. R., Turcotte, D. L., Rundle, J. B., and Malamud, B. D. (2012). Black swans, power laws, and dragon- kings: Earthquakes, volcanic eruptions, landslides, wildfires, floods, and SOC models. European Physical Journal-Special Topics, 205, 167–182.

Sornette, D. (2009). Dragon-kings, black swans and the prediction of crises. arXiv preprint arXiv:0907.4290.

Sperotto A, Molina J-L, Torresan S, Critto A, Marcomini A. (2017). Reviewing Bayesian Networks potentials for climate change impacts assessment and management: A multi-risk perspective. Journal of Environmental Management, 202:320–331.

Stahl, T., Bilderback, E. L., Quigley, M. C., Nobes, D. C., and Massey, C. I. (2014). Coseismic landsliding during the Mw 7.1 Darfield (Canterbury) earthquake: Implications for paleoseismic studies of landslides. Geomorphology, 214, 114–127.

Strahler, A. N. (1957). Quantitative analysis of watershed geomorphology. Eos, Transactions American Geophysical Union, 38, 913–920.

Taleb, N. N. and Blyth, M. (2011). The black swan of Cairo: How suppressing volatility makes the world less predictable and more dangerous. Foreign Affairs, 33–39.

Tanyas¸, H., van Westen, C. J., Allstadt, K. E., Jessee, M. A. N., Görüm, T., Jibson, R. W., Godt, J. W., Sato, H. P., Schmitt, R. G., Marc, O., and Hovius, N. (2017). Presentation and Analysis of a Worldwide Database of Earthquake- Induced Landslide Inventories. Journal of Geophysical Research: Earth Surface, 122, 1991–2015.

Tarbali, K. and Bradley, B. A. (2014). Representative ground motion ensembles for several major earthquake scenarios in New Zealand. Bulletin of the New Zealand Society for Earthquake Engineering, 47(4), 231–252.

Thompson, C. S. (2002). The high intensity rainfall design system: HIRDS. International Conference on Flood Estimation. CHR Report, No. II–17, International Commission of the Rhine Basin, Lelystad, 273–281.

UNISDR, U. N. O. (2015). Sendai framework for disaster risk reduction 2015–2030. In 3rd United Nations World Conference on DRR. Sendai, Japan: UNISDR.

Van Dissen, R., Barrell, D., Litchfield, N., Villamor, P., Quigley, M., King, A., Furlong, K., Begg, J., Townsend, D., and Mackenzie, H. (2011). Surface rupture displacement on the Greendale Fault during the Mw 7.1 Darfield (Canterbury) earthquake, New Zealand, and its impact on man-made structures. In 9th Pacific Conference on Earthquake Engineering, Auckland, New Zealand, 8.

Zerger, A. and Smith, D. I. (2003). Impediments to using GIS for real-time disaster decision support. Computers, environment and urban systems, 27, 123–141.

Zhang, L. M., Zhang, S., and Huang, R. Q. (2014). Multi-hazard scenarios and consequences in Beichuan, China: the first five years after the 2008 Wenchuan earthquake. Engineering Geology, 180, 4–20.

Chapter 3
Regional assessment of landslide dam hazards: a GIS methodology for risk preparedness

---

Alexandre Dunant[1], Tim Davies[1]

[1] Department of Geological Sciences, University of Canterbury, Christchurch

Overview

The ambition of this Ph.D. was to develop a framework that would allow for stochastic output from a multi-hazard risk assessment. Franz Josef township in the West Coast region of New Zealand is known to be at risk from multi-hazard threats (explained in more detail Chapter 4). An initial objective was to focus and test the framework for Franz Josef township. One of the identified risks to the township is from landslide dam outburst flood. Unfortunately, no forward model exists to predict potential for landslide dam break at a regional scale. To address this, Chapter 3 proposes an automated dam break flood calculation, which is described and tested for the Callery River on the West Coast. Chapter 3 summarises the creation of the tool that permits the linkage of landslide and flooding events from landslide dams. This connection is critical to the further study of the impact of cascading hazard chains after an earthquake, and is used in the work presented in Chapter 4

Contributions

The concept of the manuscript was developed through discussions between Alexandre Dunant and Tim Davies. Alexandre Dunant and Tim Davies designed the research objectives. The flood

modeling was provided by Matthew Gardner. Alexandre Dunant created the landslide dam outburst flood methodology, modelling and wrote the manuscript. Tim Davies carried out in-depth reviews of the manuscript and offered much useful discussion of results and interpretations.

3.1 Abstract

This study presents a simple automated tool to assess and map the potential outburst flood extent and backwater inundation from multiple landslide dam locations. Previously published data on landslide dams focus, in large part, on the geomorphological characteristics of existing landslide dams or the specific details of an actual blockage site. The risk of landslide damming and outburst flooding is often dealt with in a reactive manner when events occur, leaving emergency services on the back foot. The tool presented herein is built on existing knowledge and empirical relationships derived from literature review to provide a regional screening tool with GIS output. The tool is validated against known landslide dam events in New Zealand, Japan and China. The Callery gorge, upstream of the Franz Josef township, New Zealand, is used as a case study for the method, as it has been previously identified as a likely site of a future landside dam.

3.2 Introduction

Natural dams are often associated with landslides triggered by earthquakes or rainfalls (Costa and Schuster, 1988). In a large number of cases, the landslide dams fail in a relatively short time-frame, with only a minority remaining stable in the long term (Costa and Schuster, 1988). The effects of failure can be catastrophic. Many recent events demonstrate the risk associated with landslides blocking rivers and the subsequent flooding hazard (Duman, 2009; Fan et al., 2012; Hayashi et al., 2011; Nibigira et al., 2018; Safran et al., 2015; Tien et al., 2018). Landslide dams can have an impact both downstream and upstream of the naturally formed dam(s). Among the

resulting hazards are outburst flood, river aggradation and backwater inundation (Kofler et al., 2017; Korup, 2005; Pratt-Sitaula et al., 2007). Outburst floods are among the most dangerous consequences because of the suddenness and magnitude of the event. Some examples where authorities had to be involved to manage the risk of outburst floods are the Hapuku dam following the 2016 Kaikōura earthquake (Dellow et al., 2017), the Kali Gandaki dam breach following the 2015 Gorkha earthquake (Bricker et al., 2017) and the Tangjiashan dam triggered by the 2008 Wenchuan earthquake (Wang et al., 2015). The latter event led to the evacuation of two hundred thousand people initially with a follow-up plan of evacuating 1.2 million people downstream of the dam (Cui et al., 2012; Peng and Zhang, 2012a). Fortunately, due to geotechnical work undertaken, the second evacuation phase was not necessary. This example highlights the potential use of a predictive tool for preparedness for such events.

A number of papers build on an extensive global database to inform empirical studies of landslide dam morphometrics (Adams, 1981; Costa and Schuster, 1991; Ermini and Casagli, 2003; Korup, 2004; Perrin and Hancox, 1992; Stefanelli et al., 2015; Stefanelli et al., 2016; Nash et al., 2008). These studies highlight the relationship between morphological variables of landslide dams and, among others, blockage potential, time-of-failure estimates and peak discharge from outburst flood (Carrivick et al., 2011; Costa, 1985; Costa and Schuster, 1988; Dong et al., 2011; Evans, 1986; Froehlich, 2008; Peng and Zhang, 2012b; Walder and O'Connor, 1997).

Landslides can fall into drainage paths in many locations within a catchment, but many published tools focus on specific sites. Apart from the work of Korup (2004), methods to quantify landslide dam magnitude at regional and national scale, or for numerous potential dam sites in a catchment, are rare (Stefanelli et al., 2016). Indeed, modelling geomorphological features such as landslide dams is a challenging task for large areas. In addition, landslide dam geometries vary widely and the evaluation of the risk of river blockage is highly uncertain. This calls for the study of a large number of dams. One of the issues with this approach is related to hardware; modelling multiple possibilities at large scales necessitates large physical models, which themselves require heavy

computing power. An imperfect alternative to this issue is to limit the number of scenarios or the size of the area to be studied. This, however, results in downgrading the reliability of such a study. The methodology presented herein tries to circumvent this limitation by using “light” software (GIS) and a relatively simple approach to provide useful information for risk reduction and preparedness at a large scale without requiring additional investment. One of the key points of the method is to be able to generate quantifiable and mappable output that can be used for planning and further study. The ultimate objective is to inform communities and emergency services of the potential risks associated with outburst floods and backwater inundation. The following sections provide an overview of the method, test the method against three specific examples across the world, and finally apply the method to the Callery River in New Zealand.

3.3 Method

3.3.1 Overview

Due to its active tectonic and hydrological setting, the New Zealand landscape is particularly prone to landslide dam events (Perrin and Hancox, 1992; Davies and Scott, 1997; Davies, 2002; Korup, 2004). The combination of steep terrain and narrow valleys with the occurrence of earthquakes and high intensity rainfall leads to well-documented events of natural dam blockage (Hancox et al., 2005). A landslide dam database has been generated for New Zealand and empirical relationships have been derived from the dams’ geomorphological characteristics (Davies, et al., 2007; Davies and Scott, 1997; Nash et al., 2008; Korup, 2004, 2005). The geometry parameters and definitions used in this paper are specified in Figure 3.1.

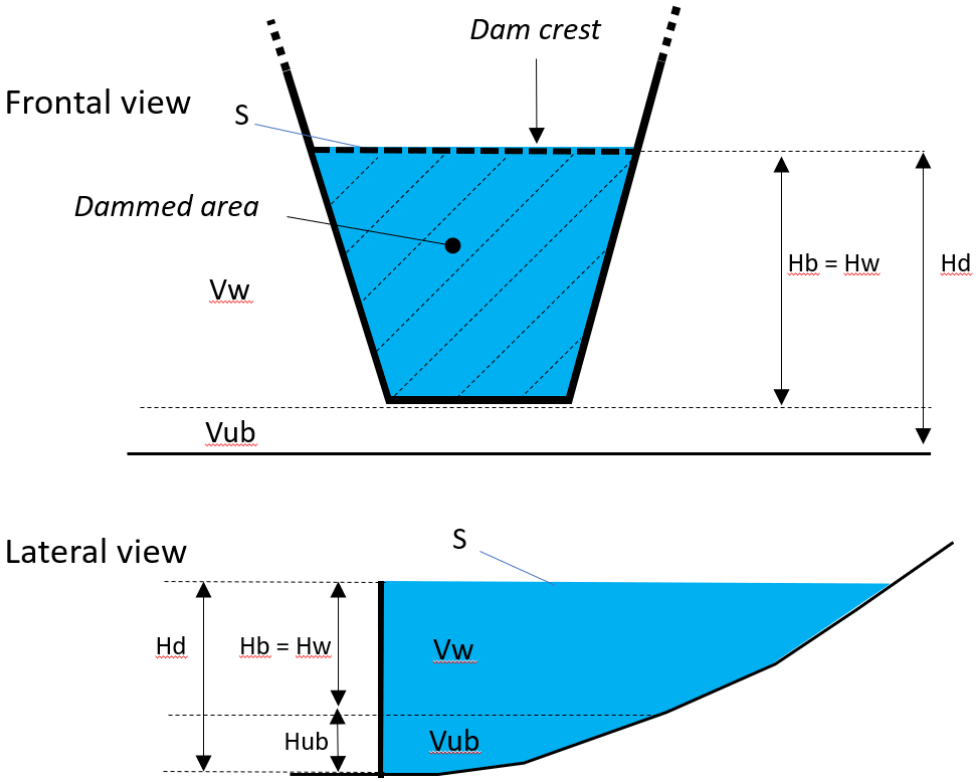

Figure 3.1 Dam geometry and parameters used in this paper. In the method presented, the dam is assumed to fail by the mechanism of overtopping when water level reaches the top of the dam. Hence, the maximum breach height (Hb in m) is equivalent to the height of the water above the final breach invert at the time of failure (Hw in m). Hd is the height of the dam from DEM (m). Hub is the height from the DEM to the bottom of breach (m). S is the total impounded volume (m^3). Vw is the volume of water stored above breach invert at time of failure (m^3).

Building on the work by Korup (2005), the aim of the method presented here is to estimate the potential outburst flood magnitude and map the inundated area at multiple sites along a river course. As landslide dams often comprise unconsolidated material, overtopping is the commonest mode of failure (Costa and Schuster, 1988). Overtopping by the impounded water is often followed by the erosion of the dam ("headcut" erosion) by overflowing water leading to rapid collapse, especially of dams with low cohesive strength (Zhang, Li, Xuan, Wang, and Li, 2009). Thus, overtopping is used as the basis for dam failure herein. The method assumes a constant dam height along the dam crest, from which the filled lake volume is calculated (Hb = Hw, Figure 3.1) from the upstream watershed area using the polygon volume algorithm available in GIS. The watershed area is defined as the upslope area contributing to a common outlet. The impounded

volume, dam height, breach height and volume released are then used to calculate the peak discharge value at the dam following failure (at this point, the “pre-failure” backwater inundation footprint is also an output). This process is repeated for defined equally set points along the river bed. An overview of the workflow is given Figure 3.2.

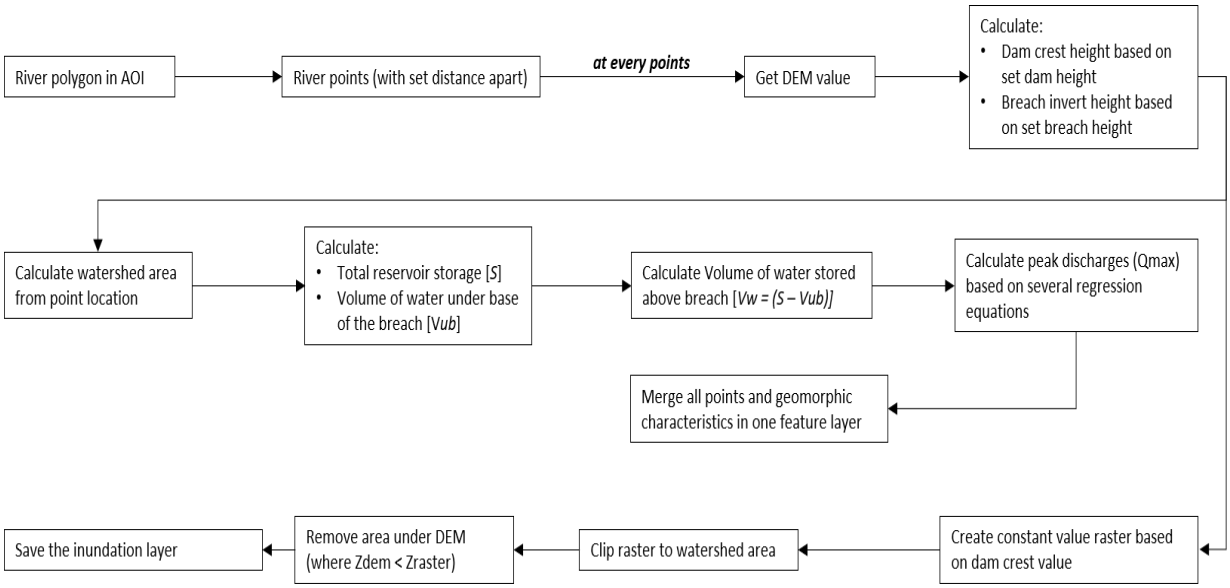

Figure 3.2 Workflow of the automated regional landslide dam outburst flood quantification method. AOI is Area Of Interest.

Once the lake volume is calculated, several equations are used to calculate peak discharge (Qmax) values (Figure 3.1 and Figure 3.2). The equations are regressions relating the peak discharge to the predicted geomorphology of the landslide dam, the resulting reservoir and the breach depth. Several published regression equations were used (Costa, 1985; Evans, 1986; Walder and O’Connor, 1997; MacDonald and Langridge-Monopolis, 1984, summarized in Table 3.1).

Table 3.1 Regression equations used for peak discharge calculation. Qp = peak discharge (m^3/s), S = reservoir storage (m^3), Hd = height of dam (m), Hb = height of breach (m), Hw = depth of water above breach invert at time of failure (m)

Reference	*Equation*
Costa (1985)	$Qp = 181(S.Hd)^{0.43}$
Walder and O'Connor (1997)	$Qp = 6.7(Hw)^{1.73}$
MacDonald and Langridge-Monopolis (1984)	$Qp = 1.154(VwHw)^{0.412}$
Evans (1986)	$Qp = 0.72(Vw)^{0.53}$

These equations have been used because their geomorphic parameters can be derived from a simple digital elevation model and, thus, can be easily applied in various locations. Also, because the regression equations use different parameters for the calculation of peak discharge (as presented Table 3.1), their results can be cross-checked.

3.3.2 Validation

In order to test the methodology and assess the validity of the first-order analysis that was envisioned for this simplified approach, actual examples of landslide dams have been selected. The aim is to validate the volume of the reservoir, the peak discharge values and the inundation footprint. Three locations have been selected, Poerua in New Zealand, Akatani in Japan and Tangjiashan in China (Figure 3.3).

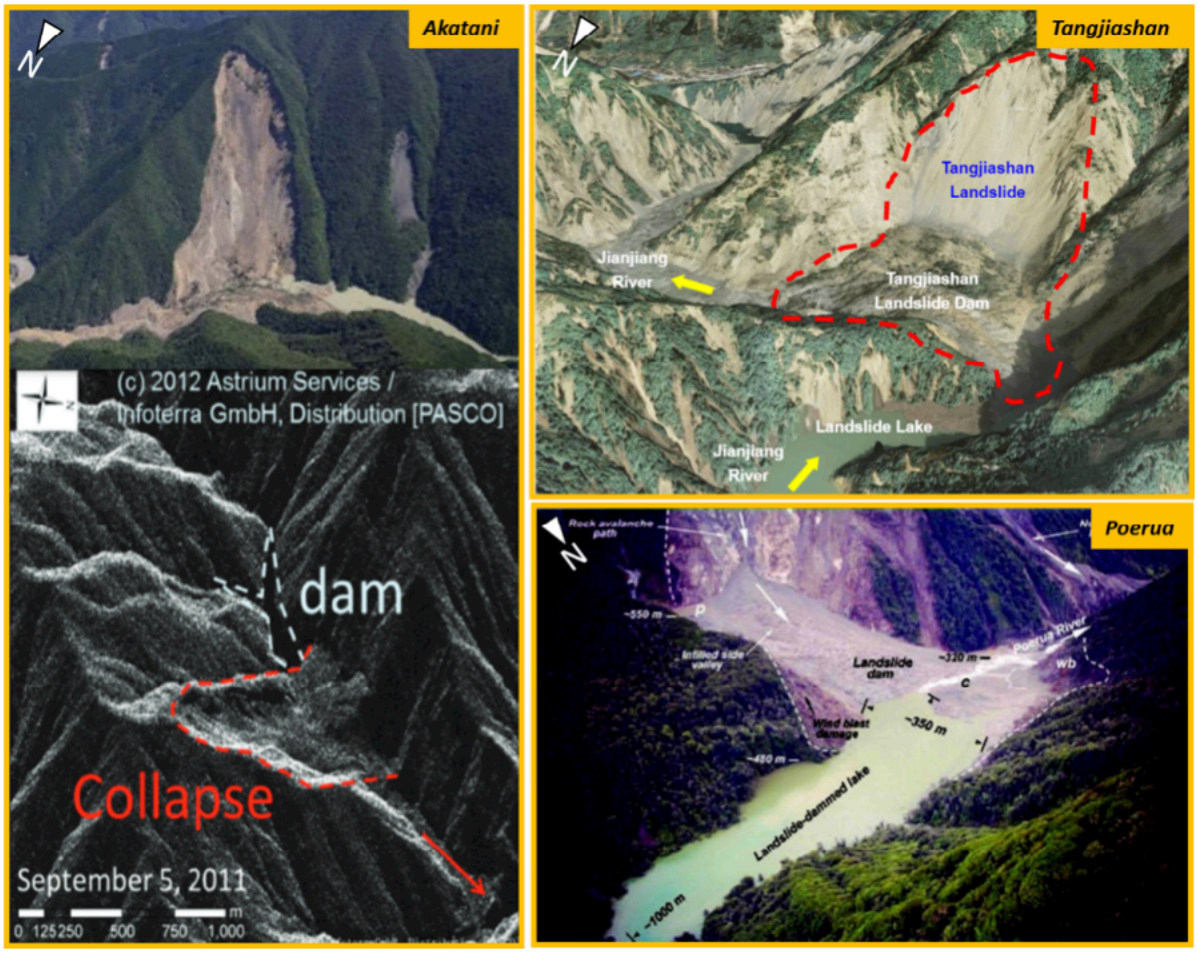

Figure 3.3 Geomorphological settings of three landslide dams used as examples for the method validation. Akatani in Japan (left), Tangjiashan in China (upper right) and Poerua in New Zealand (bottom right). Modified from existing publications (Hancox et al., 2005; Hayashi et al., 2011; Peng and Zhang, 2012a).

The events presented below have been documented in scientific publications and vary in geometries and scale (Davies et al., 2007; Fan et al., 2012; Hancox et al., 2005; Hayashi et al., 2011; Tien et al., 2018; Wang et al., 2015). It is to be noted that despite the use of regression equations based on empirical data, pre-emptive assessment of landslide dam parameters and outflows remains uncertain. Uncertainty in landslide dam assessment is intrinsic to the variety of geometries and the complex processes involved in the interaction between landslides and rivers (Wahl et al., 2010). Landslide dam scenarios are too complicated to analyse exactly; this paper presents a best attempt to test a hypothesis across multiple scenarios and generate large

numbers of outcomes that can reduce the epistemic uncertainty and hence help reduce risk.

Akatani (Japan). On the 4th September 2011, Typhoon Talas caused rainfall with cumulative precipitation of 1000-2400 mm over 5 days in the Kii peninsula, Nara Prefecture, Japan (Hayashi et al., 2011). The heavy rainfall induced seventy-two deep-seated landslides and seventeen landslide dams in the Nara and Wakayama prefectures. The Akatani deep-seated landslide failed with a total volume of 10.2 x 10^6 m^3, damming the river. The natural dam had a height of 67 m, and the reservoir filled to a lake volume of 5.5 x 10^6 m^3 (Tien et al., 2018). Geotechnical work began swiftly (drainage systems, real-time monitoring etc.) as the danger of an outburst flood was recognised early on. Discharge pipes were used to lower the water level in the lake, reducing the risk of outburst flood and preventing catastrophe. Hence the Akatani landslide dam cannot be used to calibrate peak discharge as the impounded area was drained before an outburst flood occurred (Hayashi et al., 2011).

Tangjiashan (China). On 12 May 2008, the 8.0 Mw Wenchuan earthquake caused 34 river blockages and lake formations. The largest landslide dam was formed by the collapse of 2.4x10^7 m^3 from Mt. Tangjiashan in the Jianjiang river (Wang et al., 2015). The Tangjiashan landslide dam had a height of 90 m and a reservoir capacity of 3.26 x 10^8 m^3 at the highest point. Large-scale mitigation measures were undertaken in order to reduce the risk of an outburst flood (Cui et al., 2012; Peng and Zhang, 2012a). While a drainage system was engineered to release water from the dam, 275 000 people were evacuated from the downstream town of Mianyang (Wang et al., 2015). The Tangjiashan dam lake volume was partially released using the 13 m deep and 8 m wide discharge channel (Liu et al., 2012; Liu et al., 2009). The outflow from the discharge channel peaked at 6500 m^3/s (Liu et al., 2009). In this paper, the discharge modelled is compared to the actual engineered channel geometry and resulting outflow.

Poerua (New Zealand). On 6 October 1999, a landslide of 10-15 x 10^6 m^3 fell from Mt Adams, on the West Coast of the South Island of New Zealand and blocked the Poerua river in a narrow

gorge. The rock avalanche created an 80 m high dam and a temporary lake of 5-7 million m^3 that lasted for 6 days after first overtopping; then a minor storm flow created a breach of 40-50 m depth. The failure of the dam caused a discharge estimated to be in the order of 2000-3000 m^3s^{-1} at the breach (Davies et al., 2007; Hancox et al., 2005). Five kilometers downstream, the flood peak was approximately 500 m^3s^{-1} at the State Highway bridge (Davies et al., 2007). No damage was recorded apart from erosion along riverbanks (Davies et al., 2007).

3.4 Results

The method presented in Figure 3.2 has been used for the three cases described in the previous section. Different digital elevation models (DEM) have been used to test the accuracy of the method. The ASTER Global DEM has been used for the Tangjiashan and Akatani examples (https://lpdaac.usgs.gov/dataset_discovery/aster/aster_prod_ucts_table/astgtm). The resolution of the data is 30 m and the global dataset comprises 22,702 tiles. The data quality is variable and, in the data used, the Akatani DEM seems of decent quality unlike the Tangjiashan DEM that displays acquisition or processing imprints. For Poerua, a pre-processed New Zealand South Island DEM is used. The quality is considered good with a resolution of 25 m.

In order to test whether the method provides reasonable results, despite the uncertainties inherent to the task (e.g. DEM resolution, complexity of landslide damming scenarios and geometries, epistemic uncertainty of the empirical parameters, field evaluation method for actual dam volumes etc.), volume, peak discharge and impounded area are compared between the model and the field values in the three locations presented earlier. The methodology is presented in Figure 3.2 and the results are shown in Figure 3.4:

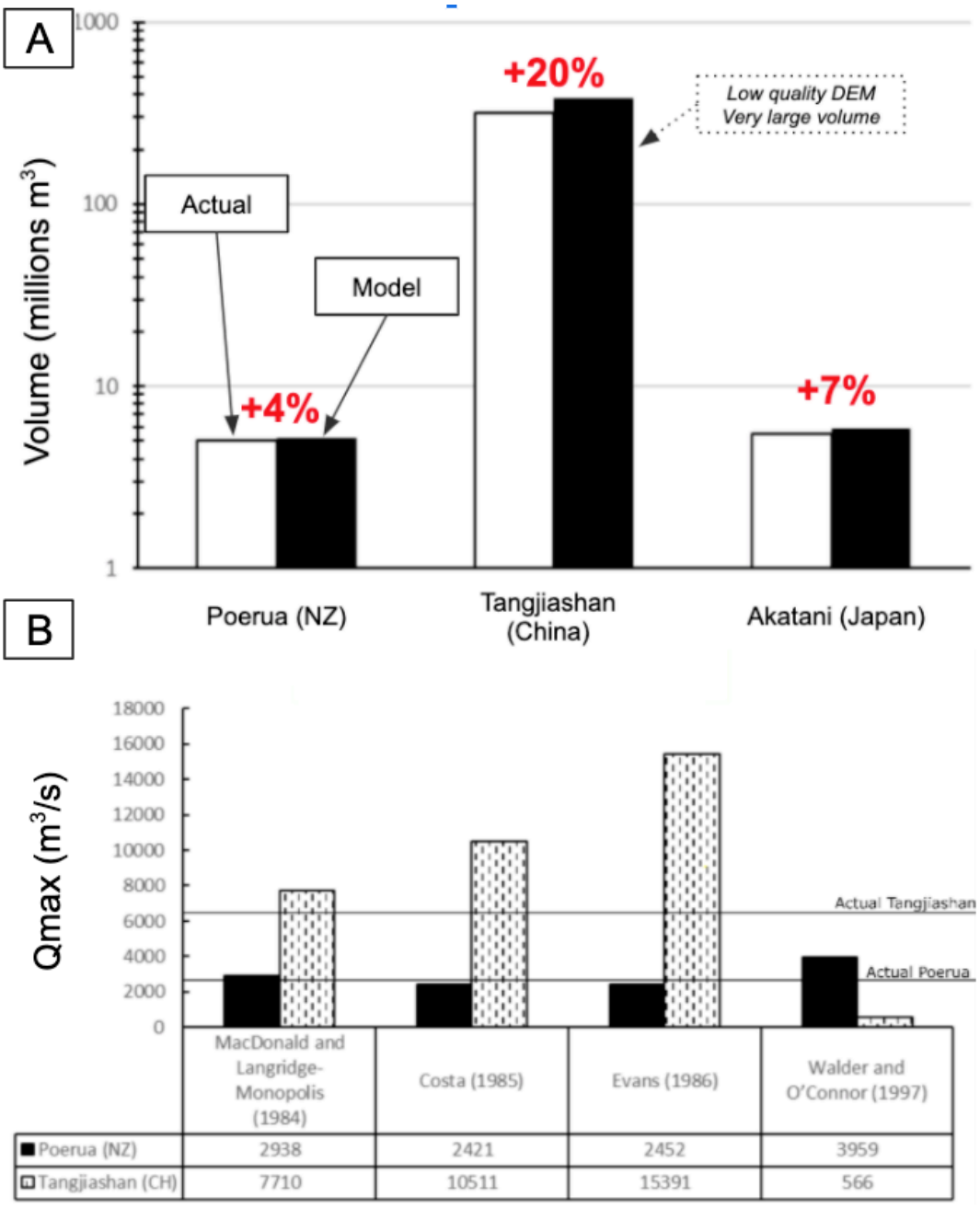

Figure 3.4 Actual and modeled backwater impounded volume (A), and for peak discharge prediction based on four regression equations (B). Due to geoengineering, no outburst occurred in Akatani, hence no comparison can be made for (B).

The results of the simulation of the reservoirs show 4% more volume than the actual volume for the Poerua dam ($5x10^6$ m^3 actual low case vs $5.2x10^6$ m^3 modelled), 20% more for the Tangjiashan dam ($320x10^6$ m^3 actual vs $383x10^6$ m^3 modelled) and 7% more for the Akatani dam

($5.5x10^6$ m^3 actual vs $5.9x10^6$ m^3 modelled). Even if errors on the Poerua and Akatani lake volumes are less than 10% and appear satisfactory, and show that the model can be considered robust, the Tangjiashan example shows significant variation from the actual occurrence. As mentioned by Korup (2005), the common overestimation of the volume can come from the assumption that the dam is analogous to a "vertical wall". Another reason for the error in the Tangjiashan example is that the combination of a poor-quality DEM and the large area under water compound the error on the volume calculation. Hence, the method should be treated carefully when used on extremely large events with poor underlying data. The prediction of peak discharge also depends on the error of the modelled volume estimate. Despite initial errors on the volume and uncertainty on the regression equations used, the actual peak discharges for Tangjiashan (6,500 m^3/s) and for Poerua (2,000-3,000 m^3/s) fall in the range of peak discharges modelled. As expected from the deviation on the total volume and the artificial nature of the breach, a wider error of peak discharge appears for the Tangjiashan dam. The results for the Poerua landslide dam fit with the estimated peak discharge at the dam (Davies et al., 2007; Hancox et al., 2005). The modelled and actual impounded areas are shown in Figure 3.5.

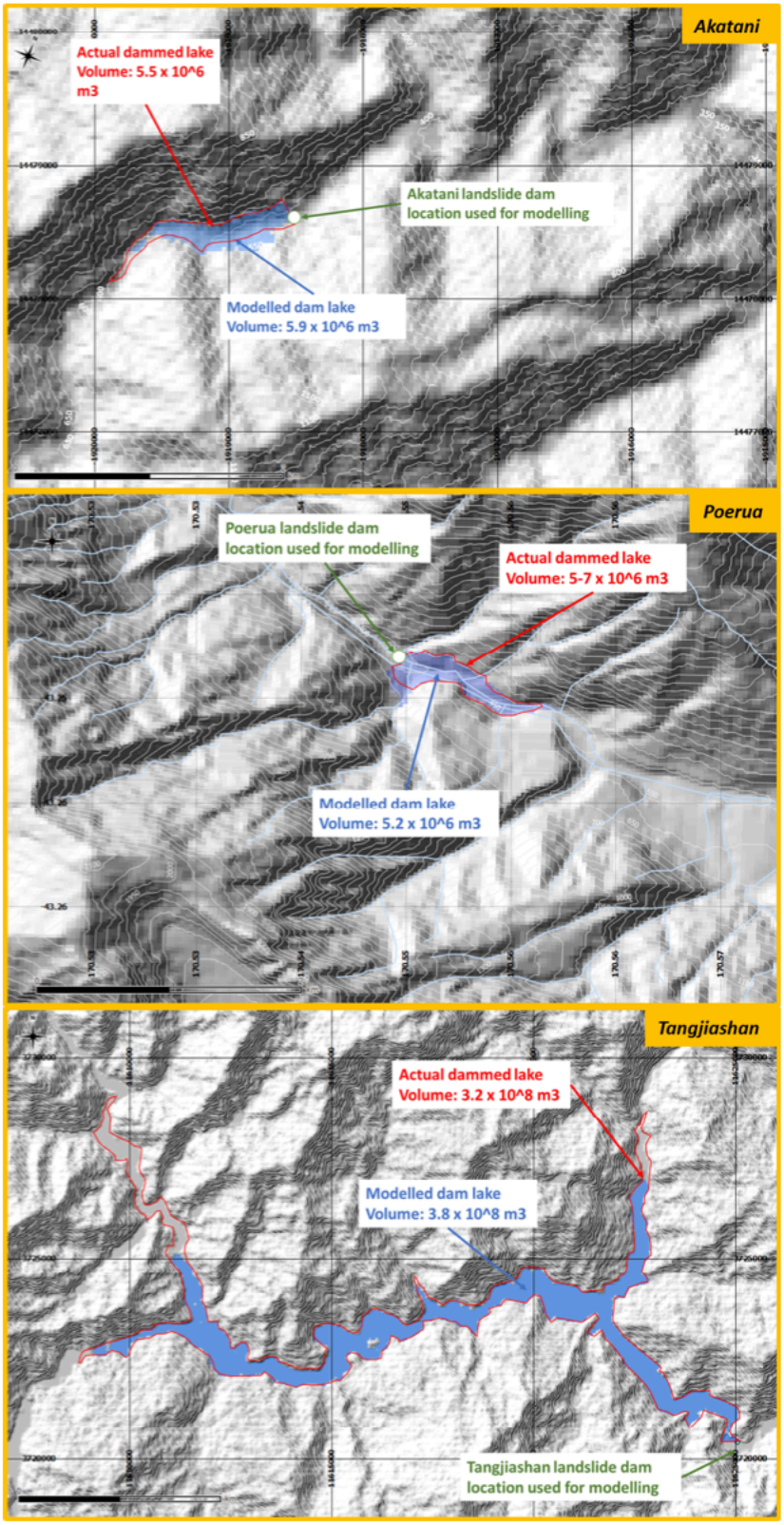

Figure 3.5 Maps highlighting the actual impounded area versus the modelled impounded area. The actual dammed lake was drawn by hand as an attempt to represent the backwater inundation from published material.

From Figure 3.5, the actual and modelled lake footprints appear to correspond well for Poerua and Akatani, but underestimate the area covered by the Tangjiashan lake. In the Tangjiashan example, this discrepancy can be explained by the quality of the DEM. The area farther from the dam represents shallower water, hence resolution becomes a critical factor to delineate the inundated area in the shallow areas. The smaller area of the modelled dammed lake and the higher volume compared to the actual dammed lake, both point toward the poor quality of the input DEM. It infers that the lack of resolution causes an increase of the volume and a reduction of the modelled lake area. The GIS volume calculation uses a triangulated irregular network (TIN) of the DEM as input. Hence, "smoothing" can cause the increase of volume in the deeper part of the lake and also a reduction of area where the water becomes shallow and where less of the reservoir volume is present. To summarise, despite some limitations of the method in dealing with poor data, and the compounding error on large areas, results from the model seem to satisfactorily fulfil the requirement of a “low demand” (in terms of data and software availability) GIS tool for regional to national assessment.

3.5 Regional case study: the Callery catchment

3.5.1 Geomorphological setting

The Callery River is a tributary of the Waiho River on the West Coast of New Zealand, upstream of Franz Josef township (Figure 3.6). The Callery river has formed a long, steep and narrow gorge on the western flank of the Southern Alps. The rapid tectonic uplift (5-10 mm a^{-1}), earthquakes (particularly on the range front Alpine fault), high rainfall intensity on the west side of the Main Divide (up to 11 000 mm/year) and the resulting steep slopes make the gorge particularly prone to landslide damming (Davies and Scott, 1997). In the case of a sudden dam failure, an outburst

flood could endanger the downstream township and put life at risk.

The Poerua landslide dam described above is a potential analogue to what could happen in the Callery Gorge. Davies and Scott (1997) mention a remnant of a landslide dam revealed by aerial photos in the Callery gorge, suggesting that the landslide dam height could have been 180 m with a subsequent "very large flow". Several sites could see a major slope failure and subsequent dam break flooding and aggradation (Davies, 2002; Davies and Scott, 1997; Korup, 2005). Ollett (2001) identified seven sites of past landslide activity from which overtopping failure models were simulated. Those sites have landslide volumes ranging from 780,000 to $45x10^6$ m^3. The simulation highlighted a range of impounded volume, discharge and flood duration of, respectively, $0.2x10^6$ m^3, 2,000 m^3/s and 4 hours for smaller dams (hd_{min} = 72 m) to $74.4x10^6$ m^3, 17,000 m^3/s and 2 hours for larger dams (hd_{max} = 180 m). An interesting point raised in Ollett's work (2001) is that the attenuation of peak flood discharge along the gorge was negligible in all cases, and sediment volume being deposited in the Waiho river ranged from 100,000 m^3 to $2x10^6$ m^3. Hence, an outburst flow would retain most of its initial discharge when it reaches Franz Josef township. The long-term impact of sediment deposition in the Waiho river system was not an objective of this study but previous works point to the risk associated with river aggradation because of sediment supplied by the release of landslide dam material (Ollett, 2001; Davies, 2002).

3.5.2 Methodology applied to the Callery river

The case study applies the workflow and geometrical approach presented in Figure 3.2 to the Callery river. The landslide dam locations are set by creating a virtual dam every 500 m along the Callery river network shapefile (Figure 3.6).

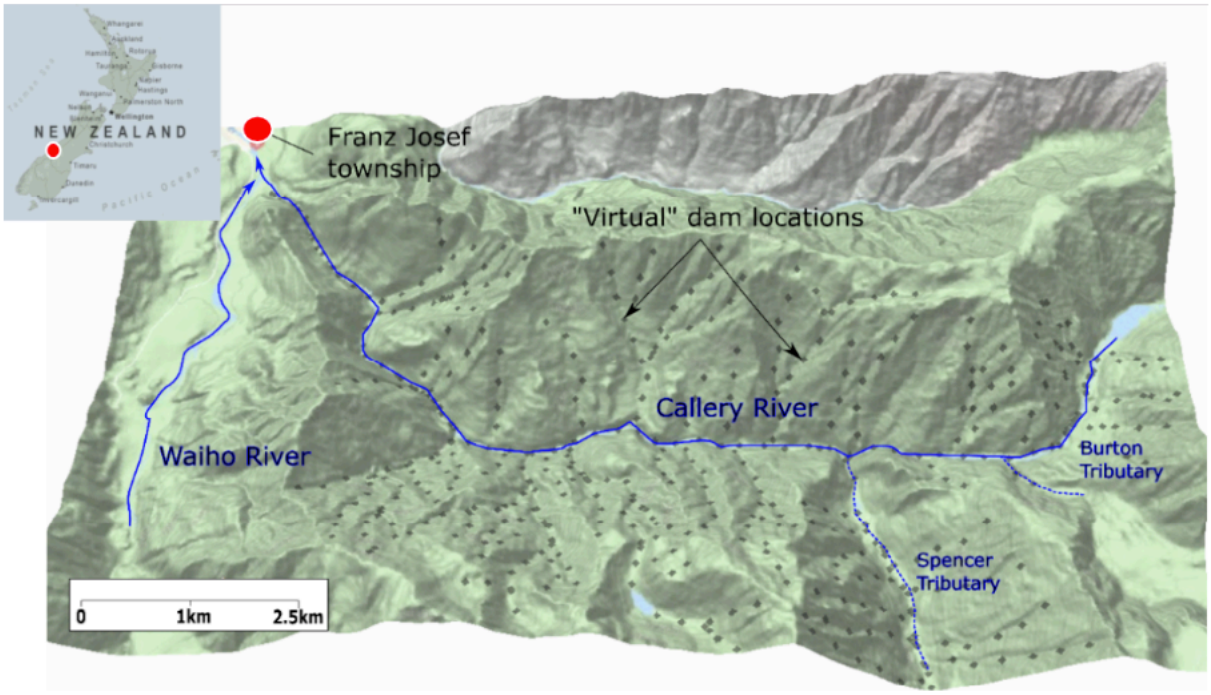

Figure 3.6 Overview of the Callery River and locations of the virtual dams. The red dots point to the Franz Josef township location. The blue arrows indicate the main rivers and streams influencing the discharge at Franz Josef.

Korup (2004) pointed out that the mean value for landslide dam height on the West Coast of New Zealand is 67 m. As the present method is automated, several dam heights, breach depths and regression equations can be tested. Dam heights of 40, 60, 70, 80, 100, 120, 170 and 200 m are used with, for precautionary reasons, a dam breach height representing the full dam height (Hd=Hb, Figure 3.1). It is to be noted that these parameters can be varied as seen fit by the user. Following the method presented, the backwater impounding areas and volumes as well as the peak discharges are calculated and mapped for every dam location along the Callery river network. An additional feature of the tool is that inundation areas can be displayed for every virtual dam.

As a validation method (Korup, 2005), the modelled lake volume-lake area relationship is plotted against the lake volume-lake area regression for New Zealand (Perrin and Hancox, 1992, Korup, 2005) (Figure 3.7).

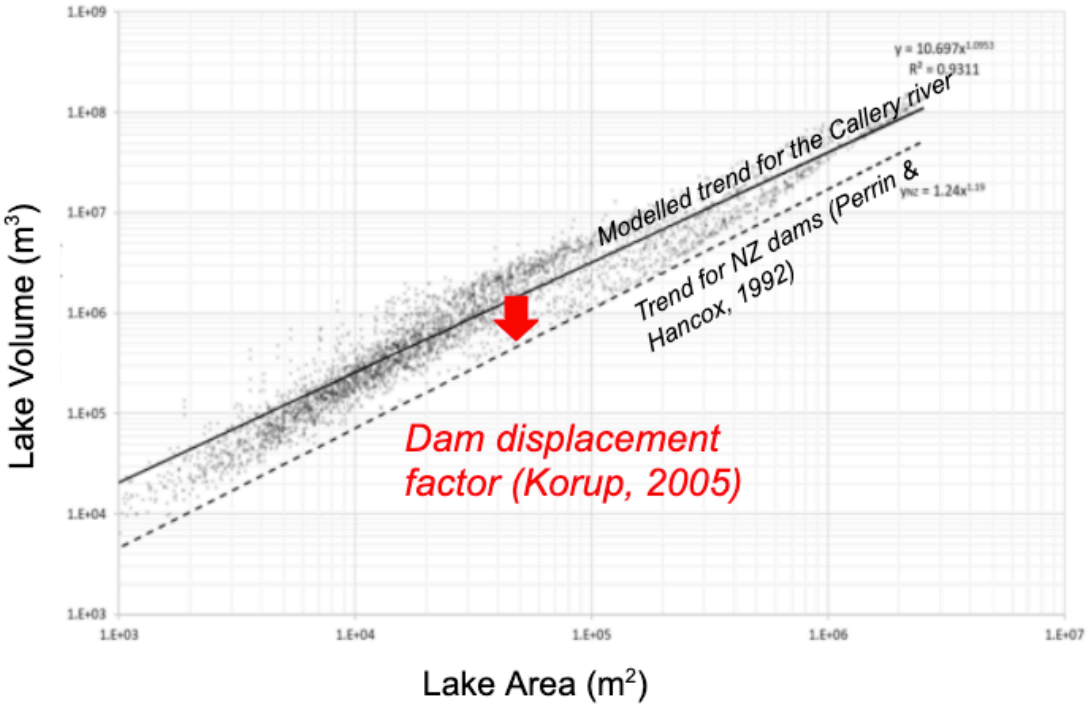

Figure 3.7 Lake volume-lake area relationship for the Callery river (solid line) compared with the regression from Perrin and Hancox (1992) for New Zealand landslide dams (dotted line).

The results give confidence that the model is realistic in the estimation despite a consistent overestimation of the lake volume. This overestimation can be attributed to the assumption that the dam has a vertical upstream face at the crest (Korup, 2005). As in the work of Korup (2005), where a "dam displacement factor" accounted for the oversimplification of the model, the modelled lake volumes have been corrected to more realistic results here. The lake volumes have been revised by subtracting the difference from the regression equation for lake area and lake volume for New Zealand dams (Perrin and Hancox, 1992; Korup, 2005). In this way, the present results are moved closer to the specific geomorphological settings of New Zealand landslide dams.

The peak discharge distribution for the pre-established sets of dam heights at the 501 dam locations along the Callery river is presented in Figure 3.8 using Costa's regression equation (Costa and Schuster, 1988). The Costa equation ($Qp = 181(S.Hd)^{0.43}$,Table 3.1) is used as it was

specifically designed for landslide-related dams. Furthermore, the Poerua case study and previous papers (Davies et al., 2007; Hancox et al., 2005) seems to point to a good fit between the actual events and the results from this regression equation.

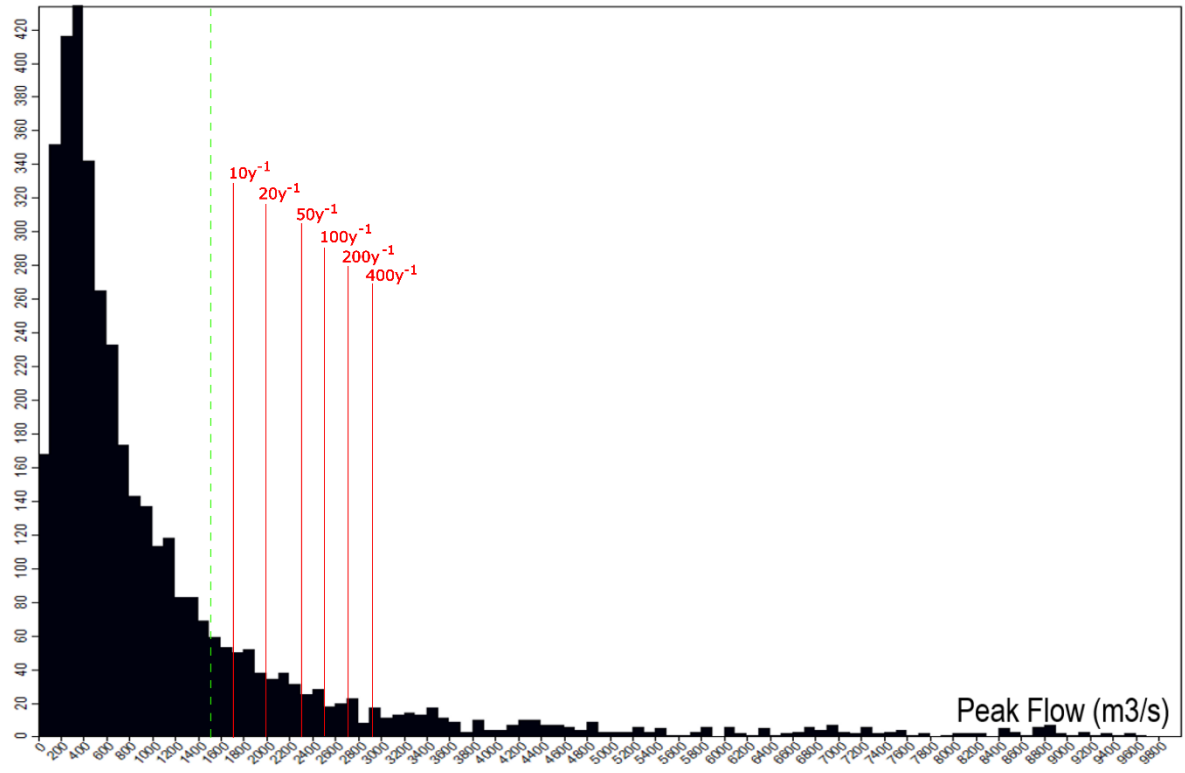

Figure 3.8 Count of peak discharge outburst floods (in m^3s^{-1}) from the modelling in the Callery catchment. As reference, the red lines represent the equivalent recurrence time of flooding for the Waiho River. The green dotted line represents the 1500 m^3s^{-1} discharge cutoff.

The resulting distribution is strongly positively skewed, which could be attributed to the known fractal dimension of mountainous landscapes and river networks (Rosso et al., 1991; Rigon et al., 1994). This distribution could be directly attributed to Horton's law (1945) in which the number of streams is correlated to the stream order by the following equation:

$$N_\omega = R_B^{\Omega-\omega} \quad (3)$$

where N_ω is the number of streams, the corresponding order ω, the order of the basin Ω and the

bifurcation ratio, R_B. Horton's law also applies to the geometric area drained by streams of a given order. Consequently, this relationship would link the impoundment capacity (of a landslide dam) and the stream order. The long tail distribution of peak flows in Figure 3.8 corresponds to this proposition.

Based on the same set of geomorphological assumptions for the dam parameters, several regression equations are tested to capture the uncertainty of the model and of the regression equations.

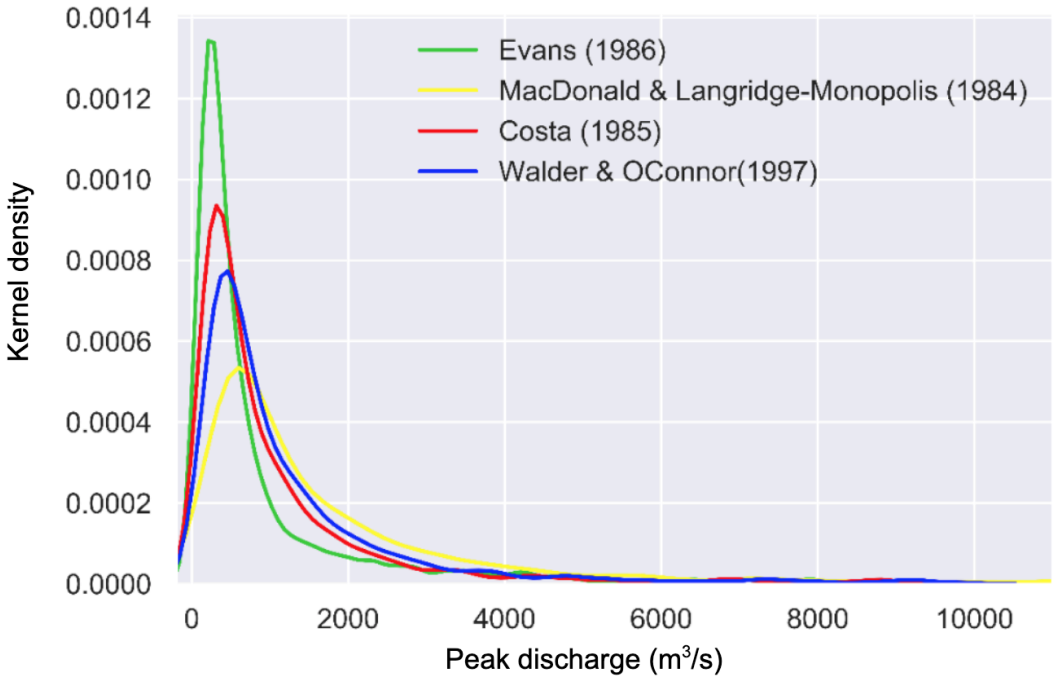

Figure 3.9 Distribution of peak discharges in the Callery river for different regression equations (see Table 3.1)

The statistical results of peak discharge values for dam heights of 40, 60, 70, 80, 100, 120, 170 and 200 m are presented in Table 3.2.

Table 3.2 Summary of results from dam break flood modelling in the Callery Gorge

Hd(m)	Stats	Qp_Evans(m3/s)	Qp_MacDonald and Langridge-Monopolis(m3/s)	Qp_Costa(m3/s)	Qp_Walder and O'Connor(m3/s)
40	mean	308	535	293	380
	std	368	482	277	331
	min	0	0	0	0
	max	1974	2482	1432	1703
60	mean	537	964	542	673
	std	683	929	548	627
	min	0	0	0	0
	max	3487	4566	2705	3077
70	mean	637	1172	665	814
	std	802	1125	669	756
	min	0	0	0	0
	max	3847	5251	3130	3525
80	mean	728	1376	786	951
	std	906	1310	784	876
	min	0	0	0	0
	max	4185	5923	3549	3962
100	mean	842	1699	979	1167
	std	1016	1561	943	1038
	min	0	0	0	0
	max	4626	7019	4237	4672
120	mean	1027	2135	1243	1457
	std	1245	1974	1204	1304
	min	0	0	0	0
	max	5288	8395	5108	5559
170	mean	1506	3307	1963	2228
	std	1853	3114	1936	2031
	min	0	0	0	0
	max	7361	12533	7759	8202
200	mean	1796	4047	2424	2709
	std	2227	3850	2415	2497
	min	0	0	0	0
	max	8814	15415	9631	10028

Figure 3.9 shows that the different regression equations generate a wide variety of results. This can be explained by the variety of geomorphological parameters used in the regression equations and the inherent uncertainty of those equations (Wahl, 2004; Yi et al., 2010). For the purpose of preparedness, the use of average, mean, minimum and "worst case" values seems to be the best option to estimate a range of outburst flood scenarios for the Callery river and to inform risk reduction measures for Franz Josef.

Ollett (2011) modelled 6 historic and potential future landslide dam sites along the Callery river. Four different models comprised of three different methods were selected to assess the potential for outburst flood: one empirical model (Costa's Regression equation), two erosion models

(Mike11 DB and BREACH) and one parametric model (OLLETT) (Ollett, 2011). Models results are compared for the various sites Figure 3.10:

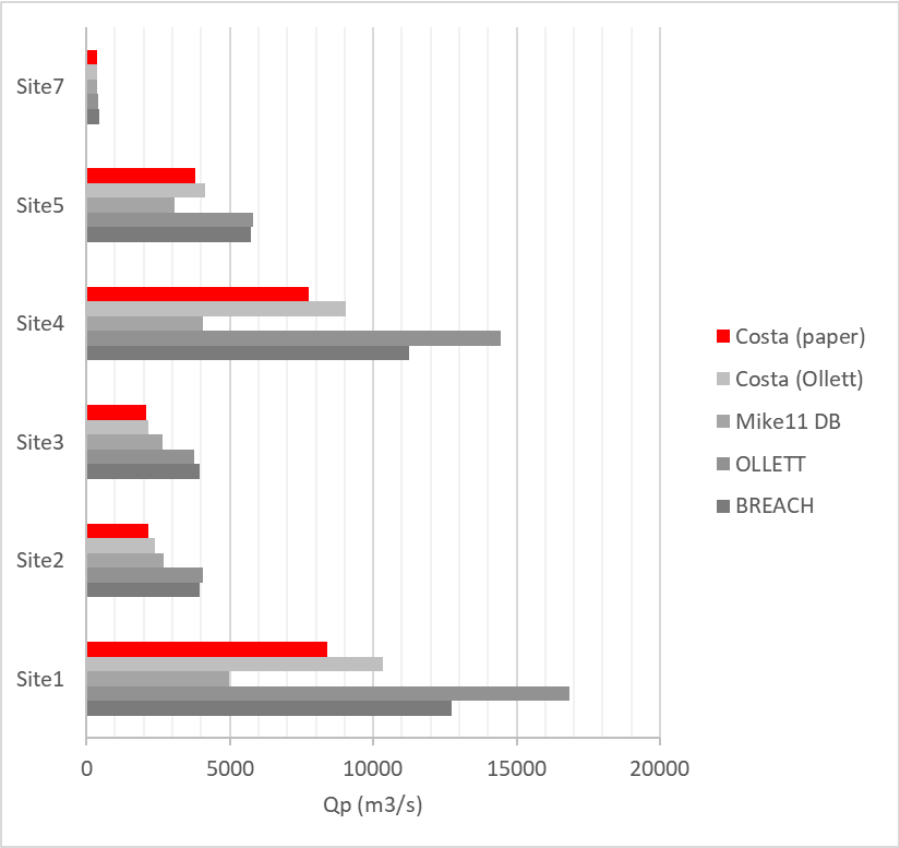

Figure 3.10 Comparison of the regional assessment results presented in this paper (in red – Costa equation) with the results from Ollett (2011) (in grey – various equations)

Figure 3.10 shows that on a site-to-site comparison, the regional model seems to give plausible results in line with previous detailed studies using advanced physical models (Ollett, 2011). As a matter of clarity, a cutoff of 1,500 m^3s^{-1} has been used to filter the results and map the base case peak discharges (for Hd=70 m, Hb=70 m) in Figure 3.11. The cutoff was established at 1,500 m^3s^{-1} as it is below the 10 year recurrence interval flood flow of 1,700 m^3s^{-1} for the Waiho river (Gardner 2014).

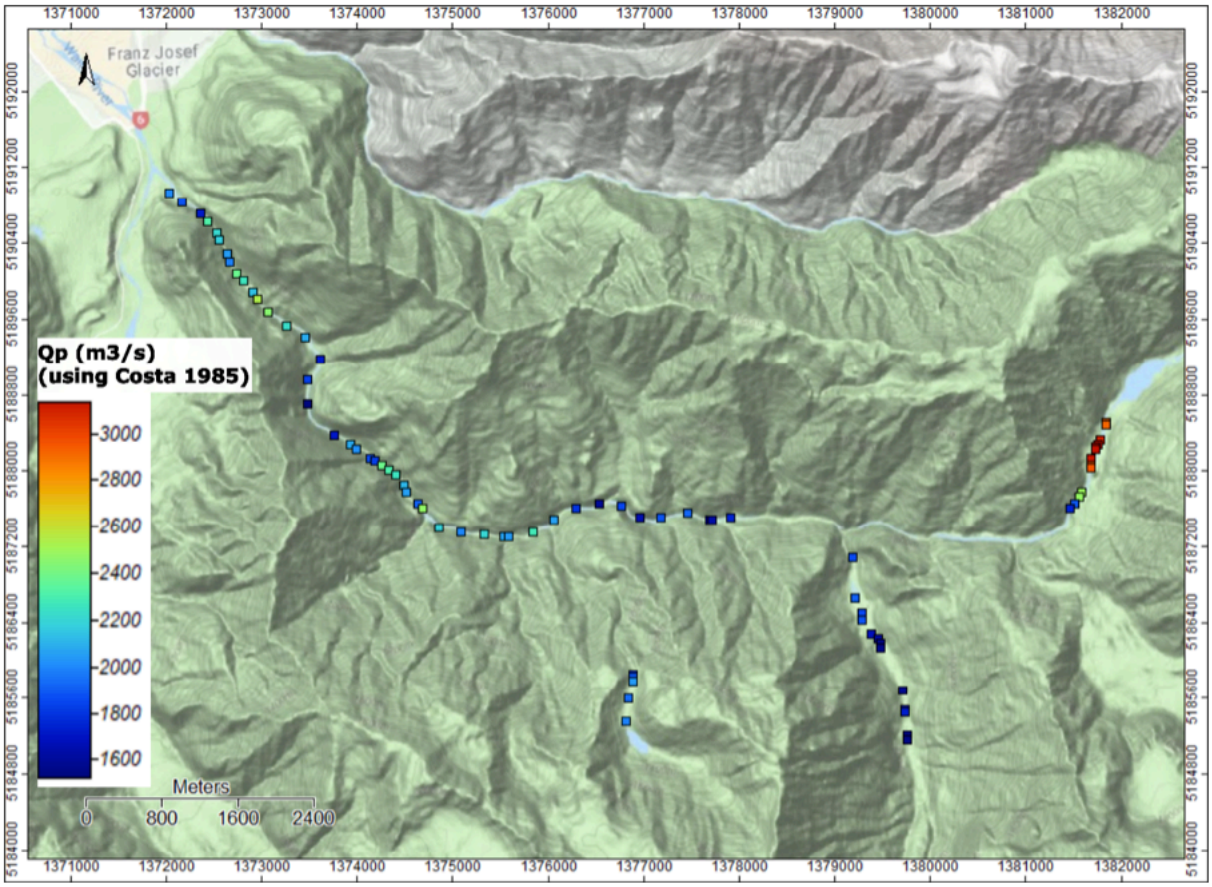

Figure 3.11 Peak outflow map calculated according to the Costa regression equation (Costa, 1985) for landslide dam height of 70 m and 70 m breach depth along the Callery river. For clarity, a cutoff of 1,500 m^3s^{-1} has been applied to display the dams.

Figure 3.11 shows, as expected, that the main channel of the river contains most of the high peak discharge potential (more than 2000 m^3s^{-1}), while the second order streams have limited peak discharge capacity. Nevertheless, it is to be noted that some locations outside of the main channel can also produce peak discharge in excess of 2,000 m^3s^{-1}. These numbers are in line with previously published material on the Callery river (Davies, 2002; Korup, 2005) and compare with a 20-years Average Return Interval (ARI) flood discharge (*Waiho River – Hydraulic Modelling and Options Analysis,* 2014). This is a reminder that careful attention should be given to second order streams because they may create high impounded volumes due to local geomorphological features.

The largest values of peak discharge modeled are located at the boundary between the river and the glacier upstream in the Callery gorge, with base case discharge in excess of 3,000 m^3s^{-1}. The increased peak discharge is most likely related to the widening of the valley closer to the glacier and corresponding increase in stored water volumes.

It is also to be noted that recent models of potential flooding for Franz Josef township showed that a discharge of 2,900 m^3s^{-1} would be equivalent to a normal rainstorm flood return period of 400 years (Gardner, 2014). According to the modeling presented here, these values of discharge are exceeded in the Callery gorge base case scenario (Hd=70 m) and could reach extreme peak discharge values in the event of a larger blockage (Figure 3.8). To give a perspective on the potential consequence of a dam break flood, the current available flood modeling for the 10, 20, 50 and 100-year ARIs are presented in Figure 3.11. It is to be noted that the presented models are based on 2014 data (e.g. bed levels, stopbanks, 3 m LIDAR DEM) and ignore bed topography changes during the event. Furthermore, the Waiho river flow is the accumulation of the Callery tributary and the Waiho river (Figure 3.6). Hence, the value of outburst flow from the Callery river would need to be added to the flow from the Waiho catchment to get the resulting downstream flood flow. From the HIRDS database (NIWA), the mean annual flood from the Waiho catchment is estimated to be 561 m^3/s. The mean value should be used as the recurrence time for the upstream flow of the Waiho is uncertain and not correlated to a landslide dam scenario from the Callery river.

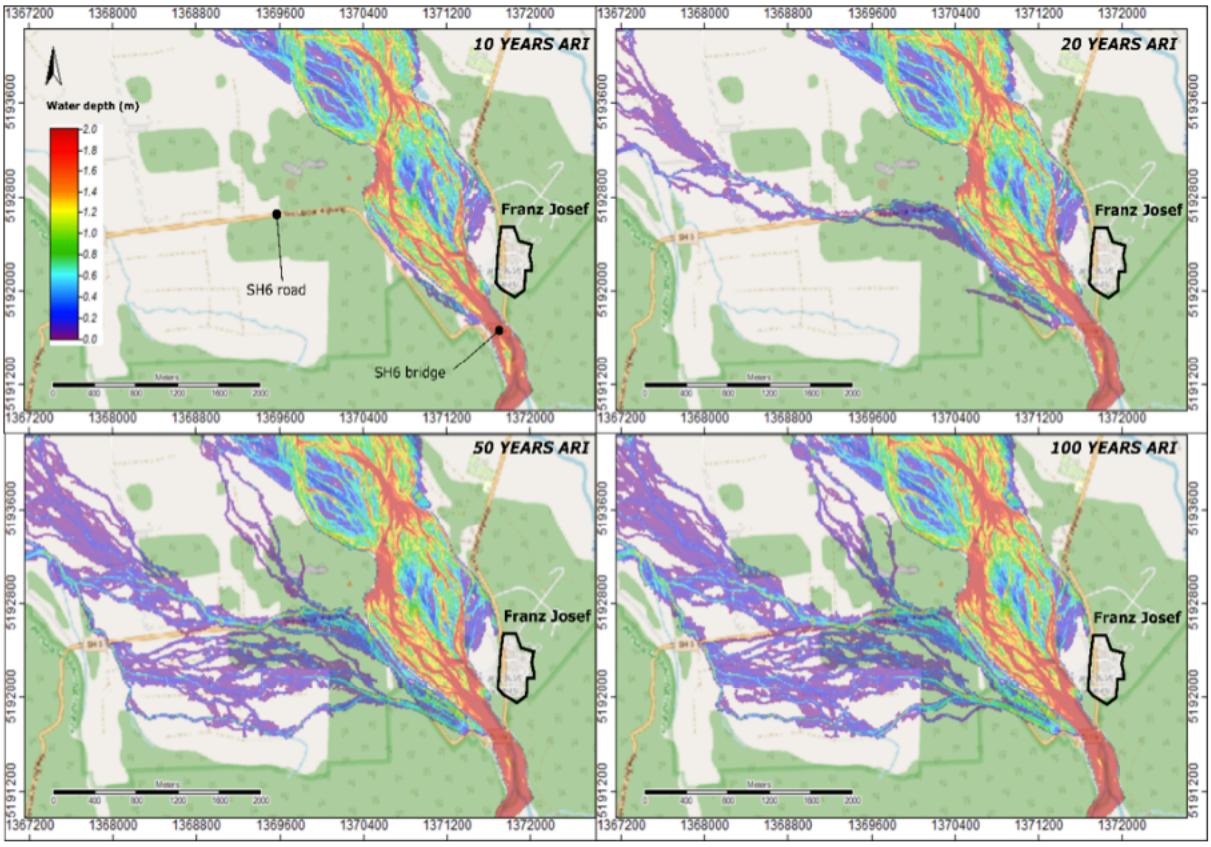

Figure 3.12 Flood maps focused on the Franz Josef township surroundings. The black outline highlights the Franz Josef town center. (Gardner, 2014). The road and bridge are labeled as reference of potential impact from flooding beyond the impact on the township itself.

Downstream of the main town side stopbank, the 10 year ARI flood scenario could overtop and flood the town terrace. Impacts on the road system and vehicle transit could be severely impaired starting from a 20 year ARI flood. As pointed out by Gardner (2014), the Southside stopbanks (left bank) could be at risk of overtopping with flow less than 1,700m^3s^{-1}, which is equivalent to an ARI of 10 years. Greater flood flow would aggravate the impact following the same pattern as lower flows with larger inundated areas and higher water depth. It is to be noted that the current flooding model does not show the sediment load, together with organic matter such as tree branches and trunks, that would be carried during a dam break flood event, making a dam break flood event more dangerous than the equivalent rainfall flood. In addition, the depth distributions of larger peak discharges (more than 3,000 m^3s^{-1}) are not known. This is in part because the flood

footprints have not yet been modelled for larger discharges, and also because the sustainability of the stopbanks protecting the Franz Josef township to larger discharge is not well known; it also results from the inevitably large sediment load carried by larger discharges, which rapidly alters the bed and land surface profiles and diverts flows unpredictably. Ollett (2011) estimated values of flows where the discharge becomes hazardous. As a reference, the hydraulic capacity through the Waiho bridge was estimated to be in the order of 3,000 m^3s^{-1} (Ollett, 2011). It is to be noted that, as this paper was being written (March 2019), the Waiho bridge collapsed due to bank erosion during a period of intense (20-year ARI; https://www.newshub.co.nz/home/new-zealand/2019/03/waiho-bridge-collapse-costing-region-1m-a-day-westland-mayor.html) rainfall and flooding with, so far, unstudied discharge; this emphasises the vulnerability of assets to extreme discharges.

3.6 Discussion

Several limitations exist in the current method. Landslide dams have highly varying morphology and the present method is optimized for narrow valley environments. Therefore, errors can arise if the area of blockage is not well constrained (e.g. partial blockage, small watershed area upstream of the dam or inadequate DEM resolution). Although the algorithm can be applied in a variety of contexts, it has to be clear to the user what the calculation entails. As observed in the Callery gorge case study, the model does not behave well outside or on the fringe of catchments. The main cause of miscalculations is related to the wrong upstream area being picked by the model to calculate reservoir volumes. The resolution and quality of the data also have an impact on the results, the Tangjiashan case study being an example of poor data leading to unreliable results.

Furthermore, for the purpose of informing emergency plans, the method assumes an immediate release and a complete failure of the dam (Hd=Hb). While this is a conservative approach, users

must bear in mind that consequences may be different if the dam failure is partial or delayed. Finally, the present work partially tackles the issue of the potential extent of downstream flooding and the attenuation of the flow between the dam and the nearest assets vulnerable to flooding, following a dam break event. As mentioned earlier, the large flood volume combined with the narrow aspect (thus the lack of storage) of the Callery gorge would likely lead to minor, if any, attenuation of the flow before it reaches the gorge mouth (Ollett, 2001); however, this might not be the case in other catchments. Models and software for estimating the spatial distribution of flooding from outburst floods are sparse. Even more unusual is the capacity to carry out this exercise on large scale with multiple river blockage locations, as in the present work. Further research needs to focus on generating cumulative susceptibility maps from outburst floods at the catchment scale.

3.7 Conclusion

Despite the limitations intrinsic to the study of complex systems such as landslide dams, the simple quantitative method presented here shows promising results. Few tools are available to give a quantitative assessment of landslide damming events at a regional scale with "light" hardware and input. The tool presented here permits the testing of various dam sizes, which could form the basis of a statistical analysis. It is suggested that, through this forecasting methodology, pre-emptive measures for reducing the risks from outburst and backwater flooding are possible - for example, regional screening can highlight areas of higher relative danger. Hence, results can inform more detailed studies over targeted sites with more accurate (and demanding) modelling, which together inform budget, policies and resource allocations for risk reduction. The investigation, recording and understanding of landslide dam occurrences remains vitally important for communities living in mountainous environments as large uncertainties persist in the understanding of transitional phenomena at the intersection between gravitational and

hydrological processes. From an engineering perspective, few data are available on New Zealand stopbanks and their capacity to withstand high discharges, accompanied by large volumes of sediment and woody debris, from landslide dams. In the case study of dam break flood risk to Franz Josef from the Callery catchment, thought should be given to this issue as the township is located on a low-lying area immediately adjacent to the Waiho River, from which it is separated by a system of stopbanks. Finally, the longer-term consequences of landslide dam failures (e.g. river aggradation, landslide-river coupling, and feedback loops) should also be a topic of research as they are not yet extensively studied.

3.8 Acknowledgements

The authors would like to thank Resilience to Nature's Challenges (RNC) for funding this research. We would like to thank the many contributors that provided models and information without whom this work would not have been possible, especially Matthew Gardner who provided the flood models.

3.9 References

Adams, J. (1981). *Earthquake-dammed lakes in New Zealand. Geology, 9(5), 215-219.*

Bricker, J. D., Schwanghart, W., Adhikari, B. R., Moriguchi, S., Roeber, V., & Giri, S. (2017). Performance of Models for Flash Flood Warning and Hazard Assessment: The 2015 Kali Gandaki Landslide Dam Breach in Nepal. *Mountain Research and Development*, *37*, 5–15. https://doi.org/10.1659/mrd-journal-d-16-00043.1

Carrivick, J. L., Jones, R., & Keevil, G. (2011). Experimental insights on geomorphological processes within dam break outburst floods. *Journal of Hydrology*, *408*(1–2), 153–163. https://doi.org/10.1016/j.jhydrol.2011.07.037

Costa, J. E. (1985). Floods from dam failures (Vol. 85, No. 560). US Geological Survey.

Costa, J. E., & Schuster, R. L. (1988). Formation and Failure of Natural Dams. *Bulletin of the Geological Society of America*, *100*(7), 1054–1068. https://doi.org/10.1130/0016-7606(1988)100<1054:TFAFON>2.3.CO

Costa, J. E., & Schuster, R. L. (1991). Documented historical landslide dams from around the world. *U.S. Geological Survey Open-File Report*, 494.

Cui, P., Dang, C., Zhuang, J., You, Y., Chen, X., & Scott, K. M. (2012). Landslide-dammed lake at Tangjiashan, Sichuan province, China (triggered by the Wenchuan Earthquake, May 12, 2008): Risk assessment, mitigation strategy, and lessons learned. *Environmental Earth Sciences*, *65*, 1055–1065. https://doi.org/10.1007/s12665-010-0749-2

Dai, F. C., Lee, C. F., Deng, J. H., & Tham, L. G. (2005). The 1786 earthquake-triggered landslide dam and subsequent dam-break flood on the Dadu River, southwestern China. *Geomorphology*, *65*, 205–221. https://doi.org/10.1016/j.geomorph.2004.08.011

Davies, T. (2002). *Landslide-dambreak floods at Franz Josef Glacier township, Westland, New Zealand: A risk assessment*. *41*(1), 1–17.

Davies, T., Manville, V., Kunz, M., & Donadini, L. (2007). Modeling Landslide Dambreak Flood Magnitudes: Case Study. *Journal of Hydraulic Engineering*, *133*(July), 713–720. https://doi.org/10.1061/(ASCE)0733-9429(2007)133:7(713)

Dellow, S., Massey, C. I., & Cox, S. C. (2017). Response and initial risk management of landslide dams caused by the 14 November 2016 Kaikōura earthquake, South Island, New Zealand. *New Zealand*, 8.

Dong, J.-J., Tung, Y.-H., Chen, C.-C., Liao, J.-J., & Pan, Y.-W. (2011). Logistic regression model for predicting the failure probability of a landslide dam. *Engineering Geology*, *117*(1–2), 52–61. https://doi.org/10.1016/j.enggeo.2010.10.004

Duman, T. Y. (2009). The largest landslide dam in Turkey: Tortum landslide. *Engineering Geology*, *104*, 66–79. https://doi.org/10.1016/j.enggeo.2008.08.006

Evans, S. G. (1986). The maximum discharge of outburst floods caused by the breaching of man-made and natural dams. *Canadian Geotechnical Journal*, *23*(3), 385–387. https://doi.org/10.1139/t86-053

Fan, X., Tang, C. X., Van Westen, C. J., & Alkema, D. (2012). Simulating dam-breach flood scenarios of the Tangjiashan landslide dam induced by the Wenchuan Earthquake. *Natural Hazards and Earth System Science*, *12*(10), 3031–3044. https://doi.org/10.5194/nhess-12-3031-2012

Fan, Xuanmei, van Westen, C. J., Xu, Q., Gorum, T., & Dai, F. (2012). Analysis of landslide dams induced by the 2008 Wenchuan earthquake. *Journal of Asian Earth Sciences*, *57*, 25–37. https://doi.org/10.1016/j.jseaes.2012.06.002

Froehlich, D. C. (1995). PEAK OUTFLOW FROM By David C. Froehlich ; Member , ASCE. *Journal of Water Resources Planning and Management*, *121*(1), 90–97.

Froehlich, D. C. (2008). Embankment Dam Breach Parameters and Their Uncertainties. *Journal of Hydraulic Engineering*, *134*, 1708–1721. https://doi.org/10.1061/(asce)0733-9429(2008)134:12(1708)

Gardner, M. (2014). Waiho River: Hydraulic Modelling and Analysis. *Land River Sea Consulting Ltd Report for West Coast District Council*. Retrieved from http://www.wcrc.govt.nz/Documents/Natural Hazard Reports/Waiho River Modelling Final Report.pdf

Hancox, G. T., McSaveney, M. J., Manville, V. R., & Davies, T. (2005). The October 1999 Mt Adams rock avalanche and subsequent landslide dam-break flood and effects in Poerua river, Westland, New Zealand. *New Zealand Journal of Geology and Geophysics*, *48*(4), 683–705. https://doi.org/10.1080/00288306.2005.9515141

Hayashi, S., Uchida, T., Okamoto, A., Ishizuka, T., Yamakoshi, T., & Morita, K. (n.d.). *Counter measures against landslide dams caused by typhoon talas 2011*.

Kofler, C., Comiti, F., Gems, B., Thiebes, B., Schneiderbauer, S., & Schlögel, R. (2017).

Advancing Culture of Living with Landslides, Volume 4 Diversity of Landslide Forms. 685–692. https://doi.org/10.1007/978-3-319-53485-5_79

Korup, O. (2004). Geomorphometric characteristics of New Zealand landslide dams. *Engineering Geology*, *73*(1–2), 13–35. https://doi.org/10.1016/j.enggeo.2003.11.003

Korup, O. (2005). Geomorphic hazard assessment of landslide dams in South Westland, New Zealand: Fundamental problems and approaches. *Geomorphology*, *66*(1–4), 167–188. https://doi.org/10.1016/j.geomorph.2004.09.013

Liu, F., Fu, X., Wang, G., & Duan, J. (2012). Physically based simulation of dam breach development for Tangjiashan Quake Dam, China. *Environmental Earth Sciences*, *65*(4), 1081–1094. https://doi.org/10.1007/s12665-011-1025-9

Liu, N., Zhang, J., Lin, W., Cheng, W., & Chen, Z. (2009). Draining Tangjiashan Barrier Lake after Wenchuan Earthquake and the flood propagation after the dam break. *Science in China Series E: Technological Sciences*, *52*, 801–809. https://doi.org/10.1007/s11431-009-0118-0

MacDonald, T. C., & Langridge-Monopolis, J. (1984). Breaching Charateristics of Dam Failures. *Journal of Hydraulic Engineering*, *110*, 567–586. https://doi.org/10.1061/(asce)0733-9429(1984)110:5(567)

Nash, Bell, D., Davies, T., & Nathan, S. (2008). Analysis of the formation and failure of Ram Creek landslide dam, South Island, New Zealand. *New Zealand Journal of …*, *51*(3), 187–193. https://doi.org/10.1080/00288300809509859

Nibigira, L., Havenith, H.-B., Archambeau, P., & Dewals, B. (2018). Formation, breaching and flood consequences of a landslide dam near Bujumbura, Burundi. *Natural Hazards and Earth System Sciences*, *18*, 1867–1890. https://doi.org/10.5194/nhess-18-1867-2018

Ollett, P. P. (2011). *Landslide dambreak flooding in the Callery River, Westland*. Doctoral dissertation, Lincoln University.

Peng, M., & Zhang, L. M. (2012a). Analysis of human risks due to dam break floods—Part 2:

Application to Tangjiashan landslide dam failure. *Natural Hazards*, *64*, 1899–1923. https://doi.org/10.1007/s11069-012-0336-9

Peng, M., & Zhang, L. M. (2012b). Breaching parameters of landslide dams. *Landslides*, *9*, 13–31. https://doi.org/10.1007/s10346-011-0271-y

Perrin, N. D., & Hancox, G. T. (1992). Landslide-dammed lakes in New Zealand preliminary studies on their distribution, causes and effects. *Landslides. Glissements de Terrain, Balkema, Rotterdam*, (1457–1466).

Pratt-Sitaula, B., Garde, M., Burbank, D. W., Oskin, M., Heimsath, A., & Gabet, E. (2007). Bedload-to-suspended load ratio and rapid bedrock incision from Himalayan Landslide-dam lake record. *Quaternary Research*, *68*(1), 111–120. https://doi.org/10.1016/j.yqres.2007.03.005

Rigon, R., Rinaldo, A., & Rodriguez-Iturbe, I. (1994). On landscape self-organization. *Journal of Geophysical Research: Solid Earth*, *99*, 11971–11993. https://doi.org/10.1029/93jb03601

Rosso, R., Bacchi, B., & Barbera, P. L. (1991). Fractal relation of mainstream length to catchment area in river networks. *Water Resources Research*, *27*, 381–387. https://doi.org/10.1029/90wr02404

Safran, E. B., O'Connor, J. E., Ely, L. L., House, P. K., Grant, G., Harrity, K., … Jones, E. (2015). Plugs or flood-makers? The unstable landslide dams of eastern Oregon. *Geomorphology*, *248*, 237–251. https://doi.org/10.1016/j.geomorph.2015.06.040

Stefanelli, C., Segoni, S., Casagli, N., & Catani, F. (2016). Geomorphological analysis for landslide dams. *Landslides and Engineered Slopes. Experience, Theory and Practice*, 1883–1887. https://doi.org/10.1201/b21520-235

Thompson, C. (2011). *HIRDSV3: High Intensity Rainfall Design System, National Institute of Water and Atmosphere, Wellington.*

Tien, P. V., Sassa, K., Takara, K., Fukuoka, H., Dang, K., Shibasaki, T., … Loi, D. H. (2018).

Formation process of two massive dams following rainfall-induced deep-seated rapid landslide failures in the Kii Peninsula of Japan. *Landslides*, *15*, 1761–1778. https://doi.org/10.1007/s10346-018-0988-y

Wahl, T. (2004). Uncertainty of Predictions of Embankment Dam Breach Parameters. *Journal of Hydraulic Engineering*, *130*(5), 389–397. https://doi.org/10.1061/(ASCE)0733-9429(2004)130:5(389)

Walder, J. S., & O'Connor, J. E. (1997). Methods for predicting peak discharge of floods caused by failure of natural and constructed earthen dams. *Water Resources Research*, *33*, 2337–2348. https://doi.org/10.1029/97wr01616

Wang, B., Zhang, T., Zhou, Q., Wu, C., Chen, Y. L., & Wu, P. (2015). A case study of the Tangjiashan landslide dam-break. *Journal of Hydrodynamics*, *27*(2), 223–233. https://doi.org/10.1016/S1001-6058(15)60476-0

Yi, S., Xie, Y., & Zuo, X. (2010). A risk analysis information model with uncertainty for flood hazard of dam-break. *2010 18th International Conference on Geoinformatics*, 1–6. https://doi.org/10.1109/GEOINFORMATICS.2010.5567620

Zhang, J., Li, Y., Xuan, G., Wang, X., & Li, J. (2009). Overtopping breaching of cohesive homogeneous earth dam with different cohesive strength. *Science in China Series E: Technological Sciences*, *52*, 3024–3029. https://doi.org/10.1007/s11431-009-0275-1}

Chapter 4
Multi-hazards risk assessment methodology, a New Zealand trial

---

Alexandre Dunant[1], Mark Bebbington[2], Tim Davies[1]

[1] Department of Geological Sciences, University of Canterbury, Christchurch

[2] Institute of Fundamental Sciences, Massey University, Palmerston North

Overview

The pilot study developed in Chapter 2 and the tool developed Chapter 3 are used in this Chapter to create a fully probabilistic multi-hazard risk assessment methodology. This quantification exercise is tested on the Franz Josef area, in the West Coast region of the South Island, New Zealand, which has been identified previously as at risk from multiple natural hazards.

Contributions

The concept of the manuscript was developed through discussions between Alexandre Dunant, Tim Davies and Mark Bebbington. Alexandre Dunant, Tim Davies, Mark Bebbington designed the research objectives. The flood modelling was provided by Matthew Gardner. The PSHA source model was provided by QuakeCoRE (University of Canterbury) and run by Alexandre Dunant. The Landslide modelling was done using the Flow-R model provided by Pascal Horton (University of Bern) and run by Alexandre Dunant. Alexandre Dunant created the graphical multi-hazard methodology, modelling and wrote the manuscript. All co-authors carried out in-depth reviews of the manuscript and offered much useful discussion of results and interpretations.

4.1 Abstract

Franz Josef in the West Coast region of the South Island, New Zealand, has been the focus of risk assessments for many years because of the geographical location of the township, at the confluence of many threats from the natural environment. Despite the obvious need for multi-hazard quantification in such locations, few methods combine complex hazard interactions and geographically intelligible outputs. For this reason, existing quantitative risk assessments of Franz Josef township have barely considered interacting natural hazards. We show that a recently developed graphical multi-hazard risk assessment method can provide an in-depth exploration of the disaster system. The spatial interaction between the elements acts as the basis for risk quantification. We consider the interactions and impacts of earthquake, rainfall, landslide, landslide dam and flooding hazards on the road network, stopbanks and housing at Franz Josef.

The results show that high probability / low magnitude losses are earthquake-dominated, while rarer events show a strong influence of landsliding on the losses, especially for the building stock. The output of this work can be further used as sensitivity analyses for more detailed studies, "real-life" drills and mitigation measures. In the current context of risk aggravation (climate change, urban development, population increase etc.), quantitative outcomes speak to the need to apply the already flourishing disciplines of complex and interconnected systems to natural-hazard-related risks.

4.2 Introduction

New Zealand is located at the focus of several dynamic environmental forces. On the Ring of Fire and in the path of the Roaring Forties, the country from time to time experiences high-impact natural events. An additional feature of the New Zealand landscape is its susceptibility to so-called

multi-hazard events, as demonstrated by numerous recent events such as the 1999 Mt Adams landslide (Hancox et al., 2005) and the 2016 Kaikōura earthquake (Dellow et al., 2017; Hughes et al., 2015; Jibson et al., 2018; Robinson & Rosser, 2017). Franz Josef township, a rapidly-developing tourist centre in the West Coast region of the South Island, New Zealand, is a prime example of vulnerability to multi-hazard events and has been a focal point of risk studies for many years – earthquakes from the Alpine fault, landslide and landslide dam risk, river aggradation leading to increased flood risk are few of the examples from scientific literature (e.g. Davies, 2002; Langridge et al., 2016; McSaveney & Davies, 1998).

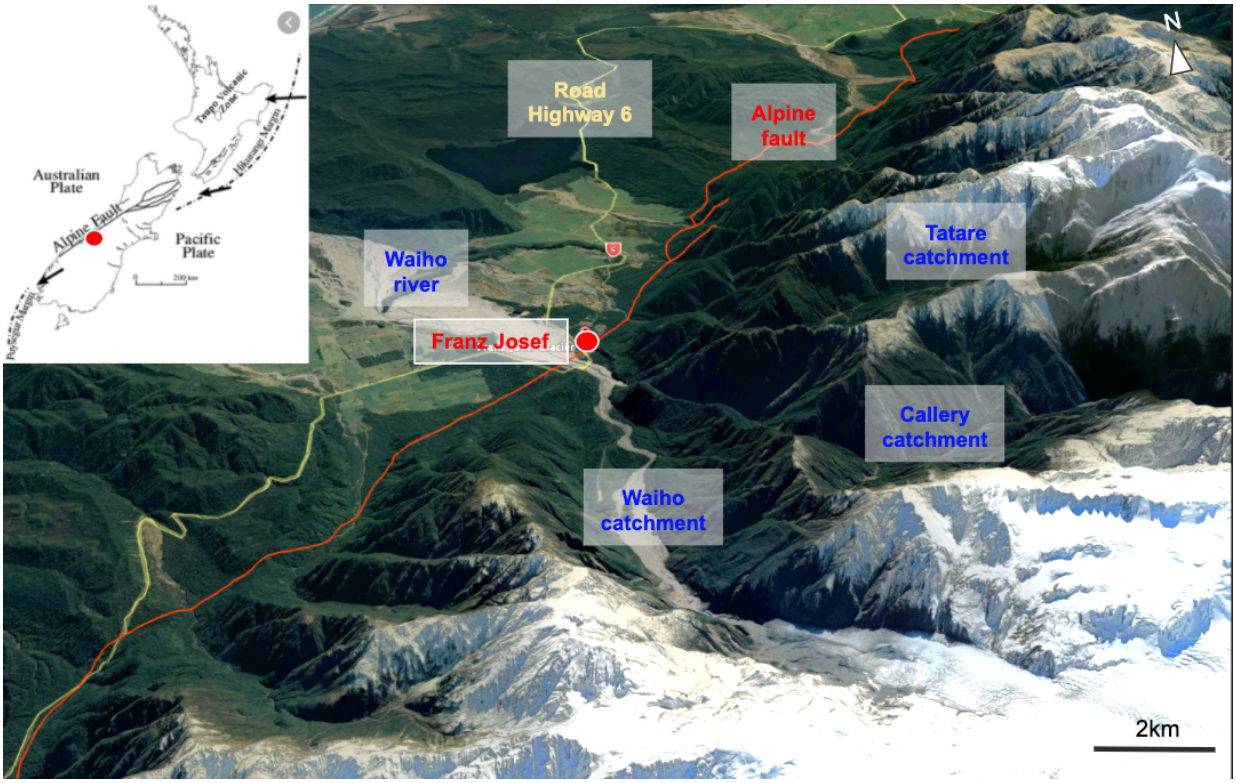

Figure 4.1 Overview of Franz Josef township and its hazardous landscape

Figure 4.1 shows Franz Josef township located on the Alpine fault - the plate-boundary fault that runs along the western range front of the Southern Alps, with the potential for large-magnitude earthquakes (Biasi et al., 2015). In addition, the mountainous environment combined with the weather pattern of the southwest Pacific brings world record rainfalls in the river catchments – up

to 700 mm in one day and 15,000 mm in one year (Henderson & Collins, 2016). Flooding of the township by the adjacent Waiho river is a well-known and well documented threat (Davies, 1997, 2002; Davies et al., 2003). The combination of climatic and tectonic processes can further cascade into landsliding (Kritikos, 2013; Robinson et al., 2016) and landslide dambreak flooding (Davies, 1997, 2002; McSaveney & Davies, 1998).

Multi-hazard risk assessment has been identified in recent years as a topic that urgently requires further research (AghaKouchak et al., 2018; Pescaroli & Alexander, 2015). Due to the complexity inherent in quantifying interacting natural events, multi-hazard risk assessment is often limited to qualitative or semi-quantitative methods (Kappes et al., 2012). Attempts to quantify risk beyond the "single-layer multi-hazard" type of assessment (Gill & Malamud, 2014) have been made, but constraints, such as the lack of geographical representation or the limited number of interacting hazards, still remain (Tilloy et al., 2019).

Dunant et al., (Chapter 2, paper in review) suggested a causal graphical approach to overcome some of the barriers to multi-hazard assessment. This method is used herein to demonstrate the value of using a complex graphical approach, by quantifying multi-hazard risk to the Franz Josef township, while also providing novel insights for planning to reduce vulnerability to future events and for fostering innovative ideas.

4.3 Material and methods

4.3.1 Overview of the graphical method

As the purpose of this paper is to test the novel methodology on the multi-hazard risk to the Franz Josef township, this section will provide only an overview of the graphical method; for more details

refer to Dunant et al., (Chapter 2). In summary, the graphical risk assessment methodology uses graphs and a complex system approach to model a distribution of multi-hazard impacts.

The workflow can be divided into two main parts: network construction and network simulation. In network construction, predetermined elements considered relevant to the risk assessment (e.g. earthquake, house, river, road etc.) are mapped out as points, also called nodes. Based on their potential impact footprint, the nodes are then linked using standard modelling techniques and expert opinion (e.g. because "earthquake" can have an impact on "house", the two are directionally connected attributes). The ensemble of the source/target links (also called edges) constitute the disaster graph. In the second part, network simulation, the graphical representation of the network is simulated iteratively; initial activations can be propagated along the network branches based on weighted conditions. Those conditions can include the attribute values initially extracted at the node location, the node type, existing empirical relationships, threshold values and, more generically, known behaviors. Certain branches of the network become then more likely to be “activated” than others (e.g. a landslide node should propagate more often to a nearby downslope house node than to a distant house node).

A large number of ‘scenarios’ are then simulated. In this context, a scenario can be defined as one complete set of discrete pathways from the initial nodes to the end nodes of the graph. The resulting scenario attributes are recorded, and a new scenario is then started that will follow a different cascading path along the network based on a randomisation exercise (for further details, see Dunant et al., (Chapter 2)). This iterative process relies on a Monte Carlo simulation to generate several hundred thousand unique individual scenarios to deliver probabilistic outputs. This process generates a large dataset that can be interrogated in the context of the purpose of the exercise. Examples of outputs are given later to characterise the multi-hazard risk to Franz Josef township.

4.3.2 Franz Josef hazard system

As identified in previous studies, Franz Josef township is threatened by a number of hazards (Langridge et al., 2016). A review of existing studies and expert judgement alongside supervisors, have identified several components of the disaster system in the Franz Josef area (Barth, 2014; Benn, 2005; Biasi et al., 2015; Davies, 1997; DTEC Consulting, 2002; Korup, 2003, 2005; Kritikos, Robinson, & Davies, 2015; Langridge et al., 2016; McSaveney & Davies, 1998; Robinson & Davies, 2013). The hazard elements used in the present modelling are earthquake shaking (due to activity of the Alpine fault and other sources), rainfall, flooding from the Waiho river, landsliding, and a landslide dam in the Callery catchment; while the potentially vulnerable elements are houses, roads and the stopbanks of the Waiho river. The risk of liquefaction has been treated in fragility functions. In the future, liquefaction might be treated as a specific hazard instead. Hazard and exposure elements have been digitised as nodes (Figure 4.2).

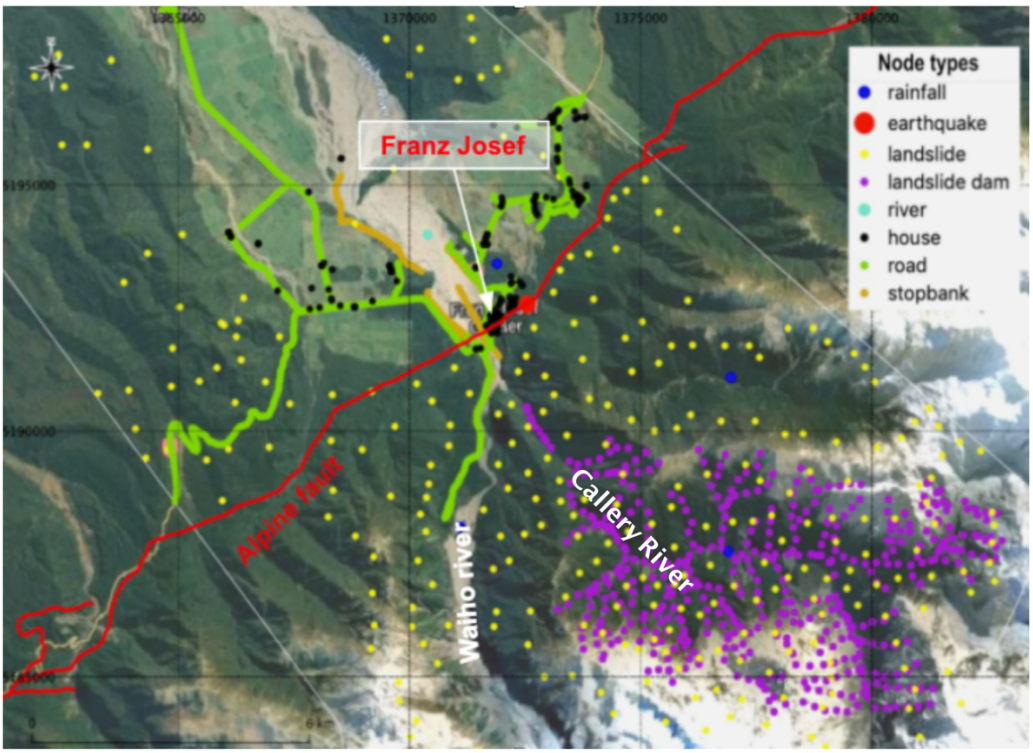

Figure 4.2 Elements of the hazard system in Franz Josef area

Based on its type, a hazard node can have a causal effect on other nodes (e.g. earthquake shaking can impact houses). These causal connections can be assumed from modeling their hazard footprint and examining intersections with the spatial location of other nodes (Dunant et al., Chapter 2). The rationale for each node type, and its associated hazard modelling, are described in the following paragraphs.

Earthquake: the node location was placed on the Alpine fault trace. The node location is nominal only. The node represents the potential earthquakes related to regional seismicity, most (but not all) of which are likely related to Alpine fault ruptures (Berryman et al., 2012; Biasi et al., 2015). The hazard footprints associated with the earthquake node are Probabilistic Seismic Hazard (PSH) expressed as maps showing the spatial distribution of peak ground velocity (PGV in cm/s). PSH maps are modeled for the recurrence intervals of 2, 5, 10, 25, 50, 100, 200, 500, 1000, 5000

and 10000 years. PSH maps have been generated using the National QuakeCoREmodel (Tarbali & Bradley, 2014), with the median percentile of the Ground Motion Prediction Equation (GMPE) model to predict the peak ground velocity associated with each recurrence interval. The limitations of using PSHA are related the size of the studied area, the tectonic setting and the number of faults contributing to the model. In the case of the area studied herein, the seismic activity above the 5-year recurrence interval is dominated by the Alpine fault. Hence, the results remain correct for damaging scenarios. In the future, the study of larger areas would be more challenging as contributions from multiple faults would cause an overestimation of shaking intensities. The option to use OpenQuake is already being implemented to generate stochastic earthquake event simulations.

Rainfall: Four rainfall nodes are part of the system studied here. One node is placed on the front of the mountain range, then one node for each main river catchment. Rainfall modelling was sourced from the National Institute of Water and Atmospheric Research (NIWA) national rainfall model (Thompson, 2011). Spatial distributions of rainfall intensity (mm/24h) were provided for recurrence intervals of 10, 20, 50 and 100 years.

Landslide: The locations of landslide nodes represent the centroid points of order 1 stream catchments in the study area. In this case, and in contrast to the earthquake and rainfall nodes, each landslide node represents a geographical landslide source area that can be triggered by either earthquake (co-seismic landslides) or rainfall (rainfall-induced landslides). Modelling of the landslide hazard footprints calculated the cumulative runout susceptibility for every slope in the catchment. To do this, the software Flow-R was used (Horton et al., 2013) to provide landslide runout susceptibility maps for the two potential triggers (earthquake and rainfall). The inputs for the Flow-R model are a DEM and a source area in a binary format (a pixel value of “0” is not triggered, a value of “1” is triggered). To capture the worst-case scenarios, a simplistic approach

was taken, assuming that every slope above 10º gradient could potentially be triggered (so given a value of 1). A volumetric distinction is made between earthquake-triggered landslides and rainfall-triggered landslides. From Larsen et al., (2010), the depths of failure (scar depth) of rainfall-triggered and of earthquake-triggered landslides were selected using the 50th percentile scar depth value for the largest soil landslide area and bedrock landslide area. Thus, the scar depths assumed for rainfall and earthquake triggered landslides are 2m and 50m respectively. Consequently, two distinct runout models were created with the parameter for the maximum angle of reach set to 0.1 for both models in order to account for long-runout scenarios (Legros, 2002). The end product of the Flow-R modelling is a distribution of cumulative susceptibility of run-out values based on the number of times a pixel has been "covered" by a modeled landslide runout. This value was normalised between 0 and 1.

The assessment of whether a landslide node would impact another node of the system was established by a step-by-step process. It is to be noted that this process is greatly simplified by the use of a graphical framework (e.g. thousands of spatial nodes modelled with specific spatial properties, requiring a relatively low computing resource).

First, the triggering event must be large enough to cause a landslide (see Table 4.1 for details). Second, as slope gradient is a driving force in landslide susceptibility (Robinson et al., 2016), a randomisation process assures that the steeper slopes are more likely to trigger landslides. Then, a landslide node is triggered. As explained earlier, each landslide node represents an area. This area value is calculated using a GIS software geometry toolbox to calculate the area of the associated polygon (order 1 catchment), and the probability of a random portion of this area contributing to a landslide can be assessed. Indeed, existing empirical relationships, established from previous landslide inventories, link source areas to their probability density (Malamud et al., 2004). Above the "roll-over" that seems to limit these correlations (Korup, 2005; Malamud et al., 2004), this relationship follows a power-law with a gradient (y). This gradient seems to be constrained to the range [-1.9, -2.6] based on previous seismic events in New Zealand (Hancox,

Ries, Parker, & Rosser, 2016; Malamud et al., 2004; Massey et al., 2018). The Kaikōura landslide inventory (Massey et al., 2018) is located in a different geological setting with a lower exponent (y)=-1.9 and the Inangahua inventory (from the 1968 Inangahua earthquake that struck the Inangahua Junction township with a moment magnitude of 7.1 M_w. The earthquake and its many aftershocks triggered numerous landslides in the surrounding mountains), with exponent (y)=-2.6, is likely to represent less damaging events than the Murchinson set with an exponent of (y)=-2.4 (C.Massey, GNS Science Ltd, PO Box 30368 Lower Hutt, New Zealand *pers. comm.*). The setting of the Murchison landsliding inventory following the 1929 earthquake (7.3 M_w with landslides impacting many roads) is somewhat different from an Alpine setting, but it could be the best available proxy for local landsliding in the Franz Josef area. Other datasets were available but treated only rainfall-triggered landslides (Hovius et al.,1997). Thus, the Murchison inventory was used as an analogue for the modeling presented herein with an exponent (y)=-2.4. Based on this empirical relationship, a random individual landslide area is triggered for each scenario generated. The lower bound of the area triggered ranges starts at 5,000 m^2 to reduce the computing time by focusing on the more damaging medium- and large-size events and to avoid the not fully understood “roll-over effect” observed in landslide inventories (Frattini & Crosta, 2013). The upper bound is limited to the source area, which is constrained by the total area that the node represents. Hence, it is expected that the most damaging landslide events will be captured by the scenario simulations. The volume of the landslide is then determined based on the power law exponent (y) existing in the literature between area (A, just calculated) and volume (V) (Larsen et al., 2010):

$$V = A^{y} \tag{4}$$

It is to be noted that a variety of specific relationships for such parameters could be used instead of the ones used herein.

The rainfall-induced and earthquake-induced landslide volumes were treated separately with respective exponents of 1.13 for New Zealand soil and 1.49 for New Zealand bedrock (Larsen et al., 2010). The Flow-R model was then used to assess the directionality of the landslide. A randomisation exercise points to the most likely target for the landslide, which allows discrimination between targets by the distance from the landslide source (is the target node far away or close?) and the topography (is the target node on a high spot or in a depression?). Finally, existing empirical relationships are used to check if the runout (L_{max} in km) and distance to target is in line with the triggered volume (V in km^3) (Legros, 2002):

$$Lmax = 8\,V^{0.25} \tag{5}$$

This was done for every landslide node previously triggered. Because of its lobate shape, a specific landslide might impact several other nodes. To calculate the impact on individual nodes, the landslide volume is divided by the number of targets. It assumes that the landslide volume is equally distributed between the targets of the landslide. Even though this approach is simple, it permits to record a more accurate volume distribution of landsliding contributing to the impact. As the vulnerability function for landsliding is currently binary (i.e. damage for a particular asset is either complete (100%) or non-existent), the volume actually doesn't matter for loss prediction. Alternative methods should be found if non-binary fragility functions are used with landsliding. Also, in the rare case that a specific node is targeted by several landslides (hence coming from different locations), the volumes are summed. This assumes that the landslide deposits will accumulate at the target location.

Landslide dam: nodes are placed every 250 m along the Callery river where the likelihood of landslide dams, and their potential impacts, are well documented (Davies, 2002; Korup, 2005). The narrow shape of the valley with steep slopes makes it a prime location for river blockage. The

dam height is calculated based on the previously logged landslide volume on a landslide dam node. This calculation is established from known geomorphological characteristics of New Zealand landslide dams which show that a relationship exists between landslide dam height and landslide dam volume (Korup, 2004). Based on a range of dam heights (40, 60, 70, 80, 100, 120, 170 and 200 m), a GIS routine algorithm was created (Chapter 3) to calculate the appropriate peak flow from an outburst flood at each node location. This resulting flow is based on the empirical equation of Costa (1985), linking the dam height (h in m) and lake volume (S in m^3) to the flow (Q in m^3/s).

$$Q = 181(S \,.\, h)^{0.43} \quad (6)$$

Flood / Waiho river: A single node is used to represent the Waiho river (flow). For display purposes this is shown on the Waiho River path in Figure 4.2, but the location is nominal (the node spatial coordinates don't have an impact on the multi-hazard model). The associated flood models (inundation depths) were obtained from Gardner (2014) for Waiho River flows of 1,700, 2,000, 2,300, 2,500 and 2,900 m^3/s. Additional modelling simulated the consequences of a stopbank breach by overtopping along the Franz Josef township side of the river (Gardner, 2016). The "overtopping" flood map was merged with the existing flood models to have a parallel set of "breaching" floods. It is recognized that each flow discharge will have a different "overtopping" flood depth, but these data were not available.

Houses: nodes represent the building stock in the area. The asset portfolio was obtained from Riskscape version 1 software. RiskScape is a risk assessment tool developed in New Zealand for analysing potential economic and social impacts from multiple natural hazards (King & Bell, 2005). The asset portfolio contains the location of each building as a point shape file. Because of the patchy quality and age of the dataset, the details of the asset types are uncertain. The project

required the use of RiskScape exposure data, and the 2005 dataset was the most up to date (asset data may easily be updated once they become available). The decision was made to consider the building stock as single-story timber frame houses (the most common type in New Zealand, https://teara.govt.nz/en/building-materials/page-1). This design is likely to resist earthquake shaking relatively well (compared to brick masonry for example) and, therefore, provide a cautious estimate of the potential losses. In the same manner, individual house prices were estimated using the median house price by region in 2018 (https://www.reinz.co.nz/residential-property-data-gallery). For the West Coast of New Zealand, the average cost of a property is estimated at NZD 219,000 and this value was used as an individual price for each node (https://www.globalpropertyguide.com/Pacific/New-Zealand/Price-History). The fragility curve for single-story timber frame housing (Table 4.1) was obtained from the RiskScape version 1 software (King & Bell, 2005).

Roads: nodes represent the road system in the Franz Josef area. The road shape file was obtained from the publicly available Land Information New Zealand (LINZ) database (https://data.linz.govt.nz/). The nodes were located every 50 m along the road lines. The cost of damage to a road segment is difficult to estimate as few pricing data are publicly available. Quotes for repair/reinstatement can vary by several orders of magnitude depending on the environment (urban or rural), road type, landscape type, traffic flow and several other factors. Hence, each 50 m road segment was estimated to have a construction cost of NZD 270,000, which is equivalent to NZD 5.4 million per km. As a comparison, information gathered put the cost of road construction in Spain at 3 million euros per km or about NZD 5 million per km in a rural environment (https://www.tecnocarreteras.es/2012/02/22/sabemos-cuanto-nos-cuesta-tener-de-forma-optima-las-infraestrcturas-y-servicios-que-garantizan-nuestra-seguridad-vial/). This cost is conservative (low) for a functioning road on the West Coast of New Zealand. Some of the potential secondary hazards from an earthquake, such as surface rupture and liquefaction, have not been

included at the hazard level in the work presented herein. However, these cascading effects have presented serious threats in the past (Bray et al., 2014) and have to be acknowledged. Liquefaction and surface deformation have been integrated at the fragility function level for the roads. The fragility curve for the road system assumes damage from liquefaction at lower level of shaking and an increase in damage at higher levels of shaking, because of increased liquefaction susceptibility and surface rupture (Table 4.1 for more details). This addition of hazard to the vulnerability is not ideal as the liquefaction has local features that should be treated at the hazard level. Future work will include the susceptibility of liquefaction (Idriss & Boulanger, 2006; Youd & Hoose, 1977) combined with local threshold shaking values as a trigger mechanism. Note that the consequential costs of road outage at Franz Josef will be much higher than replacement cost and were not considered herein (Following the Kaikōura earthquake, a large part of the impact on GDP was related to long term disruptions of infrastructure (McDonald et al., 2017)).

Stopbanks: nodes represent the stopbanks that prevent the Waiho river from flowing through the township and adjacent land (Figure 4.2). Lines represent the centerline of stopbanks of the Waiho river, with data provided by WSP Opus. The nodes were placed every 50 m along the line shapefile. The stopbanks can be impacted by seismic shaking and fault rupture, reducing their capacity to provide adequate flood protection (Green et al., 2011). Despite the lack of information on stopbank fragility, the effects of liquefaction and fault rupture on the integrity of stopbanks (Green et al., 2011; Kwak et al., 2016) have been taken into account. A simple approach was taken whereby a PGV between 14 and 80 cm/s is associated with a failure probability of 3% due to liquefaction of the stopbank or its underlying soil. For PGV between 80 and 100 cm/s, the failure probability increases to 30% because of the increased risk of surface rupture. For PGV exceeding 150 cm/s, a probability of failure of 70% due to surface rupture was assumed. A flood overtopping the stopbank is also a possibility. Because the available flood modelling didn't show an overtopping scenario and few data exist about the fragility of the stopbank inventory, a flow of

2,500 m^3/s was assumed to overtop the stopbank and create a failure of the flood protection. While this may seem high, the flow regime of the Waiho river is poorly known (there are no empirical flow data); 2,500 m^3/s is estimated to be about a 100-year return period event (Gardner, 2014), but it is acknowledged that this value is very approximate. The rationale is further presented in Table 4.1.

4.3.3 Causal network creation and simulation

Establishing the interaction between the nodes is a key component of the graphical approach presented herein, and several assumptions were required. The interactions between node types (summarised in Figure 4.3) were defined based on expert judgment (collaborative discussion between the authors and two experienced supervisors in the field of Disaster Risk Reduction) and literature review. Multi-hazard systems evolve over time (e.g. river aggradation following a landslide event in an upstream catchment), hence setting a timeline for the cascading effects at an early stage is paramount. This is because the chosen timeline will determine the events to be modelled and the ones to be left out. For the study presented herein, the timeline for the scenario was set in the immediacy of an initial trigger (earthquake or rainfall). This constrained the events of a scenario to within a few days of the initial trigger (as an example of the constraint on impacts considered, this timeline precludes consideration of longer-term cascading river hazards such as sediment-induced aggradation and flooding). From a model perspective, a continuous chain of events happens within the shortest timeframe possible.

The model recurrence intervals (probabilities) for the events are calculated on an annual basis to ensure consistency within the network.

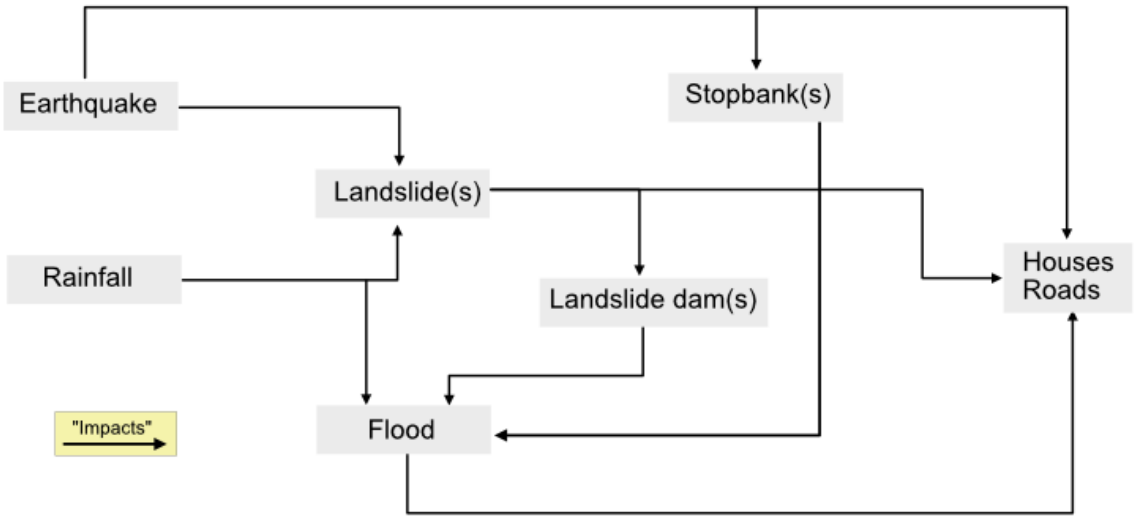

Figure 4.3 Modelled causal interaction of the disaster system in the Franz Josef area

In addition to the connections presented in Figure 4.3, the modelling outlined in the previous section is used to decide which nodes are linked or discarded. The process is automated using initial conditions based on node types (Figure 4.3) and a non-null value of the minimum applicable modelling at the node location (e.g. the shaking values for a 1-year recurrence time earthquake must be non-null at the house geographical location to establish a connection between the earthquake and the house). Other conditions apply to make sure that the node connection is realistic (e.g. landslide nodes connect only with downslope nodes). The large number of nodes and edges makes the network difficult to display clearly in a spatial way using GIS software. Thus, the resulting network is presented without spatial data (Figure 4.4) using the Fruchterman-Reingold force-directed layout algorithm to avoid cluttering (Fruchterman & Reingold, 1991). In this algorithm, the edges are springs between the nodes. The attraction and repulsion between the nodes are determined by analogy with spring forces and electrical forces respectively. In order to allow for a clearer display, highly connected node remain static while the less connected nodes will move away. Consequently, it highlights which node are strongly connected or isolated.

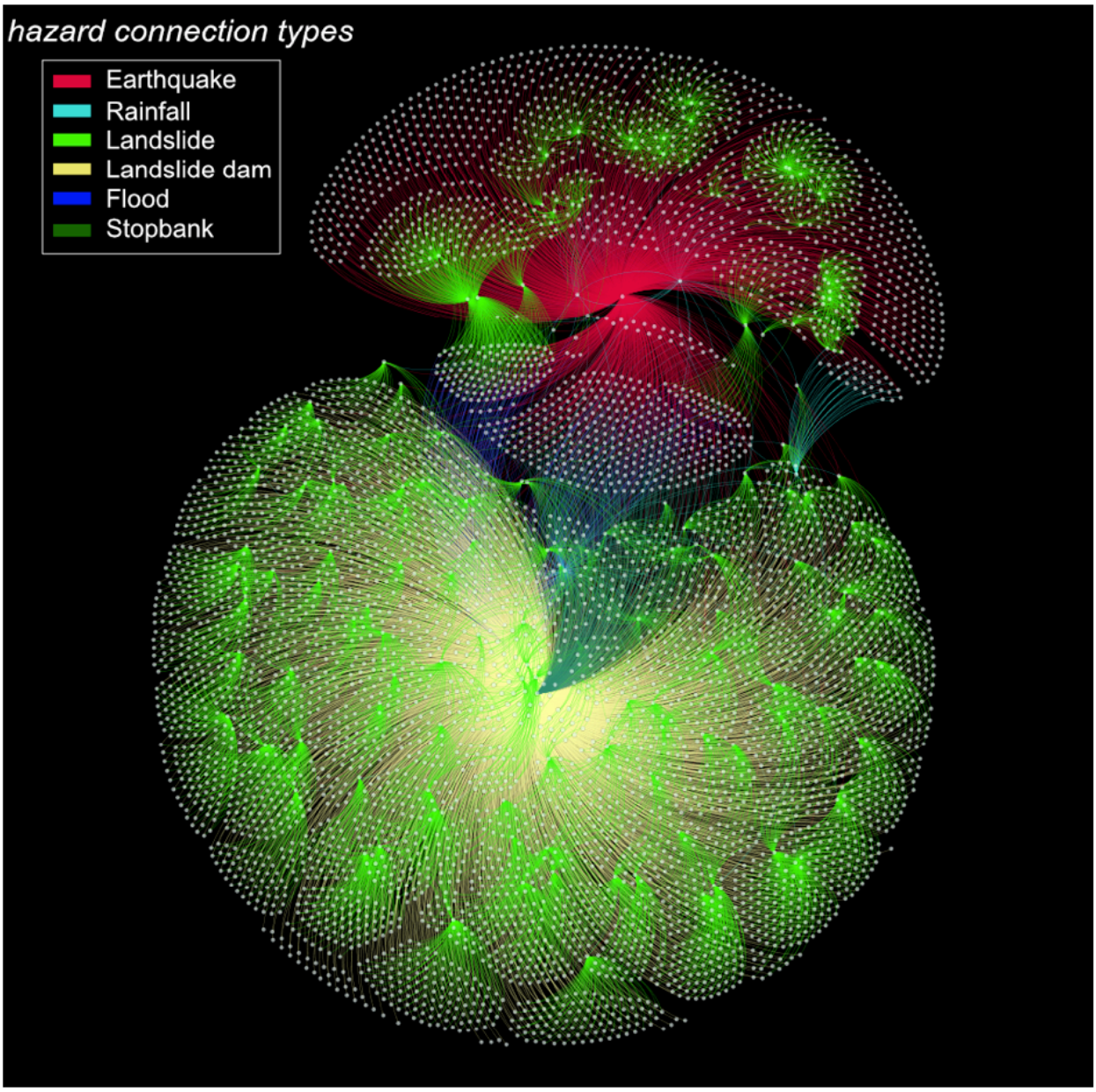

Figure 4.4 Franz Josef network presented without spatial data using the Fruchterman-Reingold force-directed layout algorithm. The white points (nodes) represent the different elements of the disaster system as presented in Figure 4.2. The lines drawn between the nodes (edges) represent the causal interactions. The colors symbolise the hazard type on each edge as per the legend (the road nodes are so numerous that they appear as a line in GIS, hence it can lead to the impression that they are more nodes on Figure 4.4 compare with the GIS layer when they are actually identical).

Figure 4.4 highlights the connectivity of the different hazards in the area. Because of their regional footprint, the earthquake and rainfall nodes connect to a majority of the nodes in the system (red and blue color edges respectively). The landslide nodes only target nodes in reach of the runout

distance (green edges). The landslide dam nodes all point to the flood/river node (light yellow edges).

Then, following the process detailed in Dunant et al., (Chapter 2), scenarios are iteratively generated by initial stimuli propagating from node to node through the network until end points are reached. During a scenario, a randomisation exercise is applied at every cascading node to trigger events based on their specific probability/magnitude pairs. Unlike the process described in Dunant et al., (Chapter 2), where a factor α is used to encourage more severe scenarios for the purpose of exercise design, the algorithm used herein is fully probabilistic, and hence suitable for risk assessment, as it relies only on uniform random numbers. Using Monte Carlo simulation, 1 million scenarios were generated for the Franz Josef area (Figure 4.5).

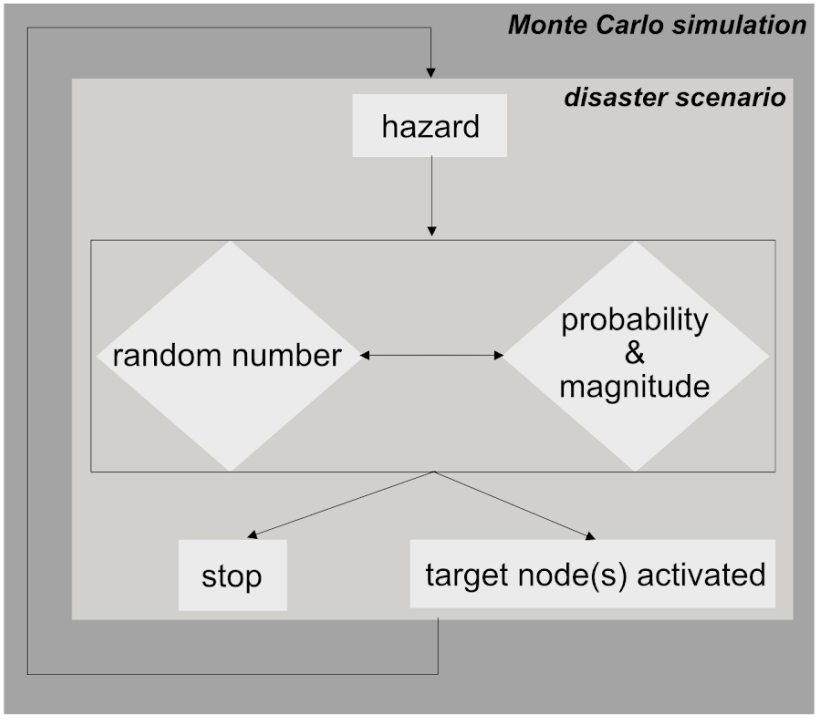

Figure 4.5 Overview of the graphical multi-hazard modelling. Disaster scenarios are nested in a Monte Carlo simulation that "explores" the branches of connectivity between the elements being studied.

The active causal interaction of the elements of the Franz Josef disaster system is further detailed in Table 4.1.

Table 4.1 Hazard-Exposure interactions matrix. The matrix displays the active interaction between nodes depending on their types

Source	Target	Correlation
Earthquake	Landslide	The minimum PGV to trigger a landslide is set at the threshold value of 0.7 cm/s (Tanyaş et al., 2017)
Earthquake	House	The impact of shaking on houses is based on the damage function currently built into Riskscape software for timber frame houses (https://www.riskscape.org.nz/) and adapted for PGV values using the MMI to PGV conversion (Worden, Gerstenberger, Rhoades, & Wald, 2012). The damage ratio function is presented graphically below: 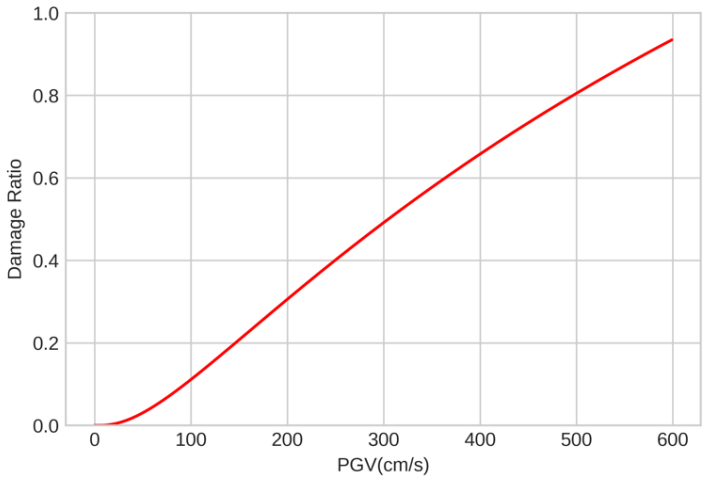
Earthquake	Road	The impact of an earthquake on roads considers the potential damage from either surface rupture and/or liquefaction. Few data exist linking surface rupture, shaking intensity and damage ratios. Nicol et al., (2016) studied the relationship between the probability of surface rupture and magnitude from the New Zealand earthquake catalogue (post 1945). These authors found an increase in the probability of surface rupture from magnitude ~6 Mw up to a maximum probability of 1 for event of ~7.5 Mw. For lower levels of shaking, liquefaction potential is possible and quickly reaches a plateau of “worse” possible liquefaction (based on the Liquefaction Severity Number (Van Ballegooy et al., 2014)). It remains challenging to estimate the impact on roads. Hence, based on the potential shaking intensities predicted for an alpine fault 7.9 Mw scenario (Bradley et al., 2017), experience from the fault

		rupture in Kaikōura (Hamling et al., 2017), current damage ratios used for buildings in Riskscape (that combine shaking and a multiplier for liquefaction) and expert judgement; the following damage ratio function was created for the impact of earthquake on the 50 m road segments: 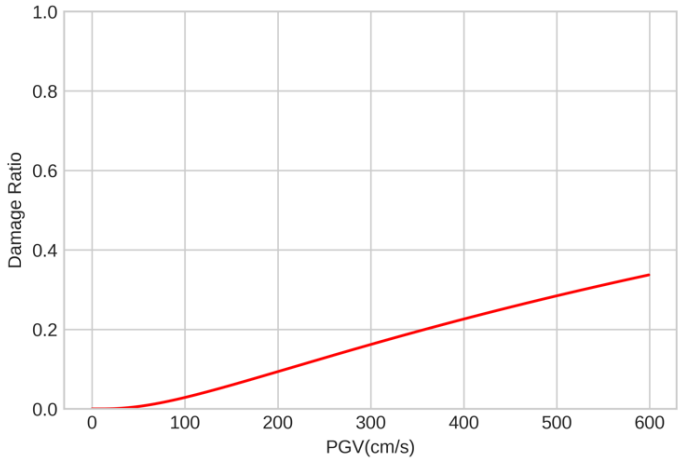
Earthquake	Stopbank	The effect of earthquakes on stopbanks is highly dependent on local geomorphological features (geology, water table etc.) and the quality of the design. Both are not well understood in the Franz Josef area. Despite ongoing initiatives, no flood protection database currently exists for New Zealand. Hence it is challenging to have a detailed understanding of the risk to stopbanks. From the work of Kwak et al., (2016), we drew the probability of failure related to earthquake shaking. In the case of Franz Josef, a simple relationship was used whereby a PGV between 14 and 80 m/s was given a failure probability of 3% due to liquefaction of the stopbank or its underlying soil. From 80 to 100 cm/s, a probability of 30% was given due to the increased risk of surface rupture. For shaking intensity exceeding 150 cm/s, a probability of failure of 70% due to surface rupture was given.
Rainfall	Rainfall	Rainfall intensities and occurrences are mainly affected by the major orography of the "Main divide" in the South Island. The literature points to regional patterns constrained by the mountain range above Franz Josef township (Caloiero, 2014; Salinger et al., 1999). Hence, it is assumed that rainfall intensity should follow similar recurrence interval patterns between catchments during a rainfall event.
Rainfall	Landslide	The minimum rainfall intensity to trigger a landslide was set at 20 mm per 24 hr (Glade, 1998).

Rainfall	Flood / River	The recurrence time of precipitation is used as an indicator of the resulting flow from each respective catchment. From the NIWA website (https://niwa.maps.arcgis.com/apps/webappviewer), peak discharge from the Waiho and Callery catchments were calculated for different recurrence intervals (mean annual, 2, 10, 20, 50, 100 and 1,000 years, based on Henderson and Collins (2018)). For consistency, the flood flow was considered dependent on the initial rainfall recurrence time. As the Waiho and Callery streams are the confluence of the Waiho river, the flood flows are added together to generate a combined flow. This flow value was then associated with the flood footprint closest to this flow value.
Landslide	Landside dam	(1) Empirical relationships exist linking the probability of a landslide to its area (Larsen et al., 2010). This is often expressed as a power law relationship with a gradient dependent of the geographical area of investigation. The Malamud (2004) empirical relationship was used to generate an area of failure based on the generation of a random probability with an exponent of -2.4, which is in range with previous earthquake events in New Zealand (Massey et al., 2018). The area of failure was bound to its maximum by the source catchment area and to its minimum by a set area of 5,000 m^2. Area/volume relationships are also represented by power law with a (y) exponent. In this case, the rainfall and earthquake induced landslides have been treated separately with respective exponents of 1.13 (New Zealand soil, Larsen et al., 2010) and 1.49 (New Zealand bedrock, Larsen et al., 2010). As some areas are more likely to see a landslide runout because of the local topography (e.g. toward accommodation space), the runout susceptibility from the Flow-R software was used. Results represent the number of times a pixel has been covered by a landslide during iterative simulations. For more details on Flow-R, refer to Horton et al., (2013). Rainfall and earthquake induced landslide models were generated as the runout will be different based on the volume activated, which will vary between a shallow and a deep scar scenario. To make sure the results are realistic, the runout distance between nodes is compared with the volume / maximum runout distance relationship from Legros (2002). The volume of landslide is logged on the target node. If a node is targeted by several events, the landslide volume is compounded.
Landslide	House	Refer to (1). The damage sustained by a house is considered binary. The house is either fully destroyed or untouched.
Landslide	Road	Refer to (1). The damage sustained by a road segment targeted is considered binary. The road segment is either fully destroyed or untouched. No long-term disruption is taken into account in this study.

Landslide dam	Flood / River	Based on the total landslide volume at the river location, the height of the dam is calculated. Empirical relationships ties the landslide volume to the dam height (Korup, 2004). The calculated dam height is used to calculate the peak outburst flow based on the equation by Costa (1988). The dimensionless blockage index (DBI) uses the dam height, landslide dam volume and catchment area to estimate the potential blockage or failure of the dam (Ermini et al., 2003). From the DBI value, if a dam is considered unstable, the outburst flow is compared with the rainfall flow and the highest value is kept per catchment. The combined flows of the Waiho river then cascad to the flood node where the appropriate flood footprint is activated.
Flood / River	House	(2) When the flood node is activated, the modelled river flow (from rainfall and/or landslide dam outburst flood) is compared with the existing flood footprints (Gardner, 2016). An additional set of flood models were generated that take into account the fact that stopbanks might have already been compromised by an earlier earthquake or flood flow if higher than 2,500 m^3/s (circa 100-year return period). From the appropriate flood footprint, the water depth at the house's location is recorded. The damage ratio for the timber frame, 1 storey houses is then calculated based on an existing damage function (derived from RiskScape damage function developed by the NIWA) presented below. 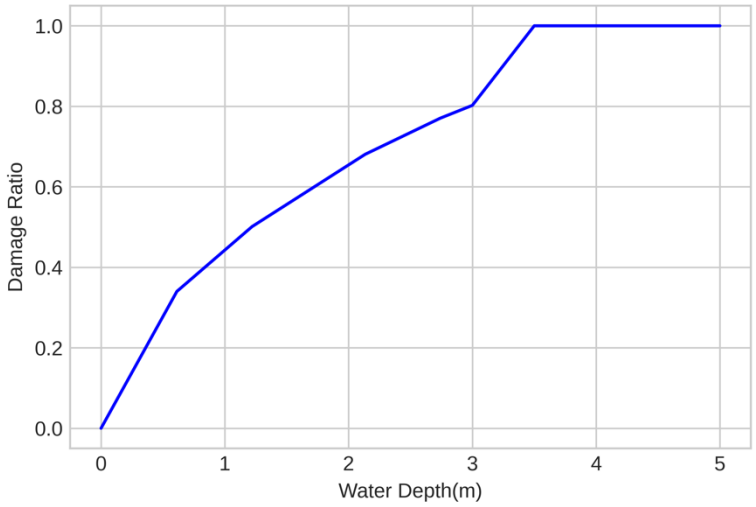
Flood / River	Road	Refer to (2) (Flood/House cell). The damage ratios for the road segments are calculated using the damage function presented below. Flood impact on roads is dependent on local features of the road and the flow speed, which would increase potential erosion

		and scour. These details were not available to us and a damage function was derived from several assumptions and the use of expert judgement. The RiskScape software uses a clean-up cost for the road of NZD 12 per m^2 of road. For the 50 m segment (if we allow for a width of road of 6-10m, it is equivalent to a surface of 300 to 500m^2) it represents close to 1-2% of the segment's initial monetary value. As water depth increases, it is more likely that the discharge would increase and hence the damage ratio, presented below, reflects the increase in damage severity with water depth for the 50 m segment. 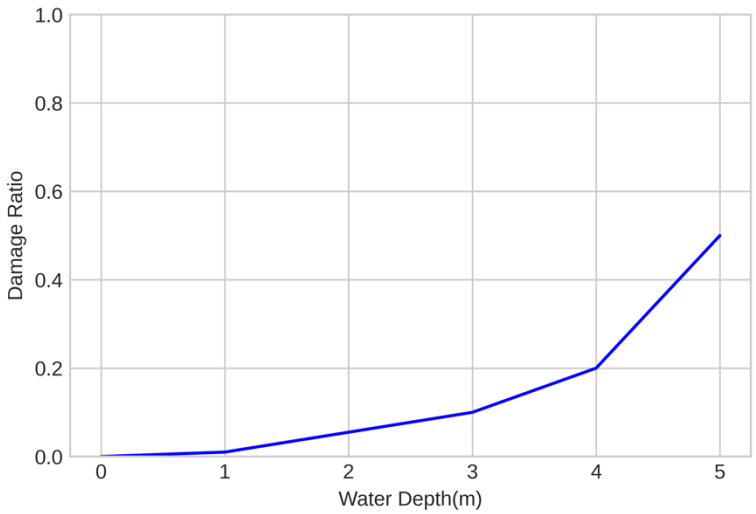
Stopbank	Flood / River	The stopbank could be compromised and feedback into the flood node. Indeed, a flood will likely be more damaging if the stopbank is compromised along the Franz Josef township. See (2) (Flood/House cell) for the effect of flood impact on houses and road segments

Modelled damage to infrastructure elements is based on fragility functions. Because of the difficulties in finding fragility curves in the literature that fulfil the present modeling requirements, expert judgement was used to create the curves required (the authors and two experts focused on the experience from New Zealand disasters and a review of scientific literature). It is to be noted that this approach brings uncertainties to the loss assessment and impacts the outcome but can be improved when improved data become available.

The cascading impacts on infrastructure are treated as follows: the first event impacting a building or road will cause a loss up to its (replacement) cost. This loss, if lower than replacement cost, can be further increased by additional damages from cascading hazards. The maximum loss is capped at the replacement value as this cannot exceed the value of the asset.

4.4 Results

The results are a compilation of the nodes impacted after completion of one million scenarios. This extensive database provides access to a variety of quantitative outputs.

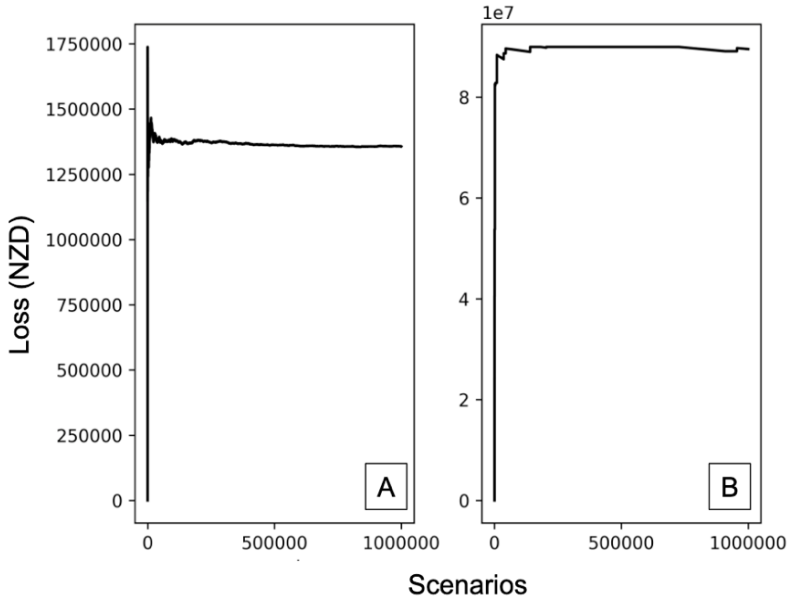

Figure 4.6 Average Annual Loss (A) and Annual 99th percentile loss (B) expressed in New Zealand dollars (NZD)

The Average Annual Loss (AAL) is the mean cumulative expected loss per year over the area of study and the Annual 99th percentile loss is the 99th percentile cumulative loss per year. Only the house stock and the roads are considered in the monetary loss calculation. The AAL reaches a convergence after 500,000 scenarios and the 99th percentile stays relatively stable after the set number of scenarios (one million). Hence, it is expected that one million simulations are sufficient

to capture the range of possible risk outcomes. The AAL reaches a steady value of close to NZD 1.4 million per year.

The distribution of Annual Exceedance Probability (AEP) was calculated and plotted Figure 4.7 for all the assets. As explained earlier, the losses per scenario have been corrected to account for compounding hazard damages where the value of losses would exceed the total value of the asset.

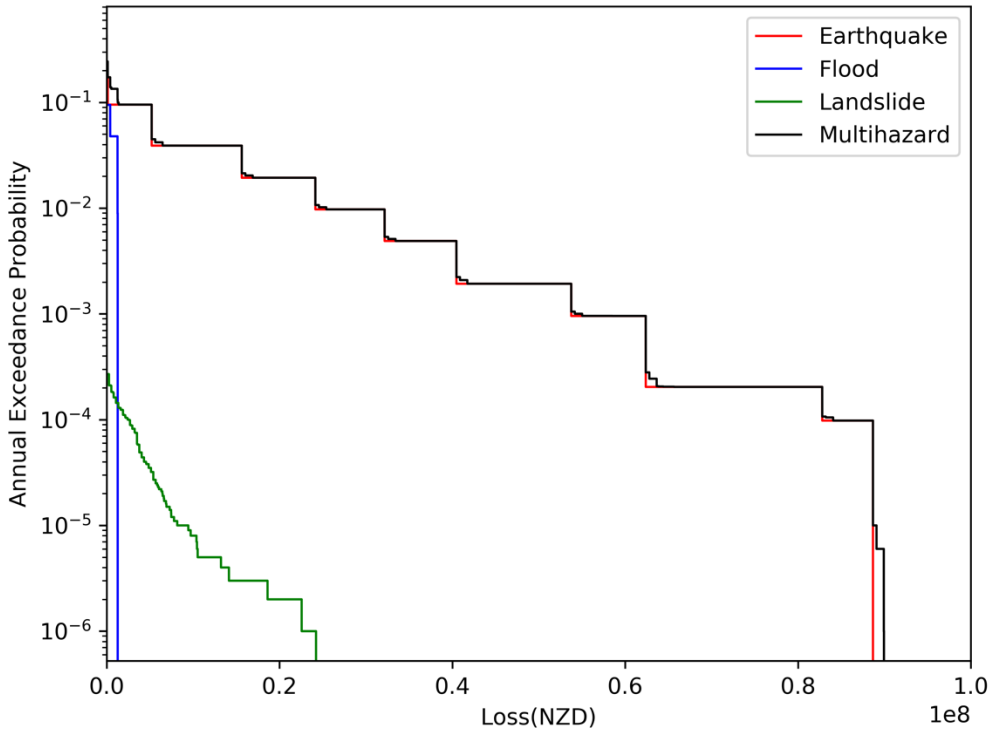

Figure 4.7 Annual Exceedance Probability plots for the Franz Josef area (in NZD)

Figure 4.7 also highlights the AEP for the different hazards to emphasise the various contributions to the monetary loss. Earthquakes appear to contribute to the majority of damage to the overall portfolio (housing, roads, stopbanks). It is worth mentioning that quantifying the probability of landsliding in Franz Josef has been recognised as a challenge due to the “complex interplay between hillslope gradient, the strength of the bedrock and dynamic stress changes operating

within slopes governed by rainfall and seismic shaking" (Langridge et al., 2016), A graphical approach simplifies this quantification as part of a cascading model.

As nodes are spatially defined, depending on the aim, several impact parameters can be mapped. Figure 4.8 shows the spatial representation of mean monetary loss (in NZD) and the distribution of the mean losses over the Franz Josef area after one million scenarios for the exposed nodes impacted. The mean loss is one of many possible outputs (e.g. minimum loss, maximum loss, standard deviation etc.). Furthermore, thanks to the graphical framework, it is possible to highlight the contribution of the causes and the recipients of losses in the study area at the node scale.

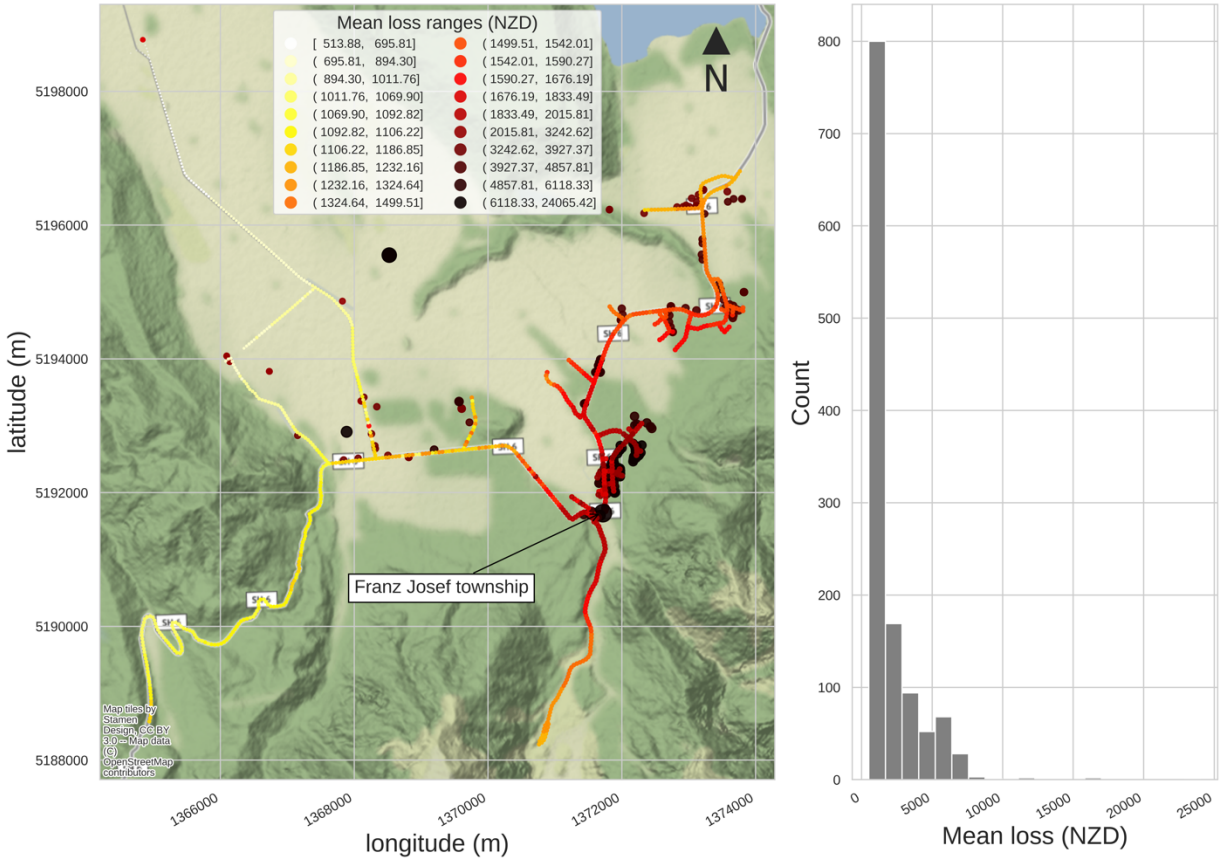

Figure 4.8 Map of modelling results. The recording of each discrete scenario allows the output to be aggregated to user needs. One example is given here with the mean monetary loss after 1 million scenarios (left) and its distribution (right). The size of the point is varied for display purpose, with higher losses having a larger diameter than smaller losses.

In addition, the range of hazard magnitudes was recorded to assess the regional threat level down to 10^{-6} AEP and is presented in Figure 4.9:

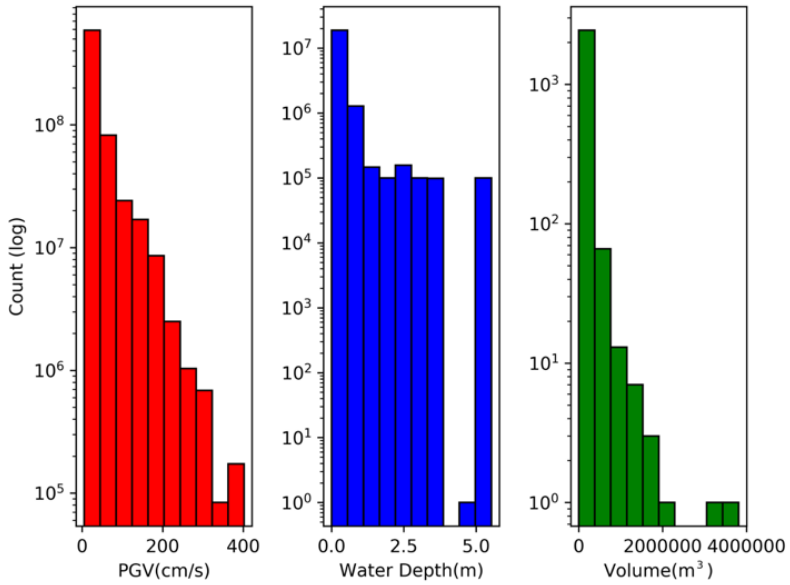

Figure 4.9 Magnitude distribution for earthquake (red, on the left), flood (blue, in the center) and landsliding (green, on the right). It is to be noted that this distribution is available for each asset or group of assets. The high-water depth readings (5m+) are likely related to a road node situated on the edge of the SH6 bridge.

In an attempt to study the discrete properties of highly damaging scenarios, one modelled damaging landslide scenario was investigated in greater detail with its spatial representation displayed in Figure 4.10.

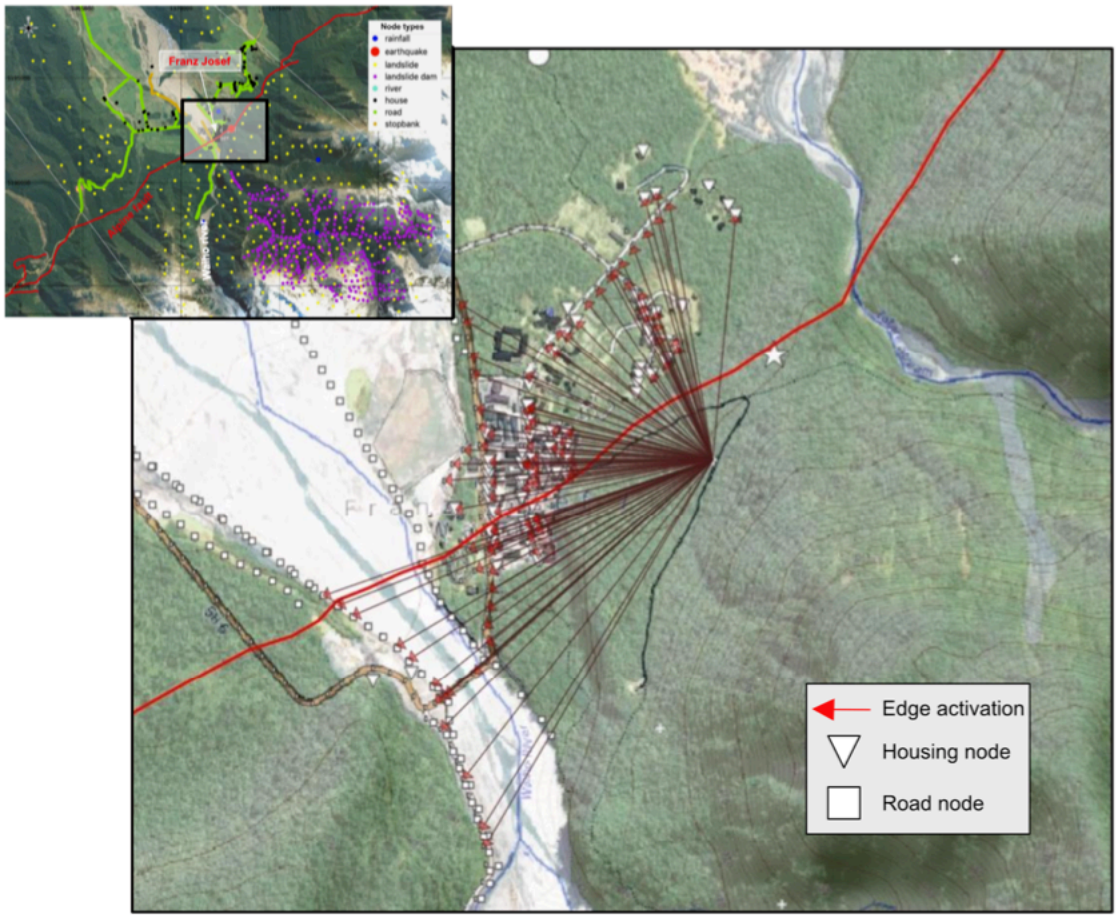

Figure 4.10 Spatial representation of a damaging landslide scenario modelled. The map shows the collapse of the hillslope on the Franz Josef township following an earthquake. Each of the arrows is coming from the hazard node, in this case a landslide node, and pointing toward the targeted exposed elements.

Figure 4.10 shows one of the highly damaging scenarios, comprising a mild 2-year recurrence interval earthquake triggering a large 3.8×10^6 m^3 landsliding event. The main damage is due to collapse of the hillslope immediately overlooking (just south-east of) the township. The runout covers a large section of the township with extensive damage to houses. The largest landslide modelled has a volume of about 3.8×10^6 m^3 and, according to the AEP plot (Figure 4.7), a minimum annual probability of 10^{-6}.

4.5 Discussion

4.5.1 Multi-hazard modeling

A large database of event scenarios has been created and used to quantify the risk from a complex hazard landscape to Franz Josef township on the West Coast of New Zealand, through the use of a causal network stimulated by a Monte Carlo algorithm. This novel risk assessment framework provides, by its granularity, more discrete data to exploit than a standard risk assessment ("Multi-layer single-hazard"; Gill & Malamud, 2016). "Discrete data" refers to the accessibility of all the detailed node interactions after one million scenarios. Accessibility of the full list of hazard cascade attributes facilitates acquisition of data that might fulfill a specific purpose beyond the probabilistic assessment (e.g. asset-specific risk assessment or scenario settings for preparedness planning). As an example, the causal graphical model highlights a specific scenario X that generates complex damage. For scenario X, it is possible to know the cascade of events, their magnitude and the loss sustained by each specific asset (as shown Figure 4.10).

Furthermore, the framework highlights the compounding effect of interacting natural occurrences (Figure 4.7), which might exceed the damage output of any isolated hazard. In the case of Franz Josef, due the proximity and scale of the Alpine fault, annual losses are dominated by earthquakes. Nevertheless, in a multi-hazard landscape, such as Franz Josef, any single-hazard assessment will underestimate the risk from natural hazards. This outcome is particularly noticeable for low-probability events where the multi-hazard losses are higher than the losses from any individual hazard (Figure 4.7). This is in line with previous work (Mignan et al., 2014) that demonstrated the emergence of extreme losses for low-probability scenarios. This can be related to the additional contribution of secondary perils where initial perils reach a "loss ceiling": with reducing probabilities. However, the increasing magnitude of the primary hazard, despite it

reaching the maximum damage, still has the capacity to cascade into greater and greater secondary perils, which cause larger and larger losses by impacting a new set of nodes.

In the current modeling, the different assets in the area sustain damages in a different manner. The assets (housing, road and stopbanks) are overwhelmingly threatened by the impact from the earthquakes. This trend will be greatly affected by the use of different fragility functions. Landsliding is also identified as a serious secondary threat. A proven advantage of the graphical approach is the capacity to quantify stochastically the risk from landsliding, which was often perceived as a difficult challenge. Flood damage is often regarded as the most serious hazard in New Zealand (https://teara.govt.nz/en/floods/page-1) (likely related to the fact that European occupation is relatively recent and that there is a bias toward frequent events); however, the flood damage seems lower than the potential damage from an earthquake for similar AEPs (Figure 4.7). It should be noted that damage is constrained to the available hazard models. Nevertheless, based on the trends for both flood and earthquake damage (Figure 4.7), it is likely that the main risk to the area of study is from the effects of earthquakes. This trend could be explained by the flood impacts being more locally constrained than earthquake impacts, which have a regional (or greater) footprint. This suggests that a scale effect exists where, when multi-hazard studies are more constrained (e.g. spatially or in the range of recurrence intervals investigated), then less “options” exist for damage. This is true also for single-hazard studies in comparison to multi-hazard studies, where the damage output is restricted by the frame of reference (one hazard versus several hazards). Indeed, potential damage from hazards is constrained to the study scope where events and losses are occurring. This may seem a trivial point, but these scale effects could have an important influence on decision-making processes, which are often supported by cost-benefit analyses. It is likely appropriate to study multi-hazard risk initially at a higher-level and then to focus on more specific studies as different loss behaviors emerge. Indeed, the combination of multi-hazard / exposure might lead to very different mitigation measures (e.g. retrofitting and relocation). Decision-making for the various options could then be handled by

different levels of authorities, substantially changing the scope of the decision-making process and engagement. This would likely be less apparent with lower granularity loss assessment (through quantitative aggregation or qualitative indexing, for example “high, medium, low”). Hence, through analytical studies and data mining, this method provides opportunities to develop insights that are only accessible through comprehensive discrete data.

As highlighted earlier, the Franz Josef results point to an overwhelming effect of earthquakes, which is in line with previous work in that location (Langridge et al., 2016; McSaveney & Davies, 1998). In areas where any single hazard impact on the overall damage output is less dominant, multi-hazard studies might even be more informative. Indeed, because the potential losses of more uniform hazard impacts are more entangled, the tipping points are less evident and the damage output less clear. In this context, a multi-hazard assessment that takes into account interactions can potentially bring out surprising loss patterns (e.g. an earthquake that causes widespread stopbank failure and also triggers a landslide, which itself generates a landslide dam cascading into an outburst flood that impacts a, now defenseless, township).

The methodological framework presented here uses triggering events to initiate landslides, thus the probability/magnitude relationship of induced landsliding is a product of the simulation. The maximum value of landslide volume and landslide recurrence time from the AEP (Figure 4.7 & 8) in our probabilistic design, seems to be in line with a recent study pointing to risk of landsliding to the Franz Josef township (Langridge et al., 2016). Furthermore, the probability of high-impact landslides affecting the township (AEP 10^{-4} - 10^{-6}, equivalent to a recurrence interval of 10,000 to 1 million years) correlates with geological observations of old terraces dating the latest landslide deposit at 11,000-12,000 years (Langridge et al., 2016).

Although peripheral to the scope of this paper, which focusses on the risk to assets, a simplistic calculation can be undertaken on the landslide risk to human life. Franz Josef township hosts an average of about 1,000 people on a daily basis throughout the year (peak and off-peak seasons combined, https://www.westlanddc.govt.nz/franz-josef), which (assuming everyone in the

township perishes as a result of the landslide, which is correct to an order of magnitude as a result of the scenario landslide described above and with no mitigation measures assumed) brings the annual risk of individual fatality close to 10^{-3} or 1 in 1000. For comparison, sea dyke failure in the Netherlands adopted a threshold of annual individual risk of 1:1,000,000 (Hungr et al., 2016), suggesting that the landslide risk-to-life at Franz Josef may be unacceptable by several orders of magnitude.

The probabilistic output can be used as a sensitivity analysis to develop and present scenarios from which can be selected a smaller set that is relevant for the preparedness of the community (Davies, 2015). Indeed, the capability of the present method to track discrete cascading pathways opens the possibility to spatially display the course of action of any scenario of interest. It adds another layer of scrutiny to the traditional single scenario selection which, often, is purely based on expert opinion.

4.5.2 Limitations

It is to be emphasised that very little quantitative information could be found on potential impacts to roads, hence the fragility functions used in this model are uncertain. An opportunity exists for more modelling work on road damage from hazards (in line with existing volcanic ashfall impact on roads (Blake et al., 2017)) as well as for the dynamic effect of compounding damages from multi-hazard scenarios. The use of hazard footprints has limitations because of their availability. As highlighted in Figure 4.7, a side effect of their use is the “stepped” aspect of the loss output. Additional options are currently being trialed based on continuous distributions at the node locations instead of using the discrete values of hazard maps. Refinement is needed in the hazard components underlying the simulation: the use of PSHA is likely valid only in limited areas and other options should be considered in the future (e.g. OpenQuake (Pagani et al., 2014)). Landslide volume distribution over impacted assets should be assessed differently if a “landslide”

vulnerability function is to be included. In addition, liquefaction and surface rupture should be treated as independent hazards (e.g. by using liquefaction susceptibility maps) instead of being incorporated in the fragility function. The framework is still in its infancy, but more focus should be given to quantify and represent the uncertainty related to the framework presented as the multi-hazard model carries uncertainty from the individual models and empirical relationships it feeds from. Finally, while the framework is currently limited by the lack of data and reliable models for natural system behavior, these can be incorporated as they become available in the future.

4.6 Conclusion

A novel causal graphical methodology for multi-hazard assessment has been trialed by focusing on multi-hazard impacts to the assets of the Franz Josef area on the West Coast of the South Island, New Zealand. The results demonstrate that the methodology is capable of assessing multi-hazard risk to a range of vulnerable assets. Model outputs show the overwhelming dominance of an earthquake on potential damage to assets at Franz Josef. They also demonstrate the value of the approach and the need for multi-hazard assessment. For example, in a low-probability event, the multi-hazard risk assessment indicates much greater loss to housing than those from any single hazard. This emphasises that the main differences between the two approaches (single- and multi-hazard) occur in the low-frequency tail of the loss distribution. Hence, because decisions are often based on higher-frequency (100-year) or quantile (99^{th} percentile) events, standard risk assessments would miss or, in the best case underestimate, risk for the purposes of infrastructure and land-use planning. Although this paper does not specifically address risk to life, the output suggests there may be a serious threat to occupants of Franz Josef.

The general contribution of this paper to risk modeling lies in two main aspects: i) the simplified aspect of the framework proposed, which allows flexibility to encapsulate multiple elements into the risk “spectrum” (hazard, exposure and vulnerability) with very little impediment, and ii) the

forward nature of the assessment, which is predictive rather than explanatory (inverse model fitting data). This last point is an important consideration as damaging disasters are often a data-poor environment.

4.7 Acknowledgments

This work was supported by the Resilience to Nature's Challenges (RNC). We would like to thank the many contributors that provided models and information without whom this work would not have been possible. Among these are Pascal Horton, Chris Massey, Matthew Gardner and Quakecore, the NZ Centre for Earthquake Resilience.

4.8 References

AghaKouchak, A., Huning, L. S., Chiang, F., Sadegh, M., Vahedifard, F., Mazdiyasni, O., Mallakpour, I. (2018). How do natural hazards cascade to cause disasters? *Nature*, *561*(7724), 458–460. https://doi.org/10.1038/d41586-018-06783-6

Barth, N. C. (2014). The Cascade rock avalanche: Implications of a very large Alpine Fault-triggered failure, New Zealand. *Landslides*, *11*(3), 327–341. https://doi.org/10.1007/s10346-013-0389-1

Benn, J. L. (2005). Landslide events on the West Coast, South Island, 1867–2002. *New Zealand Geographer*, 3–13. https://doi.org/10.1111/j.1745-7939.2005.00001.x

Berryman, K. R., Cochran, U. A., Clark, K. J., Biasi, G. P., Langridge, R. M., & Villamor, P. (2012). Major earthquakes occur regularly on an isolated plate boundary fault. *Science*, *336*(6089), 1690–1693. https://doi.org/10.1126/science.1218959

Biasi, G. P., Langridge, R. M., Berryman, K. R., Clark, K. J., & Cochran, U. A. (2015). Maximum-Likelihood Recurrence Parameters and Conditional Probability of a Ground-Rupturing

Earthquake on the Southern Alpine Fault, South Island, New Zealand. *Bulletin of the Seismological Society of America*, *105*(1), 94–106. https://doi.org/10.1785/0120130259

Blake, D. M., Wilson, T. M., Cole, J. W., Deligne, N. I., & Lindsay, J. M. (2017). Impact of volcanic ash on road and airfield surface skid resistance. *Sustainability*, *9*(8), 1389.

Costa, J. E. (1985). Floods from Dam Failures. *U.S Geological Survey*, 1–59.

Davies, T. (1997). Long-term management of facilities on an active alluvial fan—Waiho River fan, Westland, New Zealand. *Journal of Hydrology New Zealand*, *36*(2), 127–145.

Davies, T. (2002). *Landslide-dambreak floods at Franz Josef Glacier township, Westland, New Zealand: A risk assessment*. *41*(1), 1–17.

Davies, T., McSaveney, M. J., & Clarkson, P. J. (2003). Anthropic aggradation of the Waiho River, Westland, New Zealand: Microscale modelling. *Earth Surface Processes and Landforms*, *28*, 209–218. https://doi.org/10.1002/esp.449

Dellow, S., Massey, C. I., & Cox, S. C. (2017). Response and initial risk management of landslide dams caused by the 14 November 2016 Kaikōura earthquake, South Island, New Zealand. *New Zealand*, 8.

Delmendo, L. C. (2019). Globalpropertyguide. Retrieved from Globalpropertyguide website: https://www.globalpropertyguide.com/Pacific/New-Zealand/Price-History

DTEC Consulting. (2002). West coast regional council: Natural hazards review. *West Coast Regional Council: Natural Hazards Review*.

Dunant, A., Bebbington, M., & Davies, T. (In review). Multi-hazards scenario generator: A network-based simulation of natural disasters. *Risk Analysis*.

Ermini, L., & Casagli, N. (2003). Prediction of the behaviour of landslide dams using a geomorphological dimensionless index. *Earth Surface Processes and Landforms*, *28*, 31–47. https://doi.org/10.1002/esp.424

Frattini, P., & Crosta, G. B. (2013). The role of material properties and landscape morphology on landslide size distributions. *Earth and Planetary Science Letters*, *361*, 310–319.

https://doi.org/10.1016/j.epsl.2012.10.029

Fruchterman, T. M. J., & Reingold, E. M. (1991). Graph drawing by force-directed placement. *Software: Practice and Experience*, *21*(11), 1129–1164. https://doi.org/10.1002/spe.4380211102

Gardner, M. (2016). *2D Hydraulic Modelling based on LiDAR WAIHO RIVER: Hydraulic Modelling and Options Analysis*. Retrieved from http://www.wcrc.govt.nz/Documents/Natural Hazard Reports/Waiho River M21 Modelling Report - November 2016.pdf

Gill, J. C., & Malamud, B. D. (2014). Reviewing and visualizing the interactions of natural hazards: Interactions of Natural Hazards. *Reviews of Geophysics*, *52*(4), 680–722. https://doi.org/10.1002/2013RG000445

Gill, J. C., & Malamud, B. D. (2016). Hazard interactions and interaction networks (cascades) within multi-hazardmethodologies. *Earth System Dynamics*, *7*(3), 659–679. https://doi.org/10.5194/esd-7-659-2016

Glade, T. (1998). Establishing the frequency and magnitutude of landslide triggering rainstorm events in New Zealand. *Environmental Geology*, *35*(August), 160–174.

Green, R. A., Allen, J., Wotherspoon, L., Cubrinovski, M., Bradley, B., Bradshaw, A., … Algie, T. (2011). Performance of Levees (Stopbanks) during the 4 september 2010 Mw 7.1 Darfield and 22 February 2011 Mw 6.2 Christchurch, New Zealand, Earthquakes. *Seismological Research Letters*, *82*, 939–949. https://doi.org/10.1785/gssrl.82.6.939

Hancox, G. T., McSaveney, M. J., Manville, V. R., & Davies, T. (2005). The October 1999 Mt Adams rock avalanche and subsequent landslide dam-break flood and effects in Poerua river, Westland, New Zealand. *New Zealand Journal of Geology and Geophysics*, *48*(4), 683–705. https://doi.org/10.1080/00288306.2005.9515141

Henderson, R., & Collins, D. (2016). *Regional Flood Estimation Tool for New Zealand*. National Institute of Water & Atmospheric Research Ltd.

Horton, P., Jaboyedoff, M., Rudaz, B., & Zimmermann, M. (2013). Flow-R, a model for susceptibility mapping of debris flows and other gravitational hazards at a regional scale. *Natural Hazards and Earth System Sciences*, *13*(4), 869–885. https://doi.org/10.5194/nhess-13-869-2013

Hovius, N., Stark, C. P., & Allen, P. A. (1997). Sediment flux from a mountain belt derived by landslide mapping. *Geology*, *25*, 231–234. https://doi.org/10.1130/0091-7613(1997)025<0231:sffamb>2.3.co;2

Hughes, M. W., Quigley, M. C., Van Ballegooy, S., Deam, B. L., Bradley, B. A., Hart, D. E., & Measures, R. (2015). The sinking city: Earthquakes increase flood hazard in Christchurch, New Zealand. *GSA Today*, *25*(3–4), 4–10. https://doi.org/10.1130/GSATG221A.1

Hungr, O., Clague, J., Morgenstern, R., VanDine, D., & Stadel, D. (2016). *A review of landslide risk acceptability practices in various countries*. https://doi.org/10.1201/b21520

Jibson, R. W., Allstadt, K. E., Rengers, F. K., & Godt, J. W. (2018). *Overview of the geologic effects of the November 14, 2016, Mw 7.8 Kaikōura, New Zealand, earthquake* (USGS Numbered Series No. 2017–5146; p. 52). Retrieved from U.S. Geological Survey website: http://pubs.er.usgs.gov/publication/sir20175146

Kappes, M. S., Keiler, M., von Elverfeldt, K., & Glade, T. (2012). Challenges of analyzing multi-hazard risk: A review. *Natural Hazards*, *64*(2), 1925–1958. https://doi.org/10.1007/s11069-012-0294-2

King, A., & Bell, R. (2005). *Riskscape New Zealand—A Multihazard Loss Modelling Tool*. 9.

Korup, O. (2003). *Landslide-induced River Disruption: Geomorphic Imprints and Scaling Effects in Alpine Catchments of South Westland and Fiordland, New Zealand: A Thesis Submitted to the Victoria University of Wellington in Fulfilment of the Requirements for the Degree of Doctor of Philosophy in Physical Geography*.

Korup, O. (2004). Geomorphometric characteristics of New Zealand landslide dams.

Engineering Geology, *73*(1–2), 13–35. https://doi.org/10.1016/j.enggeo.2003.11.003

Korup, O. (2005). Large landslides and their effect on sediment flux in South Westland, New Zealand. *Earth Surface Processes and Landforms*, *30*(3), 305–323. https://doi.org/10.1002/esp.1143

Kritikos, T. (2013). *Geomorphic Hazard Analyses in Tectonically-Active Mountains: Application to the Western Southern Alps , New Zealand*. 299.

Kritikos, T., Robinson, T., & Davies, T. (2015). Regional coseismic landslide hazard assessment without historical landslide inventories: A new approach. *Journal of Geophysical Research*. https://doi.org/10.1002/2014JF003224.Words

Kwak, D. Y., Stewart, J. P., Brandenberg, S. J., & Mikami, A. (2016). Characterization of Seismic Levee Fragility Using Field Performance Data. *Earthquake Spectra*, *32*(1), 193–215. https://doi.org/10.1193/030414EQS035M

Langridge, R. M., Buxton, R., Howarth, J. D., & Ries, W. F. (2016). *Natural Hazard Assessment for the Township of Franz Josef, Westland District*. Retrieved from http://www.wcrc.govt.nz/Documents/Natural Hazard Reports/GNS Final Franz Josef Report 2016.pdf

Larsen, I. J., Montgomery, D. R., & Korup, O. (2010). Landslide erosion controlled by hillslope material. *Nature Geoscience*, *3*(4), 247–251. https://doi.org/10.1038/ngeo776

Legros, F. (2002). The mobility of long-runout landslides. *Engineering Geology*, *63*, 301–331. https://doi.org/10.1016/s0013-7952(01)00090-4

Malamud, B. D., Turcotte, D. L., Guzzetti, F., & Reichenbach, P. (2004). Landslide inventories and their statistical properties. *Earth Surface Processes and Landforms*, *29*(6), 687–711. https://doi.org/10.1002/esp.1064

Massey, C., Townsend, D., Rathje, E., Allstadt, K. E., Lukovic, B., Kaneko, Y., … Villeneuve, M. (2018). Landslides Triggered by the 14 November 2016 Mw 7.8 Kaikōura Earthquake, New ZealandLandslides Triggered by the 14 November 2016 Mw 7.8 Kaikōura

Earthquake, New Zealand. *Bulletin of the Seismological Society of America*, *108*(3B), 1630–1648. https://doi.org/10.1785/0120170305

McSaveney, M. J., & Davies, T. (1998). *Natural hazard assessment for the township of Franz Josef Glacier and its environs*. (July).

Mignan, A., Wiemer, S., & Giardini, D. (2014). The quantification of low-probability-high-consequences events: Part I. A generic multi-risk approach. *Natural Hazards*, *73*(3), 1999–2022. https://doi.org/10.1007/s11069-014-1178-4

Pagani, M., Monelli, D., Weatherill, G., Danciu, L., Crowley, H., Silva, V., … Panzeri, L. (2014). OpenQuake engine: An open hazard (and risk) software for the global earthquake model. *Seismological Research Letters*, *85*(3), 692–702.

Pescaroli, G., & Alexander, D. (2015). A definition of cascading disasters and cascading effects: Going beyond the 'toppling dominos' metaphor. *GRF Davos Planet@Risk*, *Volume 3*.

Reinz. (2018). Residential property data. Retrieved from https://www.reinz.co.nz/residential-property-data-gallery

Robinson, T., & Davies, T. (2013). Review Article: Potential geomorphic consequences of a future great (*M*w Combining double low line 8.0+) Alpine Fault earthquake, South Island, New Zealand. *Natural Hazards and Earth System Sciences*, *13*(9), 2279–2299. https://doi.org/10.5194/nhess-13-2279-2013

Robinson, T., Davies, T. R. H., Wilson, T. M., & Orchiston, C. (2016). Coseismic landsliding estimates for an Alpine Fault earthquake and the consequences for erosion of the Southern Alps, New Zealand. *Geomorphology*, *263*, 71–86. https://doi.org/10.1016/j.geomorph.2016.03.033

Robinson, T., & Rosser, N. (2017). Rapid landslide risk assessment of transport infrastructure following the 13 November 2016 Kaikōura, New Zealand, earthquake. *Geophysical Research Abstracts EGU General Assembly*, *19*, 2017–5180.

Tarbali, K., & Bradley, B. A. (2014). Representative ground-motion ensembles for several major

earthquake scenarios in New Zealand. *Bulletin of the New Zealand Society for Earthquake Engineering*, *47*(4), 231–252.

Teara—The encyclopedia of New Zealand. (n.d.). Retrieved from Teara—The encyclopedia of New Zealand website: https://teara.govt.nz/en/building-materials/page-1

Tecnocarreteras. (2012). Retrieved from https://www.tecnocarreteras.es/2012/02/22/sabemos-cuanto-nos-cuesta-tener-de-forma-optima-las-infraestructuras-y-servicios-que-garantizan-nuestra-seguridad-vial/

Thompson, C. (2011). *HIRDSV3: High Intensity Rainfall Design System, National Institute of Water and Atmosphere, Wellington.*

Tilloy, A., Malamud, B. D., Winter, H., & Joly-Laugel, A. (2019). A review of quantification methodologies for multi-hazard interrelationships. *Earth-Science Reviews*, *196*, 102881. https://doi.org/10.1016/j.earscirev.2019.102881

Chapter 5
Discussion and Future Research

The goal of this thesis was to create and test a novel methodology to quantify multi-hazard risk. This goal was achieved following the work presented in:

Chapter 2, where gaps in the current multi-hazard methodology were described and a new framework proposed. The methodology was then used to model the impacts of the 2016 earthquake and coseismic landsliding on the Kaikōura road system, and the approach verified by comparing model outputs with the 2016 events.

Chapter 3, which acted as “transitional” work in order to further develop the methodology presented in Chapter 2 by adding the capability to analyse landslide dams as a part of the cascading multi-hazard assessment.

Chapter 4, which presented work further building on the progress made in Chapters 2 and 3. A complex multi-hazard system was presented, and a fully probabilistic model designed. The model was used to assess the multi-hazard risk to the Franz Josef area.

The pilot study presented in Chapter 2 was used a quick-fail test that successfully demonstrated that a spatial network was a viable path forward for multi-hazard risk assessment. Quantification of the landslide dam threat (Chapter 3) facilitated further development of the method in another case study (Chapter 4) by incorporating the essential component of hazard cascades in

mountainous environments. The fully probabilistic results obtained in Chapter 4 represent the key output of this thesis, demonstrating the fulfilment of the initial goal by providing a new quantitative framework and, more importantly, new insights into the natural hazards and impacts that threaten New Zealand communities.

The precatory purpose of this work was to address several problems currently existing in multi-hazard risk assessment, namely: i) Limits on the number of hazards interacting: ii) Non-spatial output and/or difficulties in providing comprehensive output: iii) The amount of data required to assume a joint probability distribution and the intrinsic constraint of the risk analysis within the data boundaries: and iv) The computing resources necessary for combined physical models, which limits the flexibility of such models to expand to additional hazards and to provide probabilistic assessment.

The graphical framework presented (and tested) herein provides options to resolve these constraints.

As explained in the conclusion of Chapter 4, the contribution of this work to the risk modeling discipline lies in two main aspects: i) the unifying aspect of the framework proposed, which allows for the flexibility to incorporate multiple elements into the risk “spectrum” (hazard, exposure and vulnerability) with very little impediment, and ii) the forward nature of the assessment, which is predictive (use of threshold values and empirical relationships) rather than explanatory (inverse model fitting data). This last point is an important consideration as damaging disasters are often a data-poor environment.

Those advances provide new pathways for complex risk assessment, which are further described in 5.2 below.

5.1 Discussion

5.1.1 Landslide dam regional assessment

In line with the purpose of this thesis to provide a framework for integrating the various components of the disaster "system", the landslide dam regional assessment presented in Chapter 3 is an important addition to multi-hazard risk assessment in mountainous environments. Indeed, Chapter 3 presents an efficient algorithm that permits a proactive, regional-scale screening of potential outburst flood discharges from catchments. The results show a power-law trend of outburst flow size, which is likely associated with Horton's law whereby stream networks and catchment basins are characterised by numerous fractal dimensions. If we consider that catchments and river systems are Hortonian in nature, then it is likely that the power law distribution of outburst flows from landslide dams found in Chapter 3 will apply in any catchment. This must be considered carefully as human perception tends to be biased toward high frequency events – "out of sight, out of mind" (Slovic et al., 1981) – and the extreme case scenario could easily be ignored or discarded. The extreme scenario of an outburst flood could lead to discharge values well beyond "standard" river flood events. Stopbank designs would likely require consideration of this possible event, even if unlikely. As Chapter 3 used the cascading effect of a triggering hazard on subsequent hazards, the graphical framework can provide the means to assess where such impacts can occur and probability of occurrence for such events.

5.1.2 Multi-hazard graphical framework

Chapters 2 and 4 bring a new principle into risk assessment by considering a network as the framework to calculate risk instead of a hazard footprint. This framework offers many advantages, one of which is its "compactness" – the ability to store a lot of data in a computationally light

medium through pre-calculation, not dissimilar in intent to statistical emulators (Bayarri et al., 2009). Hence this provides the opportunity to simulate vast quantities of disaster scenarios flowing through large quantities of nodes using a single structure. Another advantage of the framework presented here is that the causal network uses a “bottom up” approach where the spatial data drive creation of the network thus allowing the output to be discretised. The discretisation permits results to be obtained by, for example, aggregating the outputs by exposure type, hazard type, location, event magnitude etc. Spatial information is paramount to risk reduction and preparedness actions and the results provided by the framework can be dissected and presented to fulfil specific needs (e.g. AEP losses, predictive road blockages etc.). In addition, this framework circumvents some of the issues related to lack of data. Indeed, coupling hazards together in a cascading chain reaction provides a stochastic output from a joined “activation”.

5.1.3 Coupled multi-hazard assessment

Chapter 2 and, more specifically, Chapter 4 highlight the framework difference between a “standard” multilayer single hazard and a genuine multi-hazard assessment. Multi-hazard scenarios show a compounding loss effect for rare events where the initial hazard creates losses that are then followed by secondary losses from additionally triggered perils. It was shown that the hazard spectrum behind the losses can change with diminishing probabilities of occurrence. This evolution can also be different depending on the nature of the exposure. In the case of Franz Josef, the overwhelming threat is earthquakes until the probability of exceedance reaches about the 1 in 10,000-year level where an additional threat emerges with landsliding. In terms of remediation plans, these insights could influence decisions made for the township as the nature of the two hazards suggests different options. Another aspect to keep in mind is the high probability of moderate flooding. As the compounding cost of frequent events increases, this could

overshadow the cost of rarer hazards. In this sense, the AEP plot (Figure 4.7) is quite “insurance” centric and might not be the output needed for planning or preparedness.

5.2 Future research directions

5.2.1 Graphical multi-hazard risk assessment

Future research should continue to refine the existing causal elements of the graphical method, which is at an early stage. Several projects are ongoing to test / adapt the method proposed here in other parts of the world. Computer science expertise would be beneficial to make the model more efficient.

In addition, several actions could be taken to remediate some gaps that were brought to light during the study:

- The current model is based on hazard footprints; hence the outputs show the imprints of available models. To resolve this artefact and rely less on the availability of large numbers of hazard models, precalculating a range of footprints that can be used to better inform the edge propagation probabilities would allow near continuous frequency/magnitude input at each of the nodes and, potentially, be a realistic alternative.
- The current model deals with a specific set of hazards (earthquake, rainfall, landslide etc.). Depending on needs, other hazards could be integrated into the proposed multi-hazard risk framework; fire following earthquake, volcanic unrest and related multi-hazard risk (pyroclastic density flows, Lahars, ashfall etc.), tsunami and liquefaction following earthquakes are among the possible new projects.
- The current model only deals with immediate cascading effects and should be further developed to include longer timelines (e.g. aftershocks, river aggradation etc.). It is believed that progress toward this development would be straightforward but would

require the investigation and incorporation of causality measures. Several projects are already ongoing to develop this possibility.

- The model developed in Chapter 4 creates a large dataset of discrete outputs. This output requires computing time. To gain access to lower-probability occurrences than those investigated in Chapter 4 will increase the required computing resources by an order of magnitude. Utilisation of Artificial Intelligence (AI) could help find a solution to this problem. Indeed, training an AI model on a "small" dataset (e.g. 20,000 scenarios) could permit understanding of the hidden trends of the multi-hazard loss model. Theoretically, it should then be possible to extrapolate the multi-hazard output to rarer events and extreme losses without using the multi-hazard model to its, previously required, extent (e.g. 1 million scenarios) (Bouhlel et al., 2019).
- Dynamic exposure is a difficult problem to tackle. The method presented in this thesis assumes static exposure. Proposed work is aimed at developing further the novel technique presented here toward a fully dynamic network of interactions. This new framework would drastically expand the current method capability by allowing time dimension in the exposure space (movement of population, traffic flow, evolving land use, city growth, pandemic following disaster etc.) and still provide a holistic risk assessment.
- Communication of the risk might gain from this paradigm shift in the future. I believe that the creation of discrete output can be used with maximum impact during live sessions. To be able to dig into the data to answer, dynamically, the questions of stakeholders will be a powerful tool that would lead to wider and more detailed discussion. In opposition to "pre-assembled" material (e.g. a map presenting a specific output), which is more static in nature, would focus the discussion around the material presented.
- The graphical approach might have more to give than the study presented here or the suggestions of this chapter. Making contacts with other disciplines using graphical

methodologies could foster new ideas to be used in the disaster context. Contacts have already been made to inquire into the subject of biology (Valdano et al., 2015).

5.2.2 Vulnerability functions and infrastructure fragilities

Because of the lack of data, several assumptions were necessary regarding the fragility of roads, houses and stopbanks to various hazards (Chapter 4). Apart from for housing stock, few design data are available, and the damage caused by hazards had to be approximated. Thus, the fragility of these structures is highly debatable. this suggests a lot of avenues whereby future research could considerably improve the accuracy and applicability of the graphical model, for example:

- A New Zealand stopbank inventory should be documented and design specifications made accessible. This would bring more certainty to any flood related risk assessment.
- Impact and loss estimates for the road system were difficult to incorporate as few vulnerability functions could be found for the hazards of interest. Research should create or further develop fragility models of roads to earthquake, flood and landsliding. This is especially important considering that roads are vital networks, particularly when it comes to recovery, and hence to resilience.
- Landsliding related fragilities are still sparse and the losses to exposed elements therefore remain largely binary (destroyed or intact). A vulnerability function related to volume of debris and/or velocity would be a useful addition to any loss assessment related to landsliding.
- As the method assumes a timeline of cascading events, and assuming that the primary effect will further accentuate the effect of a secondary hazard (e.g. volcanic ash loading on a building followed by an earthquake), dynamic vulnerability functions could be further developed to handle compounding hazard effects.

- If data remain scarce, expert elicitation could be use in a formal protocol to gather information (Cooke, 1991; O'Hagan, 2019).

5.3 References

Bayarri, M. J., Berger, J. O., Calder, E. S., Dalbey, K., Lunagomez, S., Patra, A. K., … Wolpert, R. L. (2009). Using Statistical and Computer Models to Quantify Volcanic Hazards. *Technometrics*, *51*(4), 402–413. https://doi.org/10.1198/TECH.2009.08018

Bouhlel, M. A., Hwang, J. T., Bartoli, N., Lafage, R., Morlier, J., & Martins, J. R. R. A. (2019). A Python surrogate modeling framework with derivatives. *Advances in Engineering Software*, *135*, 102662. https://doi.org/10.1016/j.advengsoft.2019.03.005

Slovic, P., Fischhoff, B., & Lichtenstein, S. (1981). Perceived risk: Psychological factors and social implications. *Proceedings of the Royal Society of London. A. Mathematical and Physical Sciences*, *376*(1764), 17–34.

Valdano, E., Ferreri, L., Poletto, C., & Colizza, V. (2015). Analytical computation of the epidemic threshold on temporal networks. *Physical Review X*, *5*(2), 1–9. https://doi.org/10.1103/PhysRevX.5.021005